

**Exploring the Contribution of AXIN1  
Mutation and tRNA Biology to Liver Cancer**

**Ruyi Zhang**

**张如意 著**



The studies presented in this thesis were performed at the Laboratory of Gastroenterology and Hepatology, Erasmus MC-University Medical Center Rotterdam, the Netherlands.

The research was funded by:

- Chinese Scholarship Council

Financial support for printing of this thesis was provided by:

Erasmus University Rotterdam

© Copyright by Ruyi Zhang. All rights reserved.

No part of the thesis may be reproduced or transmitted, in any form, by any means, without express written permission of the author.

Cover layout design: the author of this thesis.

Source of image: Bingting Yu & WOMBO Dream - AI Art Generator

Printed by: Ridderprint BV, Ridderkerk, the Netherlands | [www.ridderprint.nl](http://www.ridderprint.nl)

ISBN: 978-94-6483-401-7

# **Exploring the Contribution of AXIN1 Mutation and tRNA Biology to Liver Cancer**

Onderzoek naar de bijdrage van AXIN1-mutatie en tRNA-biologie aan  
leverkanker

## **Thesis**

**to obtain the degree of Doctor from the  
Erasmus University Rotterdam  
by command of the  
rector magnificus**

Prof. dr. A.L. Bredenoord

**and in accordance with the decision of the Doctorate Board**

**The public defense shall be held on**

*Tuesday 24<sup>th</sup> October 2023 at 10:30*

**by**

**Ruyi Zhang**

born in Gongzhuling, Jilin Province, China

**Erasmus University Rotterdam**



## **Doctoral Committee**

### **Promoters:**

Prof. dr. M.P. Peppelenbosch

### **Other members:**

Prof. dr. W.N.M. Dinjens

Dr. P. Hohenstein

Dr. G.M. Fuhler

### **Co-promoter:**

Dr. M.J.M. Smits

# CONTENTS

<b>Chapter 1</b> .....	1
General introduction and outline of this thesis	
<b>Chapter 2</b> .....	19
Identification of tumor-associated AXIN1 missense variants that affect $\beta$ -catenin signaling	
	<i>Manuscript in submission</i>
<b>Chapter 3</b> .....	75
Unraveling the Impact of AXIN1 Mutations on HCC Development: Insights from CRISPR/Cas9 repaired AXIN1-mutant liver cancer cell lines	
	<i>Manuscript in submission</i>
<b>Chapter 4</b> .....	115
Issues with RNF43 antibodies to reliably detect intracellular location	
	<i>PLOS ONE. 2023,18(4): e0283894.</i>
<b>Chapter 5</b> .....	141
A simplified qPCR method revealing tRNAome remodeling upon infection by genotype 3 hepatitis E virus	
	<i>FEBS letters, 2020,12(594): 2005-2015.</i>
<b>Chapter 6</b> .....	171
The biological process of lysine-tRNA charging is therapeutically targetable in liver cancer	
	<i>Liver International, 2021, 1(41): 206-219.</i>
<b>Chapter 7</b> .....	213
Summary	
<b>Chapter 8</b> .....	221
Discussion	

**Chapter 9** ..... 241

Dutch Summary (Nederlandse Samenvatting)

**Appendix** ..... 251

Acknowledgements

Publications

PhD Portfolio

Curriculum Vitae

# **Chapter 1**

## **General Introduction and Outline of This Thesis**





## Liver cancer

1

Liver cancer is the sixth most diagnosed cancer and the third most common cause of cancer mortality, which has become a serious public health issue around the world. According to data from the World Health Organization (WHO), liver cancer has been diagnosed in about 906,000 people and 830,000 related deaths in 2020, hepatocellular carcinoma (HCC) being the most common type<sup>1,2</sup>. Over the past decades, our understanding of HCC epidemiology, risk factors, and molecular profiles has progressed significantly. The most common risk factor for HCC was identified as cirrhosis. Emerging data indicate that the mortality rate of HCC associated with cirrhosis is rising and the annual rate of HCC in patients with cirrhosis is between 3% and 8%<sup>3</sup>. Cirrhosis is nearly always caused by underlying disease, including chronic infection by hepatitis B virus (HBV) or hepatitis C virus (HCV), poor diet (alcohol) and inactivity, and fungal toxins. HCC can potentially be cured if surveillance and early detection would be effective. However, sensitive and valid biomarkers for early diagnosis of HCC are lacking, resulting in a high mortality rate and global burden.

HCC is a complex and slow-developing cancer of the liver that requires multifaceted decision-making for effective management. Treatment options for HCC may vary depending on the stage of the tumor and available resources. These options may include surgical resection<sup>4,5</sup>, liver transplantation<sup>6</sup>, local ablation<sup>7</sup>, transarterial chemoembolization (TACE)<sup>8</sup>, radiotherapy<sup>8</sup>, and pharmacological approaches. Prevention of HBV and HCV infections, as well as the treatment of related liver diseases, can help reduce the global burden of HCC. However, improved detection, diagnosis, and therapy for liver cancer are also critical<sup>9,10</sup>.

A further complication is that HCC cannot be regarded as a homogeneous type of cancer. In recent years, significant advancements in the oncological classification of HCC have been made through efforts in molecular subtyping, combined with analysis of clinical, etiological, and histopathological features<sup>11,12</sup>. This has led to the identification of several subgroups (see **Figure 1**). Originally, HCC was divided in a “proliferation” and a “non-proliferation class”<sup>13</sup>. The latter is more heterogeneous and includes less aggressive, chromosomally stable tumors that are more commonly related to chronic HCV infection or alcohol consumption. On histological appearance these tumors tend to retain hepatocyte-like features. One prominent subclass is represented by HCCs carrying *CTNNB1* mutations, which

leads to aberrant activation of the Wnt/ $\beta$ -catenin signaling pathway. These  $\beta$ -catenin mutant HCCs also show a high level of TERT promoter mutations resulting in re-activation of telomerase activity. On the other hand, the "proliferation class" is stronger associated with HBV-related etiology and includes clinically aggressive tumors that are poorly differentiated. Among this group of HCCs a "progenitor subclass" is characterized by high-level expression of hepatic progenitor markers. Besides frequent TP53 mutations, this subclass also harbors a considerable proportion of AXIN1 mutant cancers, a major component of the Wnt/ $\beta$ -catenin destruction complex described in more detail below.

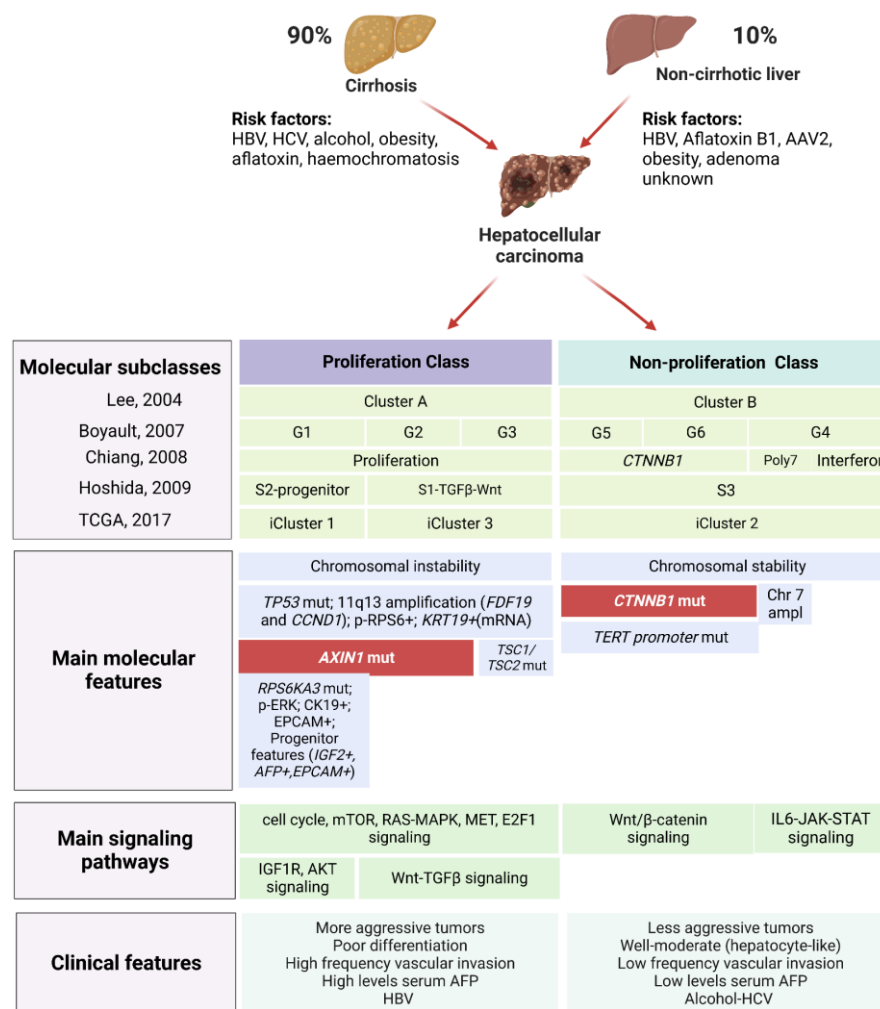


**Figure 1. Risk factors and classification of HCC.**

The classification of HCC is based on both molecular and pathological characteristics, and is derived from transcriptomic-based approaches previously reported in five studies (Lee<sup>13</sup>, Boyault<sup>14</sup>, Chiang<sup>15</sup>, Hoshida<sup>16</sup>, and TCGA<sup>17</sup>). The figure represents a modified version of the original illustrations from S. Caruso et al., and S. Rebouissou et al., with permission from the authors<sup>12,11</sup>. Ampl, amplification; mut, mutation.

## Role of Wnt/ $\beta$ -catenin signaling pathway in cancer development

The Wnt signaling pathway, which has been conserved throughout evolution, is known to be involved in a variety of processes, both normal physiological processes and abnormal pathophysiological processes<sup>18-20</sup>. It can be classified as canonical or non-canonical, with the latter divided into Wnt-planar cell polarity and Wnt/calcium pathways. However, for this thesis we will mainly focus on the canonical Wnt/ $\beta$ -catenin pathway, which is most relevant for HCC.

In this pathway,  $\beta$ -catenin is the core component, which can either be degraded or stabilized depending on the presence of extracellular Wnt protein (see **Figure 2**). Upon activation,  $\beta$ -catenin ultimately ends-up in the nucleus regulating the expression of  $\beta$ -catenin target genes, thereby influencing various cellular decisions. Aberrant activation of this pathway is observed in a large number of cancer types<sup>22</sup>. This also applies to liver cancer for which mutational analysis indicated that approximately 2/3 of HCC cases demonstrate aberrant activation of the Wnt/ $\beta$ -catenin pathway<sup>23,24</sup>. The most prominent genetic alterations observed are activating gain-of-function (GOF) mutations in *CTNNB1*, accounting for approximate 25% of cases. Most of these mutations affect amino acids encoded by exon 3 of *CTNNB1*, involved in the phosphorylation and ubiquitination of  $\beta$ -catenin, thereby preventing its degradation and promoting its nuclear translocation<sup>25</sup>. Furthermore, in a small subset of HCCs, mutations in armadillo repeat domains 5 and 6 of the  $\beta$ -catenin protein are observed, which reduce its binding to APC<sup>26,27</sup>. These latter mutations result in a small but significant increase in signaling, while the exon 3 mutants lead to a more robust activation<sup>26,27</sup>. Target genes consist of more canonical ones activated in most tissues, such as *AXIN2* and *NOTUM*, and liver specific  $\beta$ -catenin target genes, such as *GLUL* and *TBX3*<sup>28</sup>. Genes activated by  $\beta$ -catenin signaling are generally related to cancer stem cell features of HCC and promote their proliferation. Exon 3 mutations are also observed in the majority of hepatoblastomas<sup>29</sup> and a subset of hepatocellular adenomas<sup>30</sup>.

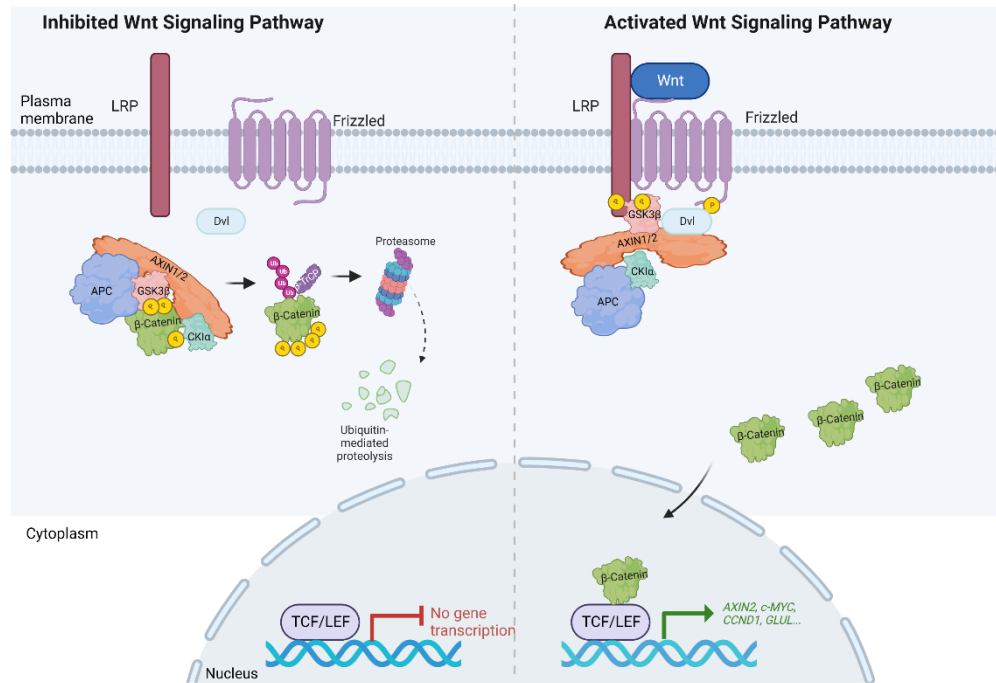


**Figure 2. The canonical Wnt/β-catenin signaling pathway.**

The canonical Wnt/β-catenin pathway is subdivided in Wnt-on or Wnt-off. **Left panel:** In the absence of Wnt, the core members of the destruction complex including adenomatous polyposis coli (APC), AXIN1/2, glycogen synthase kinase 3β (GSK3β), and casein kinase 1 (CK1) are recruited and assembled to degrade β-catenin in the cytoplasm. AXIN1 or AXIN2 is the scaffold for the destruction complex and binds to all the other complex components. CK1 handles the initial phosphorylation of β-catenin at S45, and GSK3β follows and phosphorylates it at T41, S37, and S33<sup>21</sup>. As a result, β-catenin is ubiquitinated by the E3 ligase SKP1-CUL1-F-box protein (SCF)-β-transducing repeat-containing protein (β-TrCP), which targets β-catenin for proteasome degradation. **Right panel:** Wnt/β-catenin signaling is activated when Wnt binds to its receptors Frizzled (Fz) and low-density lipoprotein receptor-related protein 6 (LRP6) or to its close relative LRP5, at the cell surface. Formation of the trimeric Wnt-Fz-LRP6 complex and recruitment of the scaffold protein Dishevelled (Dvl) leads to LRP6 phosphorylation and recruitment of the β-catenin destruction complex to the receptors. Hence, GSK3-mediated phosphorylation of β-catenin is inhibited, leading to cytoplasmic β-catenin accumulation and transferal to the nucleus, where it forms a complex with transcription factors of the Lymphoid enhancer factor/T cell factor (LEF/TCF) family and activation of Wnt target gene transcription.

Other mechanisms contributing to aberrant activation of the Wnt/β-catenin pathway include mutations in genes that regulate the degradation of β-catenin, such as *APC*, *AXIN1* and *AXIN2*, as well as changes in the levels of Wnt inhibitors or ligands<sup>31,32</sup>. *APC*, *AXIN1* and *AXIN2* are tumor suppressor genes and their alterations can involve deletions, missense, nonsense, and frameshift mutations distributed throughout the entire gene<sup>33</sup>. These genetic changes result in the nuclear translocation of β-catenin, which activates target genes and promotes

cancer development. In particular *AXIN1*, and to a lesser extent, *APC* and *AXIN2* are frequently mutated in HCC<sup>22</sup>.

Most mutations in *AXIN1* are missense variations or truncations, which are thought to disrupt the normal regulation of the  $\beta$ -catenin pathway. Missense mutations, which involve changes to a single amino acid in a protein, are the most common type of genetic alteration found in the *AXIN1* gene in human cancers. However, the functional consequences of only a handful of missense *AXIN1* mutations have been well studied<sup>34,35</sup>, while the majority of them are considered as "variants of uncertain significance" (VUS)<sup>36</sup>. Therefore, these mutations are worth exploring further as they can have significant effects on the function of the protein. Large-scale sequencing of tumor DNA is increasingly being used as a diagnostic technique to find driver genes of tumorigenesis and to identify potential gene alterations that can be used therapeutically<sup>37-39</sup>. This has however also created a new challenge in that many variants are detected for which the clinical relevance is largely unknown. Therefore, studying VUS mutations in *AXIN1* is important for advancing our understanding of their contribution to cancer, and potentially in the future to develop new treatment and management approaches for HCC and other types of cancer.

In contrast to missense mutations, truncating mutations of *AXIN1* are generally believed to be a driver of cancer development<sup>34</sup>. However, whether all truncations lead to the same level of impairment of *AXIN1* function is still largely unknown. Moreover, the exact manner in which *AXIN1* mutation contributes to HCC development is still a subject of debate. Originally, because of its contribution in the  $\beta$ -catenin breakdown complex, it was considered to contribute to cancer by activating  $\beta$ -catenin signaling. During the last decades this view has however been challenged. *AXIN1* mutant cancers rarely show nuclear accumulation of  $\beta$ -catenin, often regarded as the hallmark of active signaling<sup>40,41</sup>. In addition, RNA expression profiling of HCCs revealed that *AXIN1*-mutated cancers show no or at most a modest increase in  $\beta$ -catenin target gene expression above a set threshold<sup>28</sup>. According to this report, *AXIN1* mutant cancers are associated with the activation of the Notch and YAP/TAZ signaling pathways rather than the typical  $\beta$ -catenin-mediated transcriptional signature. Thus, these reports suggest that  $\beta$ -catenin signaling is barely increased following *AXIN1* mutation, and not relevant for HCC growth. However, Qiao and coworkers showed that *AXIN1*-driven HCC development in mice is almost entirely dependent on functional  $\beta$ -catenin<sup>42</sup>. Others argued

that this result was only obtained in the context of simultaneous overexpression of the proto-oncogene MET<sup>42-44</sup>. In further support for a role of  $\beta$ -catenin, we and others have observed increased  $\beta$ -catenin signaling in AXIN1-mutant HCC cell lines, albeit modest compared to  $\beta$ -catenin mutant HCCs<sup>45-47</sup>. This can be explained by a partial functional compensation by the AXIN2 protein. Accordingly, siRNA mediated AXIN2 knock-down leads to a dramatic increase in  $\beta$ -catenin signaling in AXIN1-mutant HCC cell lines<sup>46,47</sup>. As such, AXIN1-mutant cancers are strongly dependent on AXIN2 to counterbalance signals that induce  $\beta$ -catenin signaling, and more vulnerable to aberrantly increase this signaling pathway.

Taken together, despite two decades of research of AXIN1-driven HCC development, it is still unclear if AXIN1-mutant HCCs show increased  $\beta$ -catenin signaling, whether this is relevant to support their growth, and through which alternative mechanisms potentially it contributes to cancer growth. In conclusion, exploring the function of AXIN1 mutations in the Wnt/ $\beta$ -catenin signaling pathway is necessary in order to understand their role in the development of cancer.

Aberrant WNT receptor abundance has emerged as another contributing factor in carcinogenesis. Under normal circumstances, Ring Finger 43 (RNF43) and Zinc and Ring Finger 3 (ZNF3) E3-ubiquitin ligases, play a role in the ubiquitination and lysosomal degradation of FZD receptors, thereby affecting the WNT pathway negatively<sup>48,49</sup>. RNF43 mutations are frequently observed in cancers of the gastrointestinal tract and pancreas, but are also observed in a subtype of liver cancer, that is intrahepatic cholangiocarcinoma (9.3%)<sup>22,50,51</sup>. The functional consequence of these mutations is strongly enhanced levels of Wnt-receptors at the membrane that make these tumors hypersensitive to Wnt ligand activation<sup>49</sup>. It also means that these tumors are largely dependent on Wnt-exposure to aberrantly increase  $\beta$ -catenin signaling. This latter feature has resulted in a significant therapeutic interest, as these tumors can potentially be treated by approaches that reduce the extracellular exposure to Wnt ligands<sup>52</sup>.

The function of RNF43 to restrict Wnt receptor levels at the cell membrane is well-established. However, recent studies have suggested that RNF43 might have additional functions in the nucleus. Loregger et al. suggested that RNF43 tethers TCF7L2 (also known as TCF4) to the inside of the nuclear membrane, thereby limiting  $\beta$ -catenin signaling directly inside the nucleus<sup>53</sup>. Other demonstrated nuclear functions are a role in the DNA damage

response by potentially ubiquitinating  $\gamma$ H2AX<sup>54</sup>, a well-known marker of DNA damage, and suppressing TP53-dependent induction of P21 and BAX<sup>55</sup>. These supposed nuclear functions are supported by commonly used RNF43 antibodies that reveal nuclear staining patterns. However, a thorough testing of antibody specificity has largely been lacking, raising doubts about these claimed nuclear functions<sup>48,49,56</sup>.

## Role of tRNA biology in hepatocellular cancer development

Successful tumorigenesis requires cells to acquire capabilities to support proliferative signaling, evade growth suppressors and resist cell death, among several other features<sup>57</sup>. Cancer cells have also long been known to have higher rates of global protein synthesis compared to non-cancerous cells<sup>58</sup>. Transfer RNAs (tRNA) perform a central function in protein synthesis, as they provide the building blocks for all proteins during ribosomal translation (see **Figure 3**). Initially, tRNAs were thought to have no additional functions. However, emerging evidence has shown that dysregulation of tRNA expression is associated with a variety of physiological and pathological processes, such as cancer, diabetes mellitus, and neuronal disorders<sup>59-62</sup>.

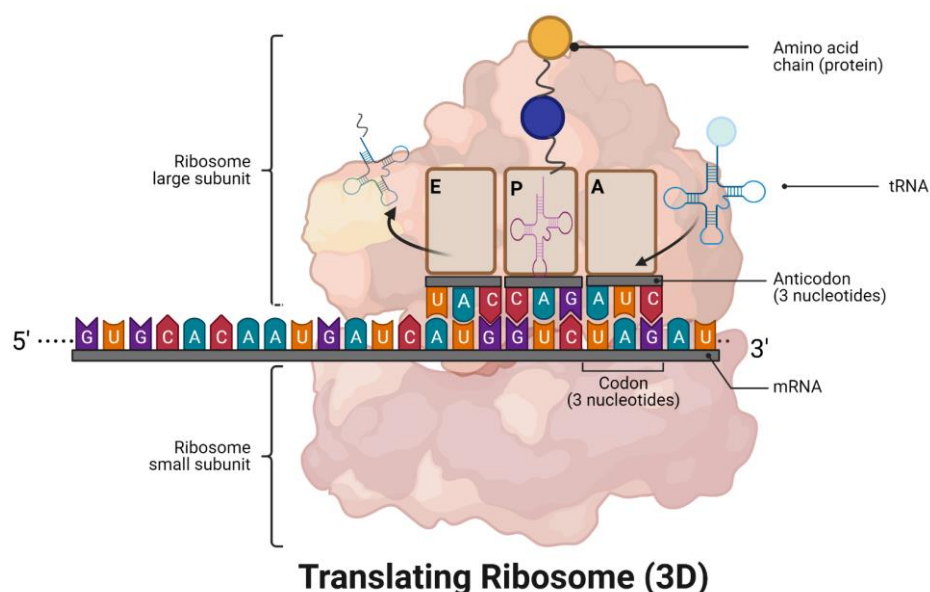


**Figure 3. Illustration of translational decoding.**

The mRNA molecule binds to the small subunit of the ribosome, and the start codon (AUG) is recognized by the initiator tRNA, which carries the amino acid methionine. The large ribosomal subunit then binds to the complex, forming the initiation complex. The A, P, and E sites are locations within the ribosome where different tRNA molecules bind during protein synthesis. The A site is where the next aminoacyl-tRNA molecule binds, the P site is where the tRNA molecule carrying the growing

polypeptide chain is bound, and the E site is where the tRNA molecule that has delivered its amino acid is released. tRNAs can recognize all the 64 triplet codons after properly base pairing by its anticodon. tRNA, transfer RNA; mRNA, messenger RNA.

The regulation of protein translation is strongly influenced by tRNA modification systems. This regulation can result in translational reprogramming of the cancer genome within various cellular processes, making it a critical factor in cancer development and progression. tRNA expression levels can influence translation based on their ability to occupy the ribosome, resulting in cancer cells having higher rates of protein synthesis. Thus, tRNA's fundamental roles in cancers are increasingly being recognized. For example, Goodzari et al. identified that upregulation of tRNA<sup>Arg</sup> (CCG) and tRNA<sup>Glu</sup> (UUC) promoted breast cancer metastasis to the lungs in mice<sup>63</sup>. Ultimately, tRNA systems may represent a potential therapeutic strategy for cancer because of its key role in codon-biased translation.

The human tRNAome is encoded by more than 600 tRNA gene loci. Following transcription, tRNAs are subjected to post-transcriptional modification, and a common CCA ribonucleotide sequence is added to the 3' end to become the mature form, which is used as the substrate for protein synthesis. They are typically 70-90 base pairs in length and charged with their cognate amino acid, which is catalysed by aminoacyl-tRNA synthetases (ARSs). The availability of amino acids and the levels of corresponding mature tRNAs are intimately related. The availability of specific aminoacyl-tRNA species that are compatible with the codon usage and amino acid composition of a particular gene is crucial for the efficient production of the protein<sup>64</sup>.

Therapies that modify the tRNA system, such as amino acid deprivation<sup>65,66</sup>, and targeting the catalytic sites of aminoacyl-tRNA synthetases (ARSs)<sup>67</sup>, have been investigated for their potential in cancer treatment<sup>67</sup>. However, the role of tRNA in hepatocellular carcinoma (HCC) remains unclear and requires further investigation<sup>68-70</sup>. Zhang et al. demonstrated that hepatitis B virus-infected HepG2 cells promote angiogenic behavior of endothelial cells, which associated with a 2-fold increase of tryptophanyl-tRNA synthetase (WARS)<sup>68</sup>. Recently, the exploration of tRNA-derived RNA fragments (tRFs) is emerging as a promising research field. Originally these tRNA fragments were considered to be innocent bystanders of cellular stress situations, but it is becoming increasingly clear that they have a potential role in immune modulation, aging, and cancer<sup>71</sup>. Zhou et al. used quantitative real-



time PCR (qRT-PCR) to observe higher expression levels of Glycine tRNA-derived fragments (*Gly-tRFs*) in HCC cell lines and tissues compared to non-HCC controls. They further showed that Gly-tRFs inhibited the Nedd4 family interacting protein 2 (NDFIP2), an activator of Nedd4 family E3 ubiquitin ligases, by binding to its 3'UTR, which could potentially contribute to the activation of the PI3K-Akt signaling pathway. This activation ultimately led to increased cell migration and epithelial-mesenchymal transition in the studied HCC cell lines<sup>69</sup>. Furthermore, the protein complex METTL1/WDR4 has been suggested to link tRNA modification and cancer progression<sup>72-74</sup>. In case of HCC, it was shown that under sublethal heat exposure METTL1/WDR4 activity and tRNA modification were increased, resulting in enhanced translation of SLUG/SNAIL in a codon frequency-dependent manner<sup>75</sup>. These limited number of examples suggest that tRNA biology may be relevant for HCC. Hence, a better understanding of the role of tRNA biology in HCC development is important for the identification of potential therapeutic targets.

## Aim of the thesis

The first objective is to investigate the altered function of the commonly mutated gene *AXIN1* in HCC. The research will examine the effect of *AXIN1* mutations in different functional domains, their impact on protein interactions, and how they enhance the  $\beta$ -catenin signaling pathway. The potential function of the *AXIN1* domain and the pathway through which HCC with *AXIN1* mutation affects cell growth will also be explored. Five HCC cell lines with *AXIN1* mutations will be repaired using CRISPR-Cas9 to achieve this goal. The second aim is to thoroughly test four commonly used RNF43 antibodies for their ability to correctly identify endogenous RNF43 protein. The third aim is to investigate the role of protein translation in HCC development. The study will analyze 57 pairs of HCC tissues to determine any abnormal expression levels of tRNA and their potential impact on HCC development.

## **This thesis is organized as follows:**

In **Chapter 1**, I presented a brief overview of the genetics of the Wnt/ $\beta$ -catenin pathway and its connection to hepatocellular carcinoma (HCC), and also explained the role of the tRNA translation process in cancer development.

In **Chapter 2**, we explore the functional consequences of missense mutations of AXIN1. critical domains for  $\beta$ -catenin regulation are identified, and the analysis of 80 tumor-associated variants reveals that only a subset of missense mutations affect  $\beta$ -catenin signaling. Truncating mutations consistently impact  $\beta$ -catenin regulation, but we observe an inverse correlation between AXIN1 truncation length and retained  $\beta$ -catenin functionality. These findings can aid in identifying the functional consequences of AXIN1 mutations and help classify tumor-associated variants.

In **Chapter 3**, we use the CRISPR/Cas9 technique to repair truncating mutations in the *AXIN1* gene in five HCC cell lines. Cell growth is consistently reduced in all AXIN1-repaired clones and accompanied by reduced  $\beta$ -catenin signaling. However, attempts to enhance  $\beta$ -catenin signaling to restore cell growth have failed to bring it back to the same level as the parental AXIN1-mutant cells. This indicates that other cellular processes are also affected by the AXIN1 mutation. Despite exploring various other signaling routes and performing RNA sequencing of all clones, we have not yet identified a common underlying mechanism related to AXIN1 mutation.

In **Chapter 4**, we thoroughly analyze the quality of four commonly used RNF43 antibodies. To this aim, we generate cell line tools that entirely lack the epitopes recognized by these antibodies. Using Western blotting, immunofluorescence and immunohistochemistry, we show that only non-specific staining patterns are observed, meaning that these antibodies cannot be used to draw conclusions about endogenous RNF43's expression levels and location.

In **Chapter 5**, we present a simpler method for detecting the mature tRNAome, which addresses the challenges encountered in tRNA research to date. We demonstrate how to use qPCR to quickly and easily analyze the tRNAome.

**In Chapter 6**, we examine the dysregulation of the tRNAome in 57 pairs of HCC samples and their controls, and show that tRNA-Lys-CUU and its corresponding essential amino acid, lysine, are associated with HCC cell growth.

1

**In Chapters 7 and 8**, I summarize and discuss the mechanisms contributing to the development of HCC, highlighting the novel insights from this thesis.

## References

- 1 Forner, A., Reig, M. & Bruix, J. Hepatocellular carcinoma. *Lancet* **391**, 1301-1314 (2018).
- 2 Sung, H. *et al.* Global Cancer Statistics 2020: GLOBOCAN Estimates of Incidence and Mortality Worldwide for 36 Cancers in 185 Countries. *CA Cancer J Clin* **71**, 209-249 (2021).
- 3 Marrero, J. A. *et al.* Diagnosis, Staging, and Management of Hepatocellular Carcinoma: 2018 Practice Guidance by the American Association for the Study of Liver Diseases. *Hepatology* **68**, 723-750 (2018).
- 4 Boleslawski, E. *et al.* Hepatic venous pressure gradient in the assessment of portal hypertension before liver resection in patients with cirrhosis. *Br J Surg* **99**, 855-863 (2012).
- 5 Teh, S. H. *et al.* Hepatic resection of hepatocellular carcinoma in patients with cirrhosis: Model of End-Stage Liver Disease (MELD) score predicts perioperative mortality. *J Gastrointest Surg* **9**, 1207-1215; discussion 1215 (2005).
- 6 Yang, J. D. *et al.* Hepatocellular Carcinoma Is the Most Common Indication for Liver Transplantation and Placement on the Waitlist in the United States. *Clin Gastroenterol Hepatol* **15**, 767-775 e763 (2017).
- 7 Shiina, S. *et al.* Percutaneous Ablation for Hepatocellular Carcinoma: Comparison of Various Ablation Techniques and Surgery. *Can J Gastroenterol Hepatol* **2018**, 4756147 (2018).
- 8 Lencioni, R., de Baere, T., Soulen, M. C., Rilling, W. S. & Geschwind, J. F. Lipiodol transarterial chemoembolization for hepatocellular carcinoma: A systematic review of efficacy and safety data. *Hepatology* **64**, 106-116 (2016).
- 9 Llovet, J. M. *et al.* Sorafenib in advanced hepatocellular carcinoma. *N Engl J Med* **359**, 378-390 (2008).
- 10 Cheng, A. L. *et al.* Efficacy and safety of sorafenib in patients in the Asia-Pacific region with advanced hepatocellular carcinoma: a phase III randomised, double-blind, placebo-controlled trial. *Lancet Oncol* **10**, 25-34 (2009).
- 11 Rebouissou, S. & Nault, J. C. Advances in molecular classification and precision oncology in hepatocellular carcinoma. *J Hepatol* **72**, 215-229 (2020).
- 12 Caruso, S. *et al.* Analysis of Liver Cancer Cell Lines Identifies Agents With Likely Efficacy Against Hepatocellular Carcinoma and Markers of Response. *Gastroenterology* **157**, 760-776 (2019).
- 13 Lee, J.-S. *et al.* Classification and prediction of survival in hepatocellular carcinoma by gene expression profiling. *Hepatology* **40**, 667-676, doi:<https://doi.org/10.1002/hep.20375> (2004).
- 14 Boyault, S. *et al.* Transcriptome classification of HCC is related to gene alterations and to new therapeutic targets. *Hepatology* **45**, 42-52 (2007).
- 15 Chiang, D. Y. *et al.* Focal Gains of VEGFA and Molecular Classification of Hepatocellular Carcinoma. *Cancer Research* **68**, 6779-6788, doi:10.1158/0008-5472.Can-08-0742 (2008).
- 16 Hoshida, Y. *et al.* Integrative transcriptome analysis reveals common molecular subclasses of human hepatocellular carcinoma. *Cancer Res* **69**, 7385-7392 (2009).
- 17 Ally, A. *et al.* Comprehensive and Integrative Genomic Characterization of Hepatocellular Carcinoma. *Cell* **169**, 1327-1341.e1323, doi:<https://doi.org/10.1016/j.cell.2017.05.046> (2017).
- 18 Klaus, A. & Birchmeier, W. Wnt signalling and its impact on development and cancer. *Nat Rev Cancer* **8**, 387-398 (2008).

- 19 Qu, B. *et al.* Wnt/ $\beta$ -catenin signaling pathway may regulate the expression of angiogenic growth factors in hepatocellular carcinoma. *Oncol Lett* **7**, 1175-1178 (2014).
- 20 Anastas, J. N. & Moon, R. T. WNT signalling pathways as therapeutic targets in cancer. *Nat Rev Cancer* **13**, 11-26 (2013).
- 21 Cruciat, C. M. Casein kinase 1 and Wnt/ $\beta$ -catenin signaling. *Curr Opin Cell Biol* **31**, 46-55 (2014).
- 22 Bugter, J. M., Fenderico, N. & Maurice, M. M. Mutations and mechanisms of WNT pathway tumour suppressors in cancer. *Nat Rev Cancer* **21**, 5-21 (2021).
- 23 Totoki, Y. *et al.* Trans-ancestry mutational landscape of hepatocellular carcinoma genomes. *Nat Genet* **46**, 1267-1273 (2014).
- 24 Cleary, S. P. *et al.* Identification of driver genes in hepatocellular carcinoma by exome sequencing. *Hepatology* **58**, 1693-1702 (2013).
- 25 Gao, C. *et al.* Exon 3 mutations of CTNNB1 drive tumorigenesis: a review. *Oncotarget* **9**, 5492-5508 (2018).
- 26 Liu, P. *et al.* Oncogenic Mutations in Armadillo Repeats 5 and 6 of  $\beta$ -Catenin Reduce Binding to APC, Increasing Signaling and Transcription of Target Genes. *Gastroenterology* **158**, 1029-1043 e1010 (2020).
- 27 Rebouissou, S. *et al.* Genotype-phenotype correlation of CTNNB1 mutations reveals different  $\beta$ -catenin activity associated with liver tumor progression. *Hepatology* **64**, 2047-2061 (2016).
- 28 Abitbol, S. *et al.* AXIN deficiency in human and mouse hepatocytes induces hepatocellular carcinoma in the absence of  $\beta$ -catenin activation. *J Hepatol* **68**, 1203-1213 (2018).
- 29 Bell, D., Ranganathan, S., Tao, J. & Monga, S. P. Novel Advances in Understanding of Molecular Pathogenesis of Hepatoblastoma: A Wnt/ $\beta$ -Catenin Perspective. *Gene Expr* **17**, 141-154 (2017).
- 30 Nault, J. C. *et al.* Molecular Classification of Hepatocellular Adenoma Associates With Risk Factors, Bleeding, and Malignant Transformation. *Gastroenterology* **152**, 880-894 e886 (2017).
- 31 Belenguer, G. *et al.* RNF43/ZNRF3 loss predisposes to hepatocellular-carcinoma by impairing liver regeneration and altering the liver lipid metabolic ground-state. *Nature Communications* **13**, 334, doi:10.1038/s41467-021-27923-z (2022).
- 32 Yu, J. *et al.* The Functional Landscape of Patient-Derived RNF43 Mutations Predicts Sensitivity to Wnt Inhibition. *Cancer Research* **80**, 5619-5632, doi:10.1158/0008-5472.Can-20-0957 (2020).
- 33 Martínez-Jiménez, F. *et al.* A compendium of mutational cancer driver genes. *Nat Rev Cancer* **20**, 555-572 (2020).
- 34 Mazzoni, S. M. & Fearon, E. R. AXIN1 and AXIN2 variants in gastrointestinal cancers. *Cancer Lett* **355**, 1-8 (2014).
- 35 Anvarian, Z. *et al.* Axin cancer mutants form nanoaggregates to rewire the Wnt signaling network. *Nat Struct Mol Biol* **23**, 324-332 (2016).
- 36 Lucci-Cordisco, E. *et al.* Variants of uncertain significance (VUS) in cancer predisposing genes: What are we learning from multigene panels? *Eur J Med Genet* **65**, 104400 (2022).
- 37 Schipper, L. J. *et al.* Complete genomic characterization in patients with cancer of unknown primary origin in routine diagnostics. *ESMO Open* **7**, 100611 (2022).
- 38 Samsom, K. G. *et al.* Feasibility of whole-genome sequencing-based tumor diagnostics in routine pathology practice. *J Pathol* **258**, 179-188 (2022).

- 39 Roepman, P. *et al.* Clinical Validation of Whole Genome Sequencing for Cancer Diagnostics. *J Mol Diagn* **23**, 816-833 (2021).
- 40 Zucman-Rossi, J. *et al.* Differential effects of inactivated Axin1 and activated beta-catenin mutations in human hepatocellular carcinomas. *Oncogene* **26**, 774-780 (2007).
- 41 Feng, G. J. *et al.* Conditional disruption of Axin1 leads to development of liver tumors in mice. *Gastroenterology* **143**, 1650-1659 (2012).
- 42 Qiao, Y. *et al.* Axis inhibition protein 1 (Axin1) Deletion-Induced Hepatocarcinogenesis Requires Intact  $\beta$ -Catenin but Not Notch Cascade in Mice. *Hepatology* **70**, 2003-2017 (2019).
- 43 Gilgenkrantz, H. & Perret, C. Letter to the Editor: Comment on Qiao et al. *Hepatology* **70**, 763-764 (2019).
- 44 Chen, X., Monga, S. P. & Calvisi, D. F. Reply. *Hepatology* **70**, 764-765 (2019).
- 45 Satoh, S. *et al.* AXIN1 mutations in hepatocellular carcinomas, and growth suppression in cancer cells by virus-mediated transfer of AXIN1. *Nat Genet* **24**, 245-250 (2000).
- 46 Wang, W. *et al.* Blocking Wnt Secretion Reduces Growth of Hepatocellular Carcinoma Cell Lines Mostly Independent of  $\beta$ -Catenin Signaling. *Neoplasia* **18**, 711-723 (2016).
- 47 Wang, W. *et al.* Evaluation of AXIN1 and AXIN2 as targets of tankyrase inhibition in hepatocellular carcinoma cell lines. *Sci Rep* **11**, 7470 (2021).
- 48 Koo BK, S. M., Jordens I, Low TY, Stange DE, van de Wetering M, van Es JH, Mohammed S, Heck AJ, Maurice MM, Clevers H. Tumour suppressor RNF43 is a stem-cell E3 ligase that induces endocytosis of Wnt receptors. *Nature*. *Nature*. **488**, 6665-6669 (2012).
- 49 Hao, H. X. *et al.* ZNRF3 promotes Wnt receptor turnover in an R-spondin-sensitive manner. *Nature* **485**, 195-200 (2012).
- 50 Schulze, K. *et al.* Exome sequencing of hepatocellular carcinomas identifies new mutational signatures and potential therapeutic targets. *Nat Genet* **47**, 505-511 (2015).
- 51 Ong, C. K. *et al.* Exome sequencing of liver fluke-associated cholangiocarcinoma. *Nat Genet* **44**, 690-693 (2012).
- 52 Yu, F. *et al.* Wnt/ $\beta$ -catenin signaling in cancers and targeted therapies. *Signal Transduct Target Ther* **6**, 307 (2021).
- 53 Loregger, A. *et al.* The E3 ligase RNF43 inhibits Wnt signaling downstream of mutated  $\beta$ -catenin by sequestering TCF4 to the nuclear membrane. *Sci Signal* **8**, ra90 (2015).
- 54 Neumeyer, V. *et al.* Loss of RNF43 Function Contributes to Gastric Carcinogenesis by Impairing DNA Damage Response. *Cell Mol Gastroenterol Hepatol* **11**, 1071-1094 (2021).
- 55 Tsukiyama, T. *et al.* A phospho-switch controls RNF43-mediated degradation of Wnt receptors to suppress tumorigenesis. *Nat Commun* **11**, 4586 (2020).
- 56 Wu, J. *et al.* Whole-exome sequencing of neoplastic cysts of the pancreas reveals recurrent mutations in components of ubiquitin-dependent pathways. *Proc Natl Acad Sci U S A* **108**, 21188-21193 (2011).
- 57 Hanahan, D. Hallmarks of Cancer: New Dimensions. *Cancer Discov* **12**, 31-46 (2022).
- 58 Silvera, D., Formenti, S. C. & Schneider, R. J. Translational control in cancer. *Nat Rev Cancer* **10**, 254-266 (2010).
- 59 Santos, M., Fidalgo, A., Varanda, A. S., Oliveira, C. & Santos, M. A. S. tRNA Deregulation and Its Consequences in Cancer. *Trends Mol Med* **25**, 853-865 (2019).

- 60 Huang, S. Q. *et al.* The dysregulation of tRNAs and tRNA derivatives in cancer. *J Exp Clin Cancer Res* **37**, 101 (2018).
- 61 Zhou, Z., Sun, B., Huang, S., Jia, W. & Yu, D. The tRNA-associated dysregulation in diabetes mellitus. *Metabolism* **94**, 9-17 (2019).
- 62 Tuorto, F. & Parlato, R. rRNA and tRNA Bridges to Neuronal Homeostasis in Health and Disease. *J Mol Biol* **431**, 1763-1779 (2019).
- 63 Goodarzi, H. *et al.* Modulated Expression of Specific tRNAs Drives Gene Expression and Cancer Progression. *Cell* **165**, 1416-1427 (2016).
- 64 Pavlova, N. N. *et al.* Translation in amino-acid-poor environments is limited by tRNA(Gln) charging. *Elife* **9** (2020).
- 65 Feun, L. *et al.* Arginine deprivation as a targeted therapy for cancer. *Curr Pharm Des* **14**, 1049-1057 (2008).
- 66 Tang, X. *et al.* Cystine Deprivation Triggers Programmed Necrosis in VHL-Deficient Renal Cell Carcinomas. *Cancer Res* **76**, 1892-1903 (2016).
- 67 Kwon, N. H., Fox, P. L. & Kim, S. Aminoacyl-tRNA synthetases as therapeutic targets. *Nat Rev Drug Discov* **18**, 629-650 (2019).
- 68 Zhang, J., Niu, D., Sui, J., Ching, C. B. & Chen, W. N. Protein profile in hepatitis B virus replicating rat primary hepatocytes and HepG2 cells by iTRAQ-coupled 2-D LC-MS/MS analysis: Insights on liver angiogenesis. *Proteomics* **9**, 2836-2845 (2009).
- 69 Zhou, Y. *et al.* Gly-tRF enhances LCSC-like properties and promotes HCC cells migration by targeting NDFIP2. *Cancer Cell Int* **21**, 502 (2021).
- 70 Pandolfini, L. *et al.* METTL1 Promotes let-7 MicroRNA Processing via m7G Methylation. *Mol Cell* **74**, 1278-1290 e1279 (2019).
- 71 Pandey, K. K. *et al.* Regulatory roles of tRNA-derived RNA fragments in human pathophysiology. *Mol Ther Nucleic Acids* **26**, 161-173 (2021).
- 72 Orellana, E. A. *et al.* METTL1-mediated m(7)G modification of Arg-TCT tRNA drives oncogenic transformation. *Mol Cell* **81**, 3323-3338 e3314 (2021).
- 73 Ma, J. *et al.* METTL1/WDR4-mediated m(7)G tRNA modifications and m(7)G codon usage promote mRNA translation and lung cancer progression. *Mol Ther* **29**, 3422-3435 (2021).
- 74 Lin, S. *et al.* Mettl1/Wdr4-Mediated m(7)G tRNA Methylome Is Required for Normal mRNA Translation and Embryonic Stem Cell Self-Renewal and Differentiation. *Mol Cell* **71**, 244-255 e245 (2018).
- 75 Zhu, S. *et al.* Targeting N(7)-methylguanosine tRNA modification blocks hepatocellular carcinoma metastasis after insufficient radiofrequency ablation. *Mol Ther* (2022).





# Chapter 4

## Issues with RNF43 antibodies to reliably detect intracellular location

Shanshan Li<sup>1</sup>, Ruyi Zhang<sup>1</sup>, Marla Lavrijsen<sup>1</sup>, Thierry P.P. van den Bosch<sup>2</sup>, Maikel P. Peppelenbosch<sup>1</sup>, Ron Smits<sup>1\*</sup>

1. Department of Gastroenterology and Hepatology, Erasmus MC Cancer Institute, University Medical Center Rotterdam, The Netherlands.
2. Department of Pathology, Erasmus MC Cancer Institute, University Medical Center Rotterdam, The Netherlands.

*PLOS ONE. 2023,18(4): e0283894.*



## Abstract

RNF43 is an important negative regulator of  $\beta$ -catenin signaling by removing Wnt-receptors from the membrane. It is often mutated in cancers, leading to aberrant Wnt-dependent nuclear translocation of  $\beta$ -catenin. RNF43 has also been suggested to regulate  $\beta$ -catenin signaling directly within the nucleus, among other proposed nuclear functions. Given the importance of RNF43 in regulating Wnt/ $\beta$ -catenin signaling and its potential therapeutic relevance, a proper understanding of RNF43 biology is required. However, the presumed nuclear location is mainly based on available antibodies. These same antibodies have also been used extensively for immunoblotting or immunohistochemical purposes. However, a proper evaluation of their quality to reliably detect endogenous RNF43 has not been performed. Here, using genome editing we have generated a cell line that entirely misses *RNF43* exons 8 and 9, encoding the epitopes of commonly used RNF43 antibodies. Using this clone in addition to various other cell line tools, we show that four RNF43 antibodies only yield non-specific signals when applied in immunoblotting, immunofluorescence and immunohistochemical experiments. In other words, they cannot reliably detect endogenous RNF43. Our results suggest that the nuclear staining patterns are an antibody artifact and that RNF43 is unlikely to localize within the nucleus. More generally, reports using RNF43 antibodies should be interpreted with caution, at least for the RNF43 protein aspects described in these papers.

## Introduction

Aberrant activation of Wnt/ $\beta$ -catenin signaling is observed in a large number of cancers originating from various tissue types(1). In normal cells the RNF43 protein, and its homologue ZNRF3, play an important role as negative regulators of this pathway. They encode for transmembrane E3-ubiquitin ligases that remove Wnt receptors from the membrane, thereby limiting the nuclear signaling of  $\beta$ -catenin(2, 3). RNF43 mutations affecting protein function have been observed in a variety of cancers among which those of the colon, stomach, pancreas, endometrium and ovarium(2). The functional consequence of these mutations is considered to be a reduced capability to remove Wnt-receptors, making such cancers hypersensitive to Wnt-ligand activation. For that reason, these RNF43-mutant cancers have gained substantial therapeutic interest, as they may identify tumors that respond to extracellular Wnt-inhibitors that have been developed, such as FZD antibodies and Wnt-secretion Porcupine inhibitors(4).

Besides this well-established role of RNF43, it has also been linked to various other cellular functions. Loregger et al. suggested that RNF43 tethers TCF7L2 (also known as TCF4) to the inside of the nuclear membrane, thereby limiting  $\beta$ -catenin signaling directly inside the nucleus(5). Other demonstrated nuclear functions are a role in the DNA damage response by potentially ubiquitinating  $\gamma$ H2AX(6), a well-known marker of DNA damage, and suppressing TP53-dependent induction of P21 and BAX(7). A direct binding of RNF43 to these nuclear proteins can only be shown by strong RNF43 overexpression. However, in support of these findings, nuclear staining patterns are observed using the commercially available HPA008079 and “home-made” 8D6 RNF43 antibodies(5, 6). These findings may have important therapeutic implications as it may indicate that RNF43 mutations contribute to tumor growth through other mechanisms than solely affecting the level of Wnt receptors.

These and other antibodies have also been instrumental in immunohistochemical approaches to evaluate RNF43 protein expression in various tumor types. For example, using such antibodies RNF43 protein was observed to be over-expressed in liver cancers(8), lost in a subset of gastric and colorectal tumors(9, 10), and to correlate with gastric and clear cell renal cancer patient survival(11-13). They have also been used to evaluate its expression in pancreatic lesions in relation to *RNF43* mutation status(14-16). In basically all these examples

nuclear staining patterns were observed, thus supporting a nuclear location of RNF43. These antibodies have also been used extensively in various reports to detect endogenous RNF43 through immunoblotting or immunofluorescence.

Given the importance of RNF43 in regulating Wnt/ $\beta$ -catenin signaling and its potential therapeutic relevance, a proper understanding of RNF43 biology is required. Antibodies are important instrumental tools for this purpose by detecting changes in RNF43 protein levels or intracellular location in various cell lines or tissue samples. However, a proper evaluation of their quality to reliably detect endogenous RNF43 has not been performed. Here, using genome editing we have generated a cell line that entirely misses *RNF43* exons 8 and 9, encoding the epitopes of three commonly used RNF43 antibodies. Using this clone in addition to various other cell line tools, we show that these and one additional RNF43 antibody recognizing a N-terminal epitope only yield non-specific signals when applied in immunoblotting, immunofluorescence and immunohistochemical experiments. Our results suggest that the nuclear staining patterns are an antibody artifact. In addition, reports using RNF43 antibodies should be interpreted with caution, at least for the RNF43 protein aspects described in these papers.

4

## Results

### Cell line tools to evaluate quality of RNF43 antibodies

Four commonly used RNF43 antibodies (rabbit polyclonal ab217787, rabbit polyclonal ab84125, rabbit polyclonal HPA008079 and rat monoclonal 8D6) were evaluated for their reliability to correctly detect RNF43. Their epitope locations are plotted in Fig 1A, showing that ab217787 maps to residues encoded by exons 2 and 3, and the other three antibodies all map to residues encoded by exons 8 and 9. For antibody testing we established a panel of cell lines and clones thereof. As positive controls for full-length RNF43 we used HT-29, and transient RNF43 transfection of HEK293T cells. DLD-1 and KM12 cells are, respectively, heterozygous and homozygous for a p.G659fs\*41 mutation, which is expected to lead to a truncated protein that can be detected by all four antibodies theoretically. As negative controls we used HCT116 cells carrying a homozygous truncation at p.R117fs\*41, and RNF43-KO KM12 cells(17). Lastly, to fully exclude that RNF43 epitopes are generated from currently unknown promoters or

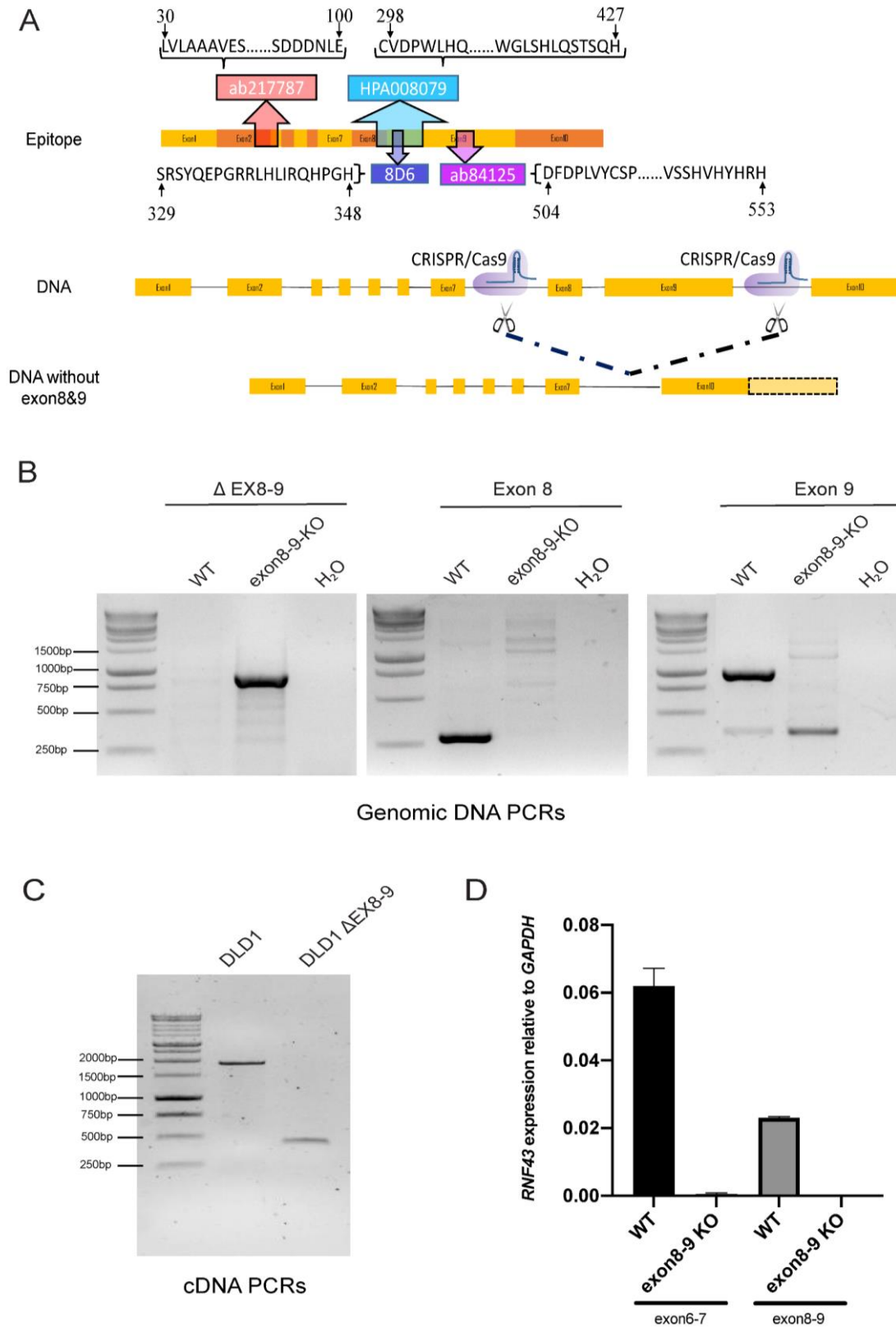


**Fig 1. Epitope location and generation of DLD-1 RNF43 ΔEX8-9 clone.**

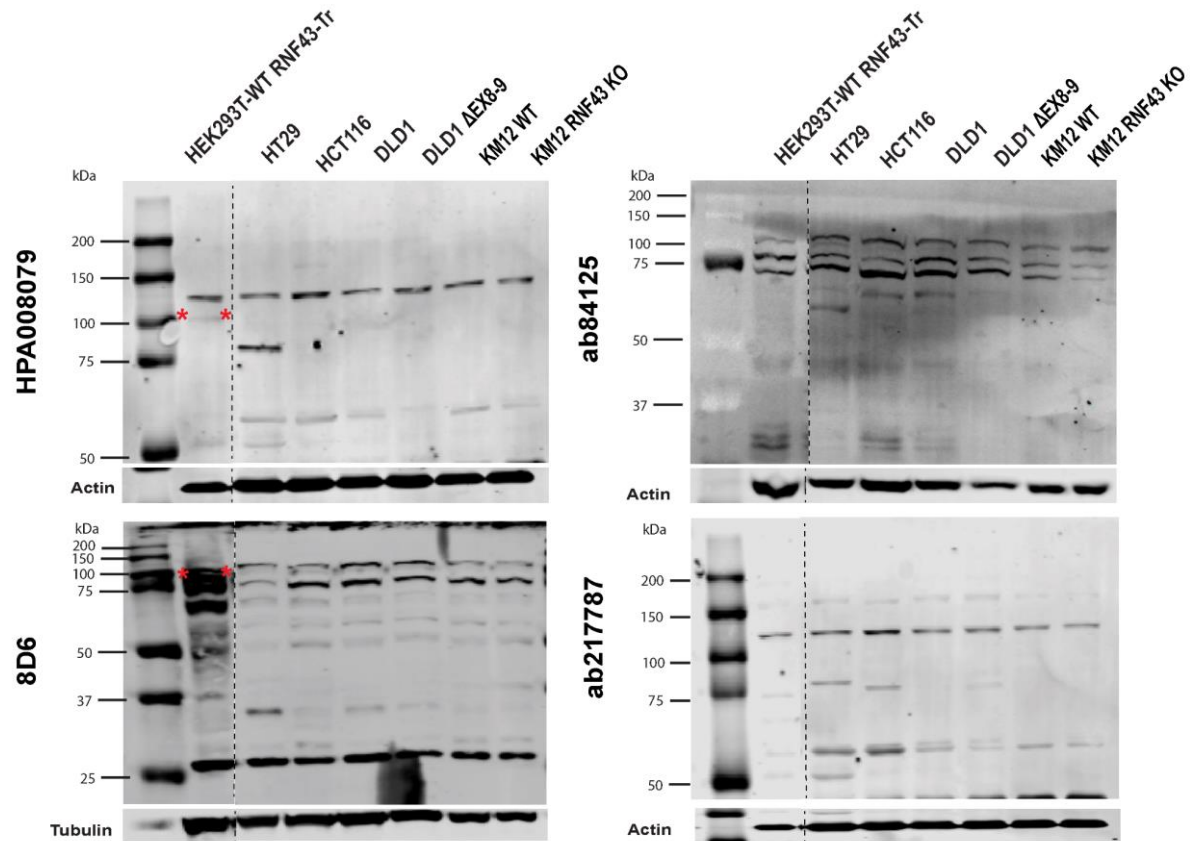
A. Schematic representation of *RNF43* mRNA and epitope location of RNF43 antibodies. The ab217787 antibody was raised against a N-terminal epitope encoded by exons 2 and 3, while the other three

antibodies were raised against epitopes encoded by exons 8 and 9. A DLD-1 cell clone was generated that entirely misses these exons leading to a p. (Glu284\_Pro769delect\*56) deletion on protein level. B. Confirmation of correct deletion of exons 8 and 9 on DNA level. Left panel shows PCR with primers flanking the deletion. The expected approximate 900bp fragment is observed in the  $\Delta$ EX8-9 clone, while the original 4kb fragment is too big to be amplified. Middle and right panels show, respectively, PCRs for exons 8 and 9, leading to the expected 283 and 914bp fragments in the wild-type cell line, whereas only non-specific bands are observed in the  $\Delta$ EX8-9 clone. DNA marker used is the 1kb DNA ladder from Promega (#G5711) C. Confirmation of correct deletion of exons 8 and 9 on mRNA level. Primers flanking exons 8 and 9 reveal the expected 1904 and 445bp fragments, respectively, for the wild-type cells and  $\Delta$ EX8-9 clone. D. A quantitative RT-PCR analysis of *RNF43* exons 8-9 shows undetectable levels in the  $\Delta$ EX8-9 clone. Interestingly, as shown by a qRT-PCR for exons 6-7, total *RNF43* levels are decreased about 200-fold in this clone. In conclusion, we have successfully generated a DLD-1 clone that shows strongly reduced levels of *RNF43* mRNA entirely lacking exons 8 and 9.

alternative usage of internal ATG start sites, we generated a DLD-1 cell clone completely lacking exons 8 and 9 (deletion of amino acids 284-769). PCRs on genomic DNA confirmed the absence of both exons (Fig 1B), while on RNA level the expected shortened cDNA fragment was observed (Fig 1C). Sequencing of the shortened genomic and cDNA PCR products revealed the expected loss of exons 8 and 9. A quantitative RT-PCR analysis validated the absence of exons 8 and 9 (Fig 1D). Interestingly, a qPCR for exons 6 and 7 retained in the transcript, showed that overall *RNF43* RNA levels are decreased about 200-fold. In conclusion, we have successfully generated a DLD-1 clone that shows strongly reduced overall levels of *RNF43* mRNA entirely lacking exons 8 and 9.

### **Non-specific binding of RNF43 antibodies revealed by immunoblotting**

Protein lysates from the cell lines described above, were used for immunoblotting (Fig 2 and Supplementary Figure 1). In all cases bands were identified that could be mistaken for RNF43. However, these same bands were also observed in the three negative control lines in our panel (HCT116, DLD-1  $\Delta$ EX8-9, and RNF43-KO KM12), clearly showing that the bands identified are not RNF43. Overexpressed RNF43 can be detected by the HPA008079 and 8D6 antibodies, while this was not the case for ab84125 and ab217787. Taken together, we conclude that these four antibodies are not suitable to identify RNF43 expressed at endogenous levels using immunoblotting.



Expected protein bands that can be detected by Western blot.

Cell line name	Predicted band size	
	HPA008079 & 8D6 & ab84125	ab217787
HEK293T-WT RNF43 transfected	86 kDa	86 kDa
HT-29	86 kDa	86 kDa
HCT116	No band	17 kDa
DLD-1	77 + 86 kDa	77 + 86 kDa
DLD-1 ΔEX8-9	No band	37 kDa
KM12	77 + 86 kDa	77 + 86 kDa
KM12 RNF43 KO	No band	No band

**Fig 2. Immunoblot analysis of RNF43 antibodies.**

The HPA008079, ab84125, 8D6 and ab217787 antibodies cannot specifically recognize endogenous RNF43 by immunoblotting. No signal is expected in the HCT116, DLD-1 ΔEX8-9, and KM12 RNF43 KO lanes for the exon 8-9 located antibodies, while ab217787 may detect 17 and 37 kDa truncated bands in, respectively, HCT116 and DLD-1 ΔEX8-9. All antibodies may detect a specific truncated band in the DLD-1 and KM12 WT lanes. However, only non-specific bands are observed. The 8D6 and HPA008079 antibodies are able to detect overexpressed RNF43 (lanes 1). The dashed lines demarcate a non-essential protein marker and/or sample lane that were removed from the image. The table at the bottom shows the expected protein bands that can be detected for each sample. Protein sizes are based on transcript ID ENST00000407977.7 and protein ID CCDS11607.1. Overexpressed RNF43 is marked with a red asterisk. Original images can be found in Supplementary Figure 1.



## Evaluation of RNF43 antibodies for immunofluorescence approaches

RNF43 immunofluorescence (IF) has been used to demonstrate a nuclear, endoplasmic reticulum (ER) or membranous location of RNF43. We used DLD-1, DLD-1  $\Delta$ EX8-9, and HCT116 cells to validate these observations. The HPA008079 antibody showed a prominent non-specific nuclear staining in all cell lines, including both negative controls (Fig 3 and Supplementary Figure 2). Similar results were obtained for 8D6, which in addition showed a non-specific staining of cellular protrusions. The ab84125 antibody revealed a weaker non-specific punctate staining of a structure adjacent to the nucleus, reminiscent of the Golgi or endoplasmic reticulum. Ab217787 detected a non-specific nuclear structure and diffuse cytoplasmic staining. In theory this antibody may detect the 17 kDa truncated protein predicted to be present in HCT116 cells. However, given that it cannot recognize even overexpressed RNF43 by immunoblotting, the observed signal is highly likely to be non-specific. As for the DLD-1  $\Delta$ EX8-9 clone, also in this case it may detect the predicted 37 kDa truncated band. This clone shows however a more than 200-fold reduced expression of RNF43, meaning that the expected signal intensity should be strongly reduced. As this is not the case, we conclude that for this and all three other antibodies, only non-specific IF signals can be obtained.

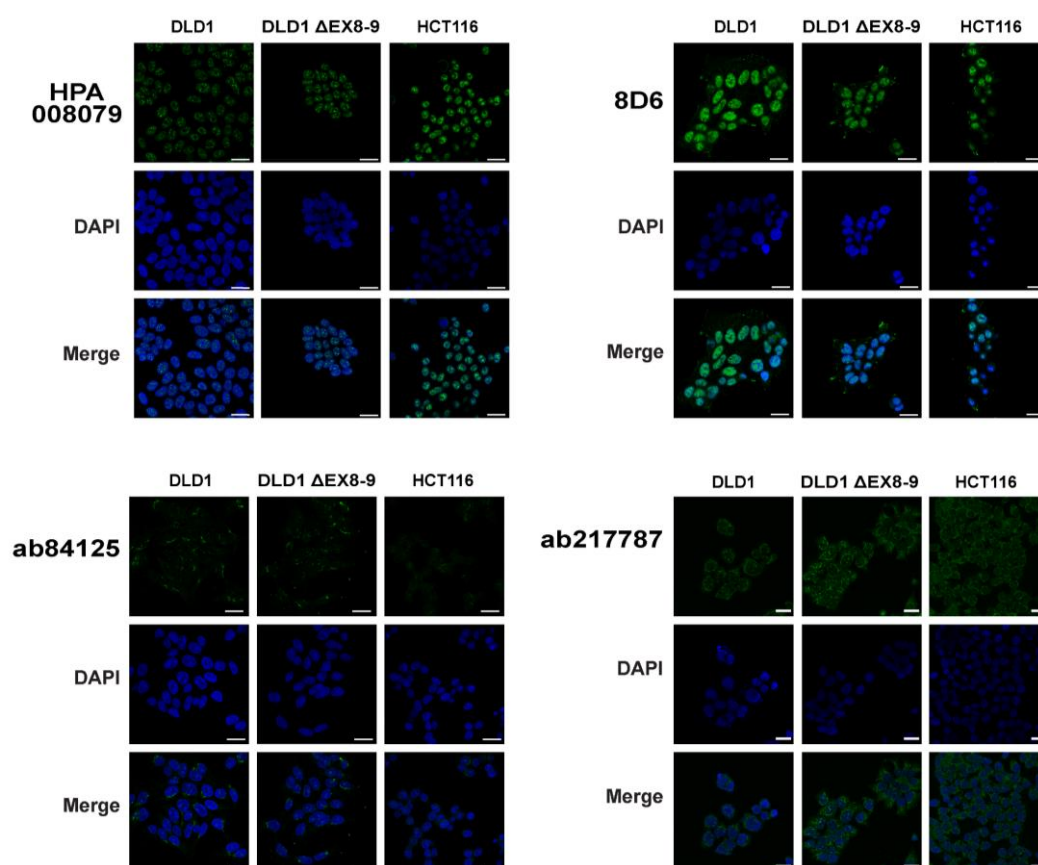


**Fig 3. Immunofluorescence analysis of RNF43 antibodies.**

DLD-1, DLD-1  $\Delta$ EX8-9, and HCT116 cells were cultured on glass slides and stained with HPA008079, ab84125, ab217787 and 8D6 antibodies. DLD-1  $\Delta$ EX8-9 and HCT116 cells are not expected to reveal any staining, but in all cases, signals are observed comparable with the wild-type control DLD1. DAPI was used to stain the nuclei. For the 8D6 antibody the DAPI-staining is coincidentally stronger in the DLD-1  $\Delta$ EX8-9 cells, giving the potential false impression that the green 8D6 signal is weaker in these cells compared with their wild-type controls. However, evaluation of multiple independent images shows that non-specific signals are of comparable intensity. Larger images, a higher intensity image for ab84125, and negative control test are shown in Supplementary Figure 2. Scale bar, 25 $\mu$ m.

Next, we tested if overexpressed RNF43 can be detected using these antibodies. To this aim, HCT116 cells were transiently transfected with HA-tagged RNF43. Staining for the HA-tag showed a clear cytoplasmic pattern (Fig 4), in line with an ER-location reported previously for overexpressed RNF43(17, 18). Overexpressed RNF43 was also detected by the HPA008079, ab84125 and 8D6 antibodies, while ab217787 was unable to detect overexpressed RNF43. Taken together, this shows that three antibodies have some potential to identify RNF43 using IF, but at endogenous levels they fail to do so in a specific manner. We also wish to stress that this latter overexpression experiment is not intended to reveal the correct endogenous RNF43 location.

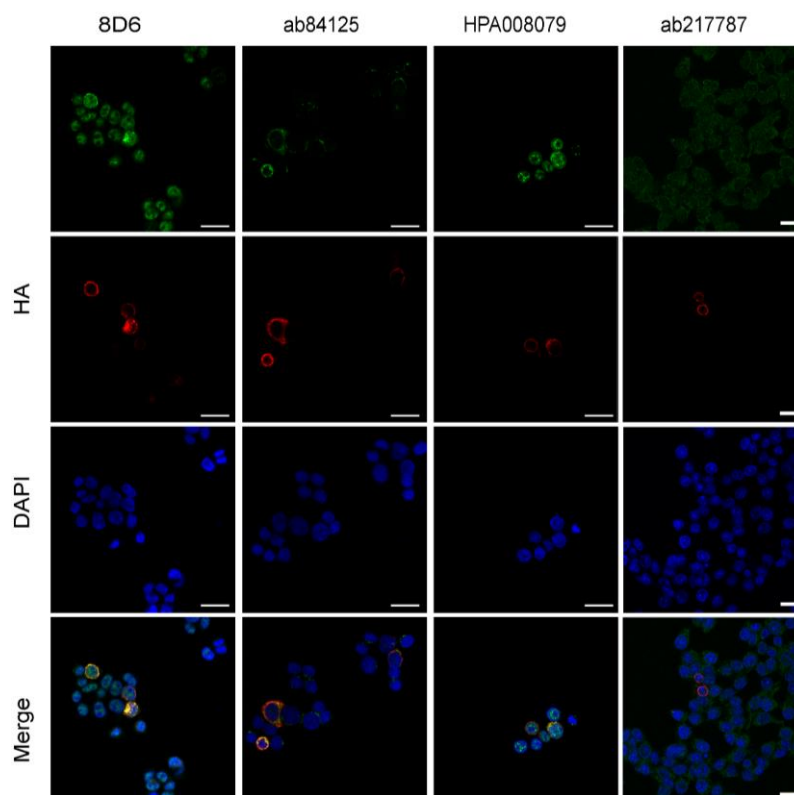


**Fig 4. RNF43 antibodies can detect overexpressed RNF43 using immunofluorescence.**

HCT116 cells were transiently transfected with HA-tagged RNF43 and simultaneously stained with each RNF43 antibody and a HA-tag antibody. DAPI was used to stain the nuclei. Overexpressed RNF43 was present in the cytoplasm and detectable with all antibodies to some extent, except for the ab217787 antibody. Scale bar, 25µm.

### Immunohistochemical staining with RNF43 antibodies

The HPA008079, ab84125 and ab217787 antibodies have been commonly used on formalin-fixed and paraffin embedded (FFPE) tissue sections, among others to show loss or retention of RNF43 protein expression in tumor samples. We generated FFPE tissue blocks from the same cell lines used for IF. As shown in Fig 5, basically identical non-specific staining patterns were observed as seen in the IF-experiments. Again, HPA008079 and 8D6 showed a prominent non-specific nuclear staining and were able to detect overexpressed RNF43, while ab84125 and ab217787 non-specifically recognized similar structures as observed in IF. Thus, also the IHC analysis shows that all four antibodies recognize strongly other proteins not being RNF43.

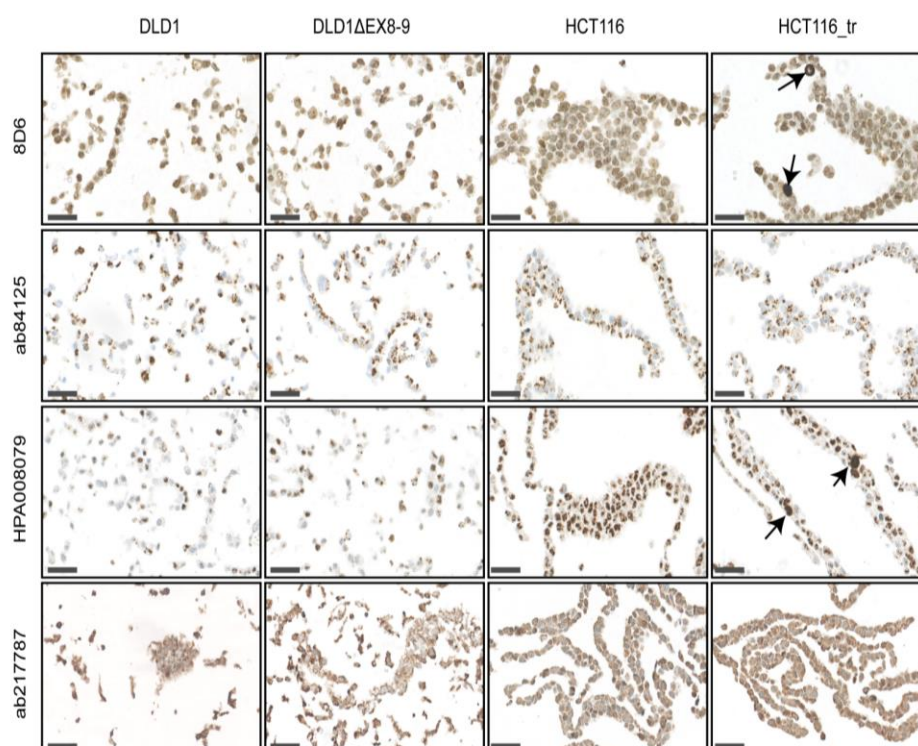


**Fig 5. Immunohistochemical analysis of RNF43 antibodies.**

The indicated cell lines were formalin-fixed and embedded in paraffin. HCT116 cells transiently overexpressing RNF43 were also included. All antibodies give the same non-specific staining

pattern as observed in the IF-experiments, showing that they all strongly recognize a non-specific protein not being RNF43. The 8D6 and HPA008079 antibodies can detect overexpressed RNF43, indicated by arrows, while this is not the case for ab84125 and ab217787. Scale bar, 50um.

### Generation and analysis of RNF43-3xFLAG knockin cell lines

Thus far our experiments show that commonly available RNF43 antibodies cannot faithfully determine the intracellular location of RNF43. This means that our current knowledge depends on overexpression experiments that are more prone to artifacts. Therefore, to obtain reliable information on RNF43's intracellular location, we generated OE19 and Caco-2 cells with knockin of a 3xFLAG, which is one of the most sensitive tags available with highly specific antibodies. OE19 and Caco-2 cells were chosen because they are among the highest *RNF43* expressing cell lines (<https://www.proteinatlas.org/ENSG00000108375-RNF43/cell+line>), which was confirmed using qPCR. Based on DNA and cDNA analysis, we successfully inserted the 3xFLAG tag preceded by a linker at the C-terminus of RNF43. However, immunoblotting using the fluorescent Odyssey system failed to detect endogenous FLAG-tagged RNF43 in both cell lines. This could be accomplished using a highly sensitive ECL Ultra Western HRP Substrate system (Fig 6A), nevertheless indicating that RNF43 protein expression is likely to be extremely low.

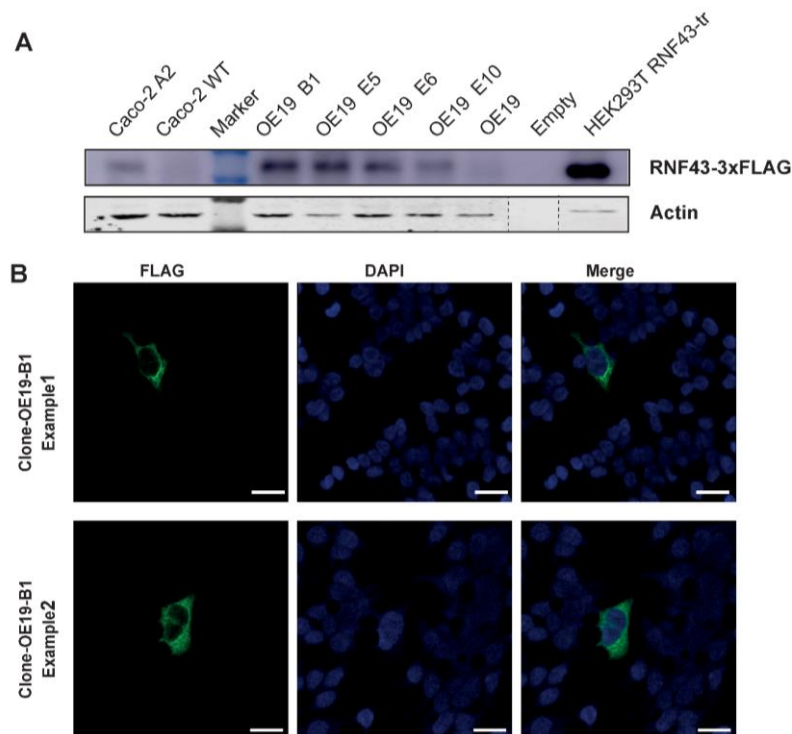


**Fig 6. Immunoblot analysis and IF of 3xFLAG RNF43 knockin clones.**

A. Immunoblot analysis of Caco-2 and OE19 clones with a 3xFLAG knockin at the C-terminus of RNF43. A sensitive ECL Ultra Western HRP Substrate system was required to reveal the bands. A 30x diluted sample of RNF43-FLAG transfected HEK293T cells is added as control. B. Using a Tyramide SuperBoost system a small number of 3xFLAG positive OE19 cells could be identified. No positive cells were observed in the parental OE19 cell line. The staining pattern resembles that of overexpressed RNF43 showing a cytoplasmic and perinuclear pattern, the latter reminiscent of an ER location. However, given the low number of positive cells in only one cell line, we cannot draw a reliable generalized conclusion about RNF43's intracellular location. Scale bar, 25 $\mu$ m.

**Immunofluorescence analysis of endogenously tagged RNF43 cells**

Next, we aimed at determining RNF43-3xFLAG's intracellular location using IF. However, using conventional secondary antibodies we failed to obtain specific signals, despite testing various fixation methods. As a last resort, we used a tyramide signal amplification method. Caco-2 RNF43-3xFLAG cells remained negative using this method, while for OE19 we identified sparse cells showing a diffuse cytoplasmic staining specifically in 3xFLAG knockin clones (Fig 6B). It should however be noted that at most a handful positive cells were identified among all the cells present in a chamber of a Lab-Tek II chamber slide. Taken together, these results suggest that it is extremely difficult to faithfully detect endogenous RNF43 using IF and other methods. When detected, its location appears to be cytoplasmic, while no clear staining is observed in the nucleus.

**Discussion**

Antibodies can be valuable tools for research. However, despite decades of warnings that the quality of antibodies should be carefully validated, it appears that more than half of the antibodies on the market are not specific to their target(19, 20). Merely showing a band of the approximate expected size on a cropped western blot, is no guarantee that the correct target protein is identified.

Unfortunately, the same appears to be true for RNF43, an important negative regulator of Wnt signaling. We have evaluated four antibodies for their ability to reliably detect RNF43 protein. However, our results show that none of these antibodies is able to correctly detect endogenous RNF43 when applied in immunoblotting, IF and IHC experiments. Using these

three methods on cell lines that express various lengths of RNF43 or that entirely miss the exons encoding the RNF43 epitopes, reveals in all cases exclusively non-specific signals for endogenous RNF43. Which non-specific proteins are recognized is currently unknown.

This has important implications, especially for its supposed nuclear location, an observation based largely on these antibodies. We consider a nuclear location unlikely for the following reasons. First, all overexpression studies yield cytoplasmic staining patterns, and show extensive overlap with markers of the ER(5, 7, 17, 18, 21, 22). Some research groups have interpreted this as RNF43 also being present at the inside of the nuclear rim(5, 7, 21). However, the ER is tightly associated with the nuclear membrane in a continuous fashion(23), meaning that an ER-staining pattern can be easily mistaken for a location on the inside of the nuclear membrane. Second, cellular fractionation of overexpressed RNF43 has also been used to support a nuclear location(5, 7, 21), but given the tight association between the ER and the nuclear membrane, it is technically challenging to prevent ER contamination in nuclear fractions(23). In fact, the fractionation experiments reported by Loregger et al. show that the Calnexin-positive ER fraction is completely isolated along with the nuclear fraction(5), thus not allowing a proper conclusion about nuclear vs ER location. Proteomic analyses dedicated to the nuclear envelope of three tissues identified over 5200 unique proteins, however, RNF43 was not observed (Dr. Eric Schirmer, personal communication)(24), further making a nuclear location less likely. Third, overexpression studies and staining of endogenous RNF43 provide strongly conflicting staining patterns. The HPA008079 and 8D6 antibodies yield a more or less homogenous nuclear staining pattern, while overexpressed RNF43 is negative inside the nucleus and shows at most staining of the nuclear border. Finally, epitope tagging endogenous RNF43 mostly fails to show its endogenous location. Tsukiyama et al. used a C-terminal HA-epitope in HEK293 cells, but failed to obtain a specific signal using IF(7). Likewise, we were unable to detect 3xFLAG-tagged RNF43 in Caco-2 cells and can only identify a small number of 3xFLAG-positive OE19 cells. These latter cells show a cytoplasmic staining and no obvious signal in the nucleus, but given the low number of positive cells in only one cell line, we cannot draw a reliable generalized conclusion about RNF43's intracellular location. Nevertheless, the difficulty to obtain signals with sensitive tags is in stark contrast to the readily obtained nuclear staining patterns observed with two commonly used RNF43 antibodies. As we show here that these antibodies are non-specific, we feel that currently no good evidence exists to support a nuclear location of RNF43.

Our results do not exclude that RNF43 indirectly affects nuclear functions. RNF43 was also shown to regulate non-canonical Wnt signaling by removing ROR1/2 from the membrane, and in concerted action with RSPO2/3 to affect BMPR1A receptor levels and BMP signaling(25-27). Thus, besides regulating nuclear Wnt/ $\beta$ -catenin signaling, RNF43 can possibly also affect nuclear functions through these alternative routes, while not having to be located in the nucleus itself.

RNF43 antibodies have also been used to evaluate protein levels in tumor samples. Various conclusions were raised, such as RNF43 being overexpressed in liver cancers(8), to correlate with gastric and clear cell renal cancer patient survival(11-13), or to be lost in a subset of gastric and colorectal cancers(9, 10). Jo et al. showed data in which RNF43 staining appeared to correlate with mutation status, as tumors with N-terminal truncating RNF43 mutations showed a negative staining(10). However, in a more recent report, Omori et al. failed to find a good correlation between *RNF43* mutation status in pancreatic lesions and IHC using HPA008079(14), which can be readily explained by the lack of antibody specificity that we observe. Based on our results, these and other reports in which RNF43 antibodies were used, should be interpreted cautiously, at least for the RNF43 protein aspects described in these papers.

Taken together, our results show that four tested RNF43 antibodies are not reliable tools to evaluate the intracellular location of RNF43 by IF and IHC, and also cannot detect endogenous RNF43 using immunoblotting. It also calls for a re-evaluation of the proposed nuclear functions of RNF43; are they the result of a direct effect of RNF43 protein within the nucleus, or an indirect consequence of RNF43 affecting one or more signaling routes? More RNF43 antibodies are commercially available. However, given the difficulty that we observe to detect endogenous RNF43, we feel that they are unlikely to detect RNF43 correctly. None of them have undergone the rigorous testing that we have performed here using cell lines in which the epitope is entirely lacking. Until such an analysis is done, we feel that they should not be used for research purposes, as this will potentially lead to misleading conclusions. If indeed no good antibodies are available and tagging endogenous RNF43 does not provide clear answers, it also means that we currently do not know the exact intracellular location of this important regulatory protein, an issue that can hopefully be resolved in the future.

## **Materials and methods**

### **Cell lines and culture**

OE19 and KM12 cells were maintained in RPMI-1640 culture medium containing 10% fetal bovine serum (FBS) and 1 mM sodium pyruvate. Caco-2, HEK293T, HCT116, DLD-1 and HT-29 cells were cultured in Dulbecco's Modified Eagle's medium (DMEM) supplemented with 10% FBS. Culture medium was changed every 2-3 days. All the cell lines were cultured in a humidified incubator maintained at 37°C with 5% CO<sub>2</sub>. All cell lines tested negative for mycoplasma based on the real-time PCR method at Eurofins GATC-Biotech (Konstanz, Germany). Identity of all cell lines and clones thereof, was confirmed by the Erasmus Molecular Diagnostics Department, using Powerplex-16 STR genotyping (Promega, Leiden, The Netherlands). RNF43 mutation status depicted in S1 Table was confirmed in all cell lines by Sanger sequencing and was consistent with those reported at COSMIC, the Catalog Of Somatic Mutations In Cancer (<http://cancer.sanger.ac.uk>).

### **The generation of a RNF43 exon8-9 deletion DLD-1 cell line and RNF43-KO KM12 cell line**

RNF43 exon8-9 deletion DLD-1 cells were generated via CRISPR-Cas9 genome editing. Two single guide RNAs (sgRNA) which target the introns between either exon 7 and 8 or exon 9 and 10 were designed using the following CRISPR design tool (<http://crispor.tefor.net/>), and cloned into pSpCas9 (BB)-2A-GFP (pX458), a gift from Feng Zhang (Addgene plasmid # 48138), using standard procedures(28). The sgRNA sequences are listed in S2 Table. Cells were seeded into six-well plates and transfected with 600 ng of both pX458 plasmids, using Lipofectamine 2000 Transfection Reagent (ThermoFisher) following the manufacturer's instructions. After transfection for 48 h, single GFP-positive cells were sorted out and plated into 96-well culture plates by a fluorescence activated cell sorter (FACS) FACS Aria II cell sorter (BD Biosciences, San Jose, CA, USA). Three weeks later, genomic DNA was extracted from expanded single cell clones by QuickExtract DNA Extraction Solution (Epicenter, Madison, WI, USA). To confirm that the correct exon8-9 deletion was obtained, clones were first screened with primers flanking the deletion (Supplementary Table2). Next, complete absence of exons 8 and 9 was confirmed



with exon-specific primers (Supplementary Table3). The generation of RNF43-KO KM12 cells has been described previously(17).

### **Quantitative real-time PCR (qRT-PCR) and cDNA PCR**

Briefly, total RNA was isolated using the NucleoSpin RNA II kit (Macherey-Nagel), after which the RNA was reverse transcribed with Primescript RT reagent kit (TaKaRa) according to the manufacturer's instruction. Quantitative PCR was performed in the StepOne Real-Time PCR System (Applied Biosystems). Analyses were performed by using the StepOne version 2.0 software (Applied Biosystems) with the comparative  $\Delta\Delta CT$  method and normalized with the human housekeeping gene *GAPDH*. All experiments were performed in triplicate. Primer sequences are provided in Supplementary Table4.

To confirm the complete absence of exons 8 and 9 in the cDNA of DLD-1  $\Delta EX8-9$  cells, a PCR was performed with flanking primers (Supplementary Table4). Generated PCR products were run on gel and sequence-verified.

### **Generation of cell lines with 3xFLAG-tag knock-in**

Using CRISPR-Cas9 genome editing, we generated Caco-2 and OE19 cells with a knockin of the 3xFLAG-tag preceded by a SGGGSGGGS linker at the C-terminus of RNF43. To this aim, a sgRNA targeting before the stop codon of RNF43 exon10 was designed using the following CRISPR design tool (<http://crispor.tefor.net/>), and cloned into pSpCas9(BB)-2A-Puro (pX459) (Supplementary Table2). A homology-directed repair (HDR) plasmid was acquired by cloning a PCR-generated 513bp fragment encompassing the stop codon of RNF43 into pEGFP-C1 (this plasmid was merely used as a backbone plasmid, not to express GFP). Next, the linker-3xFLAG sequence was cloned in frame with RNF43 using standard procedures. We noticed that Caco-2 cells harbor an uncommon heterozygous ACACCAT- ACATCAT variation in the 3'UTR. To avoid preferential targeting of the common allele, we also generated an HDR-plasmid carrying the ACATCAT variant using Q5 Site-directed Mutagenesis (New England Biolabs).

Caco-2 and OE19 cells were seeded in 10cm culture dishes and transfected with 3 $\mu$ g of pX459 and 12 $\mu$ g of HDR plasmid (6 $\mu$ g of each Caco-2 variant) using Lipofectamine 2000 Transfection Reagent. After transfection for 20 h, cells were trypsinized and separated in the ratio of 1/7, 2/7 and 4/7. Cells of each ratio were equally seeded in three 10cm culture dishes.

The next day, transfected cells were selected with 4 $\mu$ g/ml Puromycin for 3 days. Three weeks later, single clones were picked and seeded in a 96-well plate. Following Quickextract DNA isolation, correctly targeted clones were identified by PCR using primers in Supplementary Table5. Subsequently, genomic DNA and cDNA of potential correct clones was verified using Sanger sequencing.

### **Immunoblotting analysis**

Immunoblotting was carried out using standard methods. Cells were lysed in 2 $\times$  Laemmli sample buffer with 0.1 M dithiothreitol (DTT) and heated for 10 min at 95°C. Proteins were separated on 10% sodium dodecyl sulfate-polyacrylamide gel electrophoresis (SDS-PAGE). Proteins were then transferred to Immobilon-P PVDF membranes (Millipore, Bedford, MA, USA). Membranes were blocked 1 h with Odyssey blocking buffer (LI-COR-Biosciences, Lincoln, NE, USA) at room temperature and incubated overnight with primary antibodies at 4°C. After washing with TBS/0.05% Tween20 (TBST) buffer 10 min three times, the membranes were incubated for 1h with IRDye 680 goat anti-mouse (1:10.000, LI 926-68070), IRDye 800 goat anti-rabbit (1:5.000, LI 926-32211), or IRDye 680RD goat anti-rat (1:10.000, LI 926-68076) secondary antibodies (LI-COR-Biosciences), and then washed with TBST 10 min three times. The membranes were then scanned on the Odyssey Infrared Imaging System (LI-COR-Biosciences). Primary antibodies used were mouse anti-FLAG (1:1000, cat.# F1804, Sigma-Aldrich, St. Louis, MO, USA), rabbit anti-RNF43 HPA008079 (1:500, Lot 000005723, SigmaAldrich), rabbit anti-RNF43 ab84125 (1:500, Lot GR3296254, Abcam), rabbit anti-RNF43 ab217787 (1:1000, Lot 1015173-8, Abcam), and rat anti-RNF43 clone 8D6 (1:1000, a kind gift from Dr. Markus Gerhard, Technische Universität München, Munich, Germany). Mouse anti- $\beta$ -actin (1:1000, cat.# sc-47778, Santa Cruz, CA, USA), and rabbit polyclonal to alpha Tubulin (1:2000, cat.# ab4074, Abcam) were used as loading controls.

For enhanced chemiluminescence (ECL)-based detection, Immobilon Block-CH (Chemiluminescent Blocker) blocking buffer was used (cat.# WBAVDCH01, Millipore). The primary antibodies were diluted in this blocking buffer. Membranes were washed with TBS containing 0.05% Tween 20 (TBST). The following secondary antibodies were used: Goat anti-mouse/HRP (1:10.000, cat.# A16078, ThermoFisher), goat anti-rabbit/HRP (1:10.000, cat.# P0448, DAKO), or rabbit anti-rat/HRP (1:10.000, cat.# P0450, DAKO). Membranes were then

incubated with Immobilon ECL Ultra Western HRP Substrate (Millipore) and visualized by using Amersham Imager 600 (GE Healthcare).

### **RNF43 immunofluorescence analysis**

For RNF43 immunofluorescence we basically followed the procedure described by Neumeyer et al.(29). In short, DLD-1, DLD-1  $\Delta$ EX8-9, and HCT116 cells were grown on cover slips in 12-well plates in DMEM/10%FCS without phenol red. In addition, we cultured HCT116 cells transfected with a C-terminal HA-tagged RNF43 expression plasmid (a kind gift from Dr. Markus Gerhard, Technische Universität München, Munich, Germany). Cells were washed with PBS, fixed in ice-cold methanol/acetone (1:1) for 15 min, followed by 3 washes in PBS. Next, cells were incubated at RT for 30 min with blocking/washing solution (3% bovine serum albumin (BSA), 1% saponin in PBS). Cells were then stained with either ab84125, ab217787, HPA-008079 or 8D6 antibody, all at 1:400 dilution, overnight at 4°C. RNF43-HA transfected HCT116 cells were co-stained with RNF43 antibodies and HA-Tag (6E2) Mouse mAb (#2367, Cell Signaling Technology) at a 1:400 dilution. After 3 washes with blocking/washing solution, the following secondary reagents were used: Donkey anti-Rabbit-Alexa 488 (cat.# A-21206), Goat anti-Rat-Alexa 594 (cat.# A-11007), Goat anti-Mouse-Alexa 488 (cat.# A-32723), Donkey anti-Mouse-Alexa 594 (cat.# A-21203); all from Thermo Fisher Scientific, at 1:400 dilution at RT for 1 h. Following 3 times washing with PBS containing 1% saponin, and one PBS wash, slides were mounted with Vectashield antifade mounting medium with DAPI (cat.# H-1200, Vector Laboratories, Burlingame, CA, USA). Images were captured by a Zeiss LSM510 Meta confocal laser scanning microscope using ZEN 2009 software with constant parameter setting.

### **Using Tyramide SuperBoost to detect RNF43-3xFLAG-tag**

RNF43-3xFLAG Caco2 cells, RNF43-3xFLAG OE19 cells, Caco2 cells and OE19 cells were grown on 8-well Lab-Tek II chamber sides (Thermo Scientific). After 48h cells were fixed in ice-cold methanol/acetone (1:1) for 15 min, followed by 3 washes in PBS and stained using Tyramide SuperBoost Kits (Alexa Fluor 488 Tyramide SuperBoost Kit, goat anti-mouse IgG, ThermoFisher) according to the manufacturers' protocol. The optional step to block endogenous peroxidases was applied. Cells were stained with anti-FLAG antibody (1:500, cat.# F1804, Sigma-Aldrich) overnight at 4°C. Slides mounting and generation of images were performed as described above.

## **Preparation of paraffin blocks from cell lines**

The generation of formalin-fixed paraffin-embedded cell lines was basically performed as described previously(30). In short, cells were grown in three 150cm<sup>2</sup> plates until near-confluency. Next, the cells were scraped, washed with PBS, fixed in PBS-buffered 10% formalin and mixed with 1% agarose, prior to embedment in paraffin according to routine protocols. HCT116 cells transiently transfected with a FLAG-tagged RNF43 expression plasmid were also included.

## **Immunohistochemistry**

Immunohistochemical analyses for the RNF43 antibodies (all 1:200 diluted, except for ab217787 which was diluted 1:300) were performed in an automated stainer (Benchmark-Ultra, Ventana Medical Systems, Tucson, AZ). Sections were deparaffinized and pretreated with standard cell conditioning 1 solution (CC1) at 100°C for 64 min, followed by incubation with the specified antibodies at 37°C for 60 min. The antibodies were visualized with the OptiView IHC DAB Detection Kit.

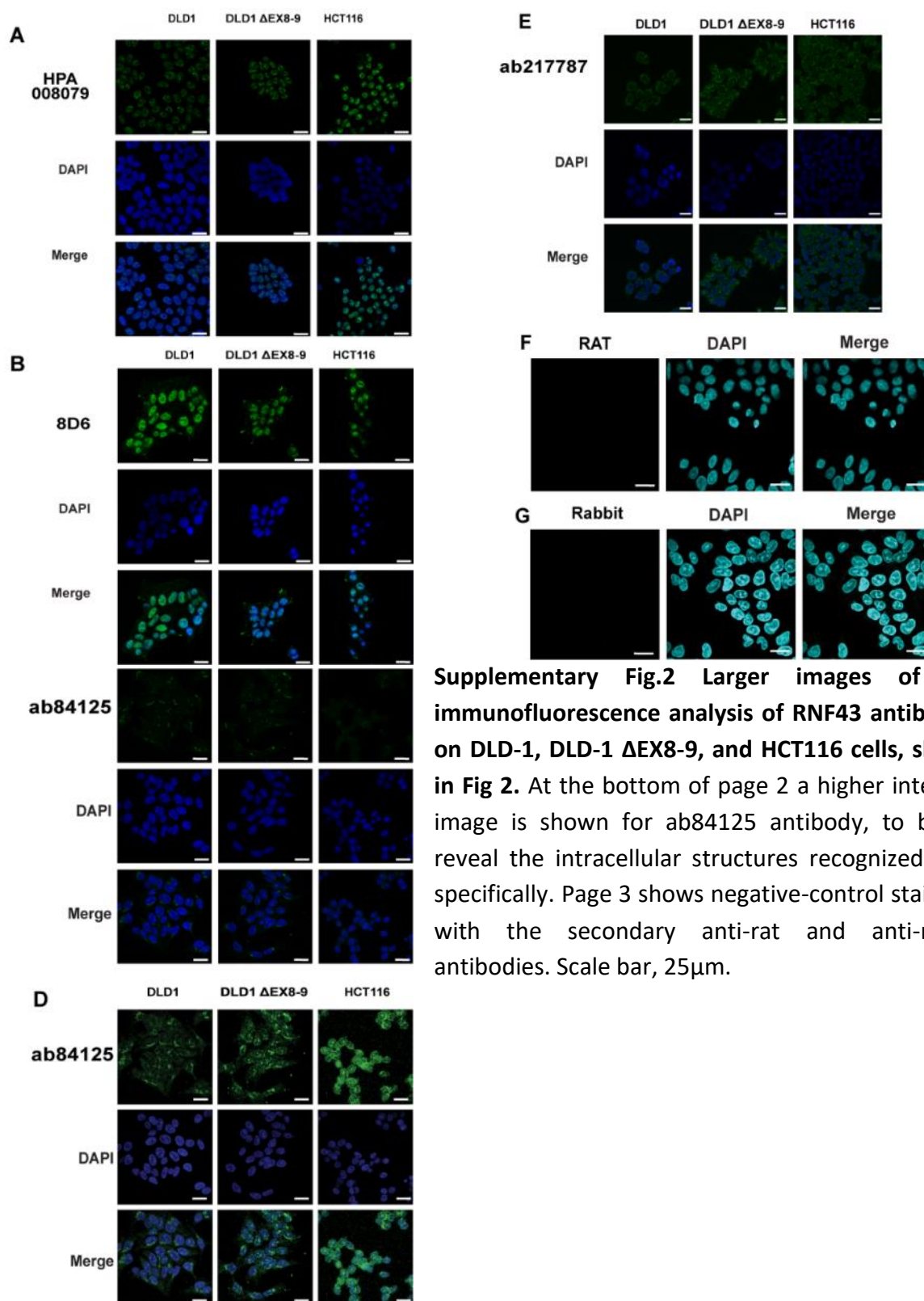
## **Acknowledgements**

We wish to thank Dr. Markus Gerhard (Technische Universität München, Munich, Germany) for generously providing the 8D6 rat monoclonal antibody and the HA-tagged RNF43 expression plasmid. We also wish to thank Dr. Eric Schirmer (University of Edinburgh, UK) for helpful discussions on the nuclear envelope and its isolation challenges.

## Supplemental information

Supplemental Figure 1 original immunoblot images not shown.

## Supplemental Figure 2



**Supplementary Table 1.** Cell lines used in this study. RNF43 mutation status is depicted. homo., homozygous; het., heterozygous.

Cell line name	RNF43 mutation status
HCT116	p.R117fs*41 homo.
DLD-1*	p.G659fs*41 het.+ p.L214M het.+ p.P231L het
KM12	p.G659fs*41 homo.
HEK293T	
HT-29	
Caco-2	
OE19	

\* Sequence analysis of cloned cDNA products from DLD-1 showed that the p.G659fs\*41 and p.P231L are present on the same allele, while the p.L214M variant is present on the other chromosome. The P231L variant was shown to represent a common germline variant [5], while the L214M variant behaves like wild-type RNF43 in a  $\beta$ -catenin reporter analysis.

**Supplementary Table 2.** The sgRNA sequences used for CRISPR-Cas9 genome editing

sgRNA used for CRISPR-Cas9 genome editing	Forward primer (5'-3')	Reverse primer (5'-3')
RNF43 intron7	caccgACCATTCTATTCTACTGTG	aaacCACAGTAGAATAGGAATGGTc
RNF43 intron9	caccGGTGCTACCCCTTAGTTGG	aaacCCAATAAGGGGTAGCACC
RNF43 exon10	caccgACTCGAGGAGCTGTGTGAAC	aaacGTTACACAGCTCCTCGAGTc

**Supplementary Table 3.** Primers used to identify DLD-1 clones with exon 8-9 deletion.

RNF43 deletion check	Forward primer (5'-3')	Reverse primer (5'-3')
Exon8-9 primers flanking deletion	CCTGTGTGTGCCATCTGTCT	ACTGAGCTGTGAGCATTGGT
Exon8 specific primers	GTCCTGATTCTGGCAATTC	ATGGTGGCAGTTCTGCTTTC
Exon9 specific primers	CATGGCTCTCCAGTGACTC	CTTCCCTCTGAAAACCTCACC

**Supplementary Table 4.** Primers for qRT-PCR and for confirming exon 8-9 deletion in cDNA.

<b>RNF43 deletion check</b>	<b>Forward primer (5'-3')</b>	<b>Reverse primer (5'-3')</b>
Exon6&7	CTGTGTGTGCCATCTGTCTG	GTCCGATGCTGATGTAACCA
Exon8&9	CCTTCTGAATGGAGTTCTGAC	GCTAGGCCTGAACATCTCACA
Exon8-9 primers flanking deletion	TCCGCTTCAGCAGAGAACAG	TGGCTGGACATGGATTTGCT

4

**Supplementary Table 5.** RNF43-3xFLAG-tag clones screening primers

<b>primers</b>	<b>sequences</b>
RNF43-5intch-F	TCCAAAAAGGTTACCAGGTCCC
RNF43-5intch-R	GGTTTGGGTCCCCTCGTAT
RNF43-3intch-F	CACGGGTGGTATGGACGAACT
RNF43-3intch-R	CCAGGGTTGCCCTGATGTA
RNF43-Gslink-F	AGCAAGCTGTGTCCGGAGGT
RNF43-FLAGlink-R	CCTGAACATCTCACTTGTCATCGT
RNF43-ex9_cbFin	ACCCACAGAGGAAAAGGCG

## References

1. Bugter JM, Fenderico N, Maurice MM. Mutations and mechanisms of WNT pathway tumour suppressors in cancer. *Nat Rev Cancer*. 2021 Jan;21(1):5-21.
2. Hao HX, Jiang X, Cong F. Control of Wnt Receptor Turnover by R-spondin-ZNRF3/RNF43 Signaling Module and Its Dysregulation in Cancer. *Cancers (Basel)*. 2016 Jun 8;8(6):10.3390/cancers8060054.
3. Koo BK, Spit M, Jordens I, Low TY, Stange DE, van de Wetering M, et al. Tumour suppressor RNF43 is a stem-cell E3 ligase that induces endocytosis of Wnt receptors. *Nature*. 2012 Aug 30;488(7413):665-9.
4. Yu F, Yu C, Li F, Zuo Y, Wang Y, Yao L, et al. Wnt/beta-catenin signaling in cancers and targeted therapies. *Signal Transduct Target Ther*. 2021 Aug 30;6(1):307.
5. Loregger A, Grandl M, Mejias-Luque R, Allgauer M, Degenhart K, Haselmann V, et al. The E3 ligase RNF43 inhibits Wnt signaling downstream of mutated beta-catenin by sequestering TCF4 to the nuclear membrane. *Science signaling*. 2015 Sep 8;8(393):ra90.
6. Neumeyer V, Brutau-Abia A, Allgauer M, Pfarr N, Weichert W, Falkeis-Veits C, et al. Loss of RNF43 Function Contributes to Gastric Carcinogenesis by Impairing DNA Damage Response. *Cell Mol Gastroenterol Hepatol*. 2021 Nov 11;11(4):1071-94.
7. Tsukiyama T, Zou J, Kim J, Ogamino S, Shino Y, Masuda T, et al. A phospho-switch controls RNF43-mediated degradation of Wnt receptors to suppress tumorigenesis. *Nat Commun*. 2020 Sep 15;11(1):4586.
8. Xie H, Xing C, Cao G, Wei B, Xu X, Song P, et al. Association of RNF43 with cell cycle proteins involved in p53 pathway. *Int J Clin Exp Pathol*. 2015;8(11):14995-5000.
9. Bond CE, McKeone DM, Kalimutho M, Bettington ML, Pearson SA, Dumenil TD, et al. RNF43 and ZNRF3 are commonly altered in serrated pathway colorectal tumorigenesis. *Oncotarget*. 2016 Sep 20.
10. Jo YS, Kim MS, Lee JH, Lee SH, An CH, Yoo NJ. Frequent frameshift mutations in 2 mononucleotide repeats of RNF43 gene and its regional heterogeneity in gastric and colorectal cancers. *Hum Pathol*. 2015 Nov;46(11):1640-6.
11. Niu L, Qin HZ, Xi HQ, Wei B, Xia SY, Chen L. RNF43 Inhibits Cancer Cell Proliferation and Could be a Potential Prognostic Factor for Human Gastric Carcinoma. *Cell Physiol Biochem*. 2015;36(5):1835-46.



12. Holm B, Barsuhn S, Behrens HM, Kruger S, Rocken C. The tumor biological significance of RNF43 and LRP1B in gastric cancer is complex and context-dependent. *Sci Rep.* 2023 Feb 23;13(1):3191.
13. Zhu D, Shi X, Tian Y, Li H, Tang B, Zhang Z, et al. Combining expression of RNF43 and infiltration level of CD163(+) tumor associated macrophage predicts prognosis of clear cell renal cell carcinoma. *Cancer Med.* 2022 Sep 12.
14. Omori Y, Ono Y, Tanino M, Karasaki H, Yamaguchi H, Furukawa T, et al. Pathways of Progression From Intraductal Papillary Mucinous Neoplasm to Pancreatic Ductal Adenocarcinoma Based on Molecular Features. *Gastroenterology.* 2019 Feb;156(3):647-61 e2.
15. Aoki Y, Mizuma M, Hata T, Aoki T, Omori Y, Ono Y, et al. Intraductal papillary neoplasms of the bile duct consist of two distinct types specifically associated with clinicopathological features and molecular phenotypes. *The Journal of pathology.* 2020 May;251(1):38-48.
16. Sakihama K, Koga Y, Yamamoto T, Shimada Y, Yamada Y, Kawata J, et al. RNF43 as a predictor of malignant transformation of pancreatic mucinous cystic neoplasm. *Virchows Arch.* 2022 Jun;480(6):1189-99.
17. Li S, Lavrijsen M, Bakker A, Magierowski M, Magierowska K, Liu P, et al. Commonly observed RNF43 mutations retain functionality in attenuating Wnt/beta-catenin signaling and unlikely confer Wnt-dependency onto colorectal cancers. *Oncogene.* 2020 Apr;39(17):3458-72.
18. Yu J, Yusoff PAM, Woutersen DTJ, Goh P, Harmston N, Smits R, et al. The Functional Landscape of Patient-Derived RNF43 Mutations Predicts Sensitivity to Wnt Inhibition. *Cancer research.* 2020 Dec 15;80(24):5619-32.
19. Bradbury A, Pluckthun A. Reproducibility: Standardize antibodies used in research. *Nature.* 2015 Feb 5;518(7537):27-9.
20. Acharya P, Quinlan A, Neumeister V. The ABCs of finding a good antibody: How to find a good antibody, validate it, and publish meaningful data. *F1000Res.* 2017;6:851.
21. Sugiura T, Yamaguchi A, Miyamoto K. A cancer-associated RING finger protein, RNF43, is a ubiquitin ligase that interacts with a nuclear protein, HAP95. *Exp Cell Res.* 2008 Apr 15;314(7):1519-28.
22. Tu J, Park S, Yu W, Zhang S, Wu L, Carmon K, et al. The most common RNF43 mutant G659Vfs\*41 is fully functional in inhibiting Wnt signaling and unlikely to play a role in tumorigenesis. *Sci Rep.* 2019 Dec 6;9(1):18557.

23. Korfali N, Florens L, Schirmer EC. Isolation, Proteomic Analysis, and Microscopy Confirmation of the Liver Nuclear Envelope Proteome. *Methods in molecular biology* (Clifton, NJ. 2016;1411:3-44.
24. Korfali N, Wilkie GS, Swanson SK, Srsen V, de Las Heras J, Batrakou DG, et al. The nuclear envelope proteome differs notably between tissues. *Nucleus*. 2012 Nov-Dec;3(6):552-64.
25. Tsukiyama T, Fukui A, Terai S, Fujioka Y, Shinada K, Takahashi H, et al. Molecular Role of RNF43 in Canonical and Noncanonical Wnt Signaling. *Molecular and cellular biology*. 2015 Jun 01;35(11):2007-23.
26. Radaszkiewicz T, Noskova M, Gomoryova K, Vondalova Blanarova O, Radaszkiewicz KA, Pickova M, et al. RNF43 inhibits WNT5A-driven signaling and suppresses melanoma invasion and resistance to the targeted therapy. *Elife*. 2021 Oct 27;10.
27. Lee H, Seidl C, Sun R, Glinka A, Niehrs C. R-spondins are BMP receptor antagonists in *Xenopus* early embryonic development. *Nat Commun*. 2020 Nov 4;11(1):5570.
28. Ran FA, Hsu PD, Wright J, Agarwala V, Scott DA, Zhang F. Genome engineering using the CRISPR-Cas9 system. *Nature protocols*. 2013 Nov;8(11):2281-308.
29. Neumeyer V, Grandl M, Dietl A, Brutau-Abia A, Allgauer M, Kalali B, et al. Loss of endogenous RNF43 function enhances proliferation and tumour growth of intestinal and gastric cells. *Carcinogenesis*. 2019 Jun 10;40(4):551-9.
30. Dubbink HJ, Hollink I, Avenca Valente C, Wang W, Liu P, Doukas M, et al. A novel tissue-based  $\beta$ -catenin gene and immunohistochemical analysis to exclude familial adenomatous polyposis among children with hepatoblastoma tumors. *Pediatr Blood Cancer*. 2018 Jun;65(6):e26991.

# Chapter 5

## **A simplified qPCR method revealing tRNAome remodeling upon infection by genotype 3 hepatitis E virus**

Xumin Ou<sup>1,2#</sup>, Buyun Ma<sup>2#</sup>, Ruyi Zhang<sup>2#</sup>, Zhijiang Miao<sup>2</sup>, Anchun Cheng<sup>1,3,4</sup>, Maikel P Peppelenbosch<sup>2</sup>, Qiuwei Pan<sup>2</sup>

1. Institute of Preventive Veterinary Medicine, Sichuan Agricultural University, Chengdu, China.
2. Department of Gastroenterology and Hepatology, Erasmus MC - University Medical Center Rotterdam, The Netherlands.
3. Key Laboratory of Animal Disease and Human Health of Sichuan Province, Sichuan Agricultural University, Chengdu, China.
4. Research Center of Avian Diseases, College of Veterinary Medicine, Sichuan Agricultural University, Chengdu, China.

#These authors contributed equally to this article

*FEBS letters, 2020, 12(594)*



## Abstract

The landscape of tRNA-viral codons regulates viral adaptation at translational level, presumably through adapting host codon usage or modulating host tRNAome. We found that the major zoonotic genotype of hepatitis E virus (HEV) has not adapted to host codon usage, prompting exploration of HEV infection on host tRNAome. However, tRNAome quantification is largely impeded by their extremely short sequence and redundant tRNA genes. Hereby, we present a length-extension and stepwise simplified qPCR method by utilizing a universally DNA/RNA hybrid tRNA adaptor and degenerate primers. Using this novel methodology, we observe that HEV infection dramatically reprograms the hepatic tRNAome that is likely to facilitate translation of viral RNAs. This tRNAome quantification method bears broad implications for future tRNA research and possibly tRNA-based diagnostics.

5

**Keywords:** hepatitis E virus; length-extension and simplified qPCR method; tRNAome

This research was supported by the National Key Research and Development Program of China (2017YFD0500800), China Agricultural Research System (CARS-42-17), China Scholarship Council (Joint-Ph.D. fellowships 201706910003 to X.O.; Ph.D. fellowship 201508330291 to B.M.; Ph.D. fellowship 201808530490 to R.Z.).

## Introduction

Viral adaptation is shaped by a variety of effectors, including the need to hijack the cellular protein synthesizing machinery for efficient translation of viral genes [1]. Rate-limiting steps in the production of viral proteins differ depending on host species and the virus involved. But in many cell types, efficiency of the translational machinery is critically dependent on the tRNAs availability that decode both cellular and viral codons [2,3]. Accordingly, many viruses show adaptation with respect to codon usage towards their host [4-7]. Conversely, it has been reported that interferons, the potent antiviral cytokines [8], can alter the availability of tRNAs to facilitate the production of antiviral proteins and to attenuate decoding of viral codons [9,10]. Thus, studying the interplay between viral codons and cellular tRNAome is essential for understanding the infection biology.

tRNAs are the recognition modules that decode the mRNA in the ribosome and are covalently charged by amino acids [11]. Following recognition, the corresponding intramolecular bond is hydrolysed and the released amino acid is covalently linked to nascent peptide chain. The tRNAs encoded in genomic DNA are typically 70 to 90 base pairs in length often with multiple genomic copies of the same tRNA [12]. The human tRNAome is encoded by more than 600 tRNA gene locus [12]. Following transcription, tRNAs are subjected to post-transcriptional modification, and a common CCA ribonucleotide sequence is added to the 3' end of tRNA [13]. Accurate detection of the mature tRNAome is technically challenging and especially hampered by the short length and redundant tRNA genes [14,15]. As the number of different tRNA sequences is relatively limited, we believe that optimized qPCR-based techniques hold possibility for quantifying tRNAs.

Hepatitis E virus (HEV) is a ssRNA (+) virus and is the leading cause of acute viral hepatitis [16]. Globally, HEV causes annually 20 million infections with over 56,000 lethal cases and especially in pregnant women [17]. Among the major genotypes, genotype 1 and 2 HEV only infects human, whereas genotype 3 and 4 are zoonotic. Genotype 3 is highly prevalent in western countries with a broad host spectrum [18,19]. In this study, we aim to first develop a simplified qPCR method for quantifying mature tRNAs, and then to investigate how codon usage of the zoonotic HEV genotype relates to the human tRNAome composition.

## Materials and methods

### Experimental models

For HEV infectious model, a full-length genotype 3 HEV genome (Kernow-C1 p6 clone, GenBank Accession Number: JQ679013) was used [20]. The human hepatoma Huh7 cell line was used to harbor the HEV genome and produce infectious virus particles for secondary infection of naïve Huh7 cells [21]. The HEV subgenomic model was based on Huh7 cells containing the subgenomic genotype 3 HEV sequence (Kernow-C1 p6/luc) coupled to a *Gussia luciferase* reporter gene [21,22]. The cell line was regularly checked for identity using STR verification as provided by the pathology department of the Erasmus MC. Key reagents, viral strains and software used in this study were listed in **Table S1**.

### Bioinformatic analysis

Codon usage bias and codon adaptation index (CAI) of HEV ORF (1-3) and ISGs were analyzed by Codon W software (<http://www.molbiol.ox.ac.uk/cu>, version 1.4.2) using standard genetic codes. Correlation analysis were performed by Python Matplotlib package. Codon usage and tRNAome data were visualized by Hemi software with hierarchical clustering analysis (<http://hemi.biocuckoo.org/>).

### The qPCR protocol for quantifying mature tRNAs

#### Preparation of samples and reagents •TIMING 1d

1| Prepare primary cells, cell lines or tissues to yield 1-4 µg total RNA for each sample. This amounts to roughly 10<sup>5</sup>-10<sup>6</sup> mammalian cells. These values are rough guidelines for experimental design, but yields will vary according to the cell types and amounts.

**(Optional)** Protocol can begin with isolated RNA samples. In this case, we recommend to adjust RNA concentration to 214 ng/µL. Then, mix 4 µL RNA sample with 1 µL 5×deacylation buffer (step 9) and incubate at 37 °C for 40 min, after that add 10 µL TE buffer for PH adjustment (step 10). Finally, 7 µL of the RNA containing deacylated tRNAs (400 ng ≈ 214 ng/µL × 4/15 × 7 µL) are ready for following annealing with U-adaptor (step 11).

#### Total RNA isolation and tRNA deacylation •TIMING 1.5-2h

2| Wash cells. Remove cell medium, and wash cells with warm PBS buffer.

3| Lyse cells. Add 350  $\mu$ L of RA lysis buffer to each well, then suck up whole cell lysate into 1.5 EP tube. All the reagents for RNA extraction except deacylation buffer are provided by NucleoSpin<sup>®</sup> RNA kit.

4| Adjust RNA binding condition. Add 350  $\mu$ L 70% ethanol to the homogenized lysate and mix by pipetting up and down. (minimal 5 times)

5| RNA binding. For each sample take one Nucleospin<sup>®</sup> RNA Column place in a collection tube. Pipette lysate up and down 2-3 times and load the lysate to the column. Centrifuge for 30 s at 11,000 $\times$ g. Place the column on a new collection tube (2 ml).

6| Desalt silica membrane. Add 350  $\mu$ L MDB (Membrane Desalting Buffer) and centrifuge at 11,000 $\times$ g for 1 min to dry the membranes.

7| Digest DNA. Prepare DNase reaction mixture in a sterile 1.5 ml tube. For each isolation, add 10  $\mu$ L DNase to 90  $\mu$ L reaction buffer for DNase. Mix by flicking the tube. Add 95  $\mu$ L DNase reaction mixture directly onto the center of the silica membrane of the column. Incubate at room temperature for 15 min.

8| Wash and dry the silica membrane.

1st Wash: Add 200  $\mu$ L RAW2 buffer to the Nucleospin<sup>®</sup> RNA Column. Centrifuge for 30 s at 11,000 $\times$ g. Place the column on a new collection tube (2 ml).

2nd Wash: Add 600  $\mu$ L RA3 buffer to the Nucleospin<sup>®</sup> RNA Column. Centrifuge for 30 s at 11,000 $\times$ g. Place the column on a new collection tube (2 ml).

3rd Wash: Add 250  $\mu$ L RA3 buffer to the Nucleospin<sup>®</sup> RNA Column. Centrifuge for 2 min at 11,000 $\times$ g to dry the membrane completely. Place the column on a new collection tube (2 ml).

9| Deacylation. Prepare deacylation mixture. Add 2  $\mu$ L of 5 $\times$ Tris-HCl (100 mM, PH 9.0) into 8  $\mu$ L ddH<sub>2</sub>O; mix it by pipetting up and down (minimal 5 times). Add 10  $\mu$ L Deacylation mixture to the Nucleospin<sup>®</sup> RNA Column. Incubate at 37 °C for 40 min.

10| Elute RNA. Place the column on a new 1.5 EP tube. Elute the RNA by adding an additional 20  $\mu$ L TE buffer on the Nucleospin<sup>®</sup> RNA Column directly. Centrifuge for 1 min at 11,000 $\times$ g.



**Adaptor ligation •TIMING 1.5-2h**

11| Annealing. Measuring RNA concentration by Nanodrop. Prepare mixture of 400 ng RNA and 20 pm adaptor (2  $\mu$ L); then the final volume is adjusted to 9  $\mu$ L. Incubate at 90 °C for 3 min.

12| Add 1  $\mu$ L 10 $\times$ Tris-HCl (50 mM, PH8.0) annealing buffer at 37 °C for 20 min.

13| Ligation reaction. 2  $\mu$ L ligase buffer, 7.9  $\mu$ L H<sub>2</sub>O and 0.1  $\mu$ L T4 RNA ligase was added into the above mixture, then incubate at 37 °C for 1 h.

**Reverse Transcription •TIMING 0.5h**

14| Annealing with mixture of specific tRNA reverse primers. 20  $\mu$ L of above mixture is added with 3.42  $\mu$ L (1.14  $\mu$ L $\times$  3 = 3.42  $\mu$ L) of mixture of tRNA reverse primers (**Table S2**). Incubate the mixture at 65 °C for 5 min. Place on ice immediately.

15| Co-reverse transcript with random and oligo dT Primers. Add 6  $\mu$ L 5 $\times$  Prime Script RT Master Mix and 0.58  $\mu$ L H<sub>2</sub>O into the above tube. Mix by flicking the tube. Incubate the mixture at 37 °C for 15 min followed by 85 °C for 5 s.

**qPCR •TIMING 1-2h**

16| qPCR mix preparation (**Table S3**). Prepare qPCR mixture according to the following recipe (10  $\mu$ L). To cover all 57 tRNA types, we recommend adding 220  $\mu$ L ddH<sub>2</sub>O into above 30  $\mu$ L of reverse transcription solution.

Notice: Because of the large number of tRNA sets, it is recommended to prepare tRNA-X-R and tRNA-X-F primer mixture to minimize loading variation. For example, to prepare 80 times of tRNA-R/F mix, we recommend that 20  $\mu$ L (10 pm) of tRNA-X-R and tRNA-X-F was diluted by 200  $\mu$ L ddH<sub>2</sub>O. Therefore, the finally used volume of tRNA primers mix is 3  $\mu$ L.

17| Perform qPCR with the designed cycling condition according to **Table S4**.

**Quantification**

The  $2^{-\Delta\Delta C_t}$  was used to calculate the relative expression of each tRNA species, and the  $\Delta C_t$  values were determined by subtracting the average  $C_t$  values of the endogenous control gene *GAPDH* from the average  $C_t$  values of the each tRNA type.

## Statistical Analysis

Linear correlations between the relative synonymous codon usage (RSCU) of human and animal HEV strains were estimated by Pearson coefficients. Statistical comparisons of tRNAome data were performed with Mann-Whitney U test for non-paired independent samples. \* $P < 0.05$  was indicated as significant. The statistical analysis was performed using the SPSS19.0 software.

## Results

### The codon usage of genotype 3 HEV has not adapted to its human host

As in many biological systems tRNA availability [23] and codon context [24] constitute the rate limiting step for protein synthesis. Viruses are expected to adapt codon usage as to fit host codon usage patterns. With respect to the zoonotic genotype 3 HEV, however, this has not yet been analyzed. Hence, we compared the RSCU of three open reading frames (ORFs) of genotype 3 HEV isolated from human to the counterpart of the human host. Similar analysis was also performed for HEV strains isolated from animals, including swine, deer, mongoose and wild boar (Table 1). Strikingly, we did not find evidence that the codon usage of genotype 3 HEV isolated from human and the animal host has adapted to the human codon usage pattern for any of the three ORFs investigated (Fig. 1). Because linear correlations between the RSCU of human and animal HEV strains are very poor (Pearson coefficients less than 0.40). Moreover, the RSCU analysis of HEV between the non-human primate (e.g., monkey) and human also indicated that the usage of major codons is similar except serine codon (UCU) (Fig. S1). Besides RSCU, the codon adaption index (CAI) has also been suggested to predict the efficiency of translation elongation [25]. Our results indicated that the CAI of HEV was similar among different host species-derived strains, and much lower than that of human housekeeping gene (e.g., *GAPDH*) (Fig. 1). We conclude that there has been very little evolutionary pressure on genotype 3 HEV to adapt the codon usage of its human host. Thus, we decided to investigate how HEV infection regulates host tRNAome.

Table 1. list of HEV genotype 3 strains used in this study.

Host	Source material	Country of origin	Collection data	Accession #
<i>Homo sapiens</i>	Hepatocytes	United Kingdom	Jul-2010	JQ679013
<i>Sus domesticus</i>	Serum	United States	1997	AF082843
<i>Sus scrofa</i>	Liver	Germany	2006	FJ705359
<i>Cervus nippon</i>	Liver or serum	Japan	22 Feb 2003	AB189071
<i>Herpestes javanicus</i>	Serum	Japan	2002	AB236320
<i>Cynomolgus</i>	Serum	Japan	Nov-2009	JQ026407.1

5

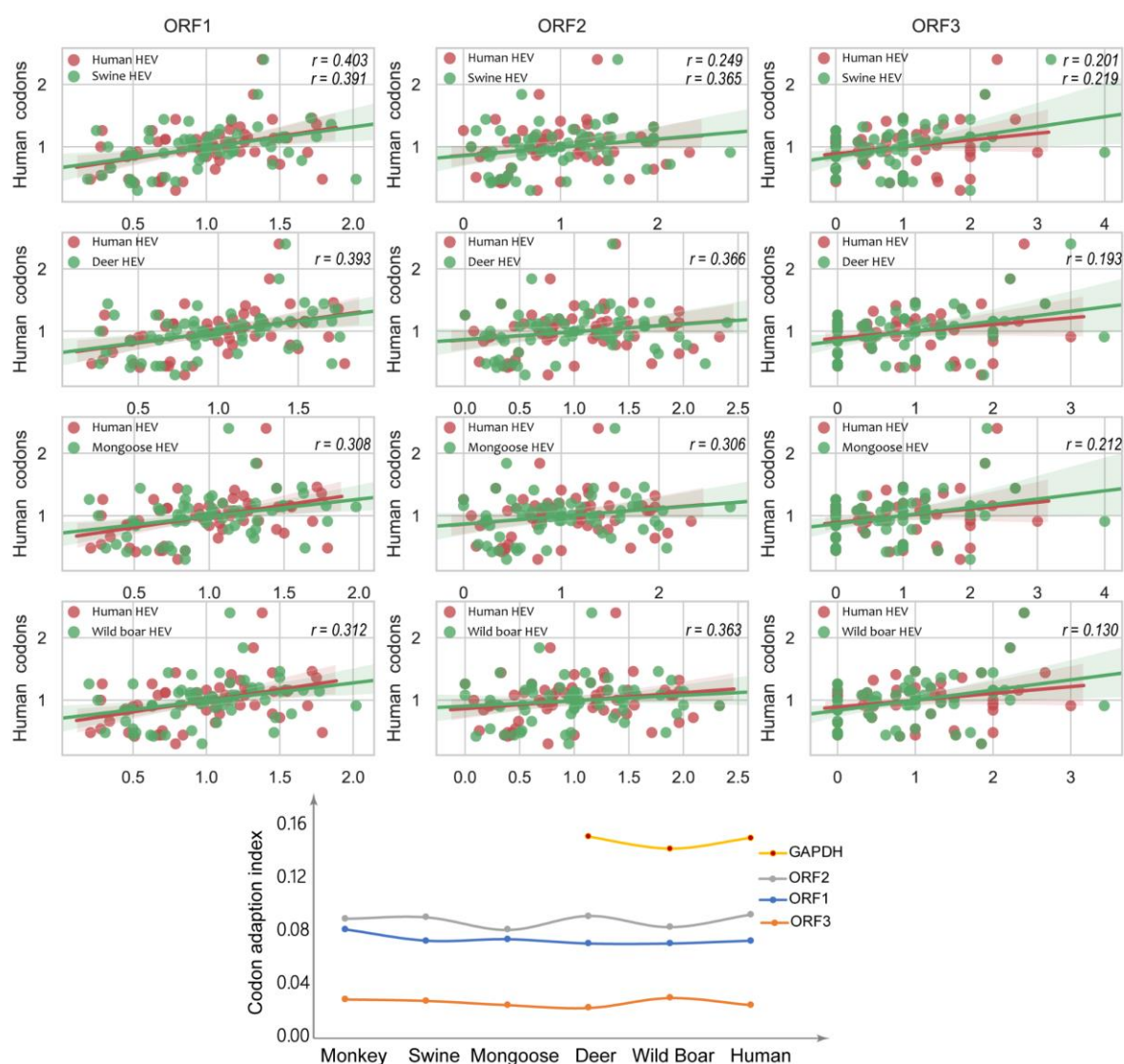


**Fig. 1. Lack of adaptation of genotype 3 HEV codon usage to host codon usage.**

Codon usage of human HEV was correlated to overall human codon usage. The codon usage of swine, wild deer, mongoose and wild boar HEV was also related to human codon usage. For each possible codon and 64 in total, its RSCU in the human genome is plotted against the Y axis and the corresponding RSCU in the relevant viral ORF on the X axis. Results were shown for all three ORFs in the upper panels. In the lower panel, codon adaption index of genotype 3 HEV isolated from different host species were compared for ORF1-3. The CAI of GAPDH from deer, wild boar and human are also indicated. The CAI calculation was performed by Codon W software with *Saccharomyces cerevisiae* as reference set.

**A simplified qPCR method for characterizing the human mature tRNAome**

To develop a novel qPCR method for easy quantification of mature tRNAs, we first designed a DNA/RNA hybrid adaptor (Universal adaptor, U-adaptor). It is compatible with all types of mature tRNAs with a common 3' CCA acceptor (**Fig. 2**). Following binding of the adaptor to the tRNA molecule, the adaptor can be ligated to both the 5' end and 3' end of the mature tRNAs. Of note, the mature tRNAs are frequently charged by amino acids that hamper the above ligation reaction. Thus, a deaminoacylation reaction for the charged tRNA is needed during RNA isolation (see Materials and methods). Importantly, the adaptor is designed to form a loop and hybridize on tRNA itself. This hybridization is compatible for any types of base-pairs adjacent to 3' CCA tail of tRNAs, as the pairing base of the U-adaptor involved is degenerately designed. The ligation reaction specifically links the 5' end and 3' end of the adaptor to the corresponding ends of tRNA molecule that is catalyzed by T4 RNA ligase (**Fig. 2**). Finally, a hybrid pseudocircular molecule, containing the deaminoacylated original mature tRNA molecule and the U-adaptor, is formed. This strategy serves two important ends: it extends length of tRNA for subsequent qPCR while simultaneously eliminating unmature tRNAs. Afterwards, tRNAs can be determined by conventional qPCR (see the experimental strategy **Fig. 3**).

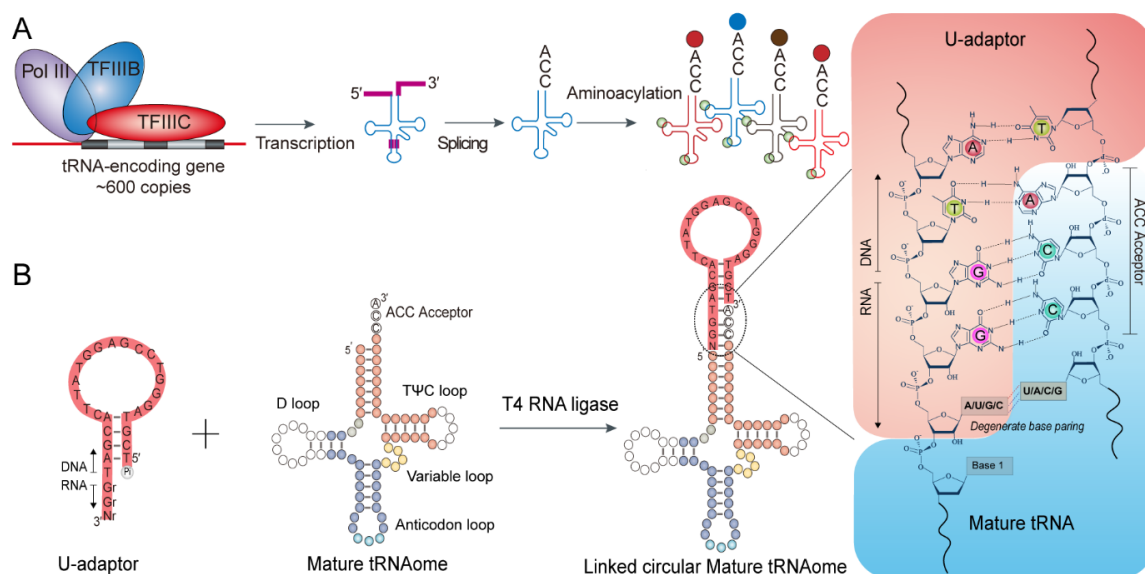


**Fig. 2. A universal U-adaptor that interacts specifically with all mature tRNAs.**

**A)** More than 600 tRNA-encoding genes can be transcribed by RNA polymerase III. After post-transcriptional processing, splicing and adding of ACC acceptor to these new tRNA transcripts. The resulting mature tRNAome is available for all cellular mRNA translation and also for viral RNA decoding. The final step in tRNA maturation is adding the CCA sequence to which the acylating amino acid is coupled. The CCA tail is thus common and specific to all mature tRNAs. **B)** A universal(U) DNA/RNA hybrid adaptor was designed. The -2 to -4 of 3' terminal bases (TGG) of the U-adaptor are specifically designed to pair CCA acceptor. To further improve the compatibility of U-adaptor to all mature tRNAs, the last 3' terminal nucleotide was degenerately designed. The interface of U-adaptor and mature tRNA are detailed at the right of the panel.

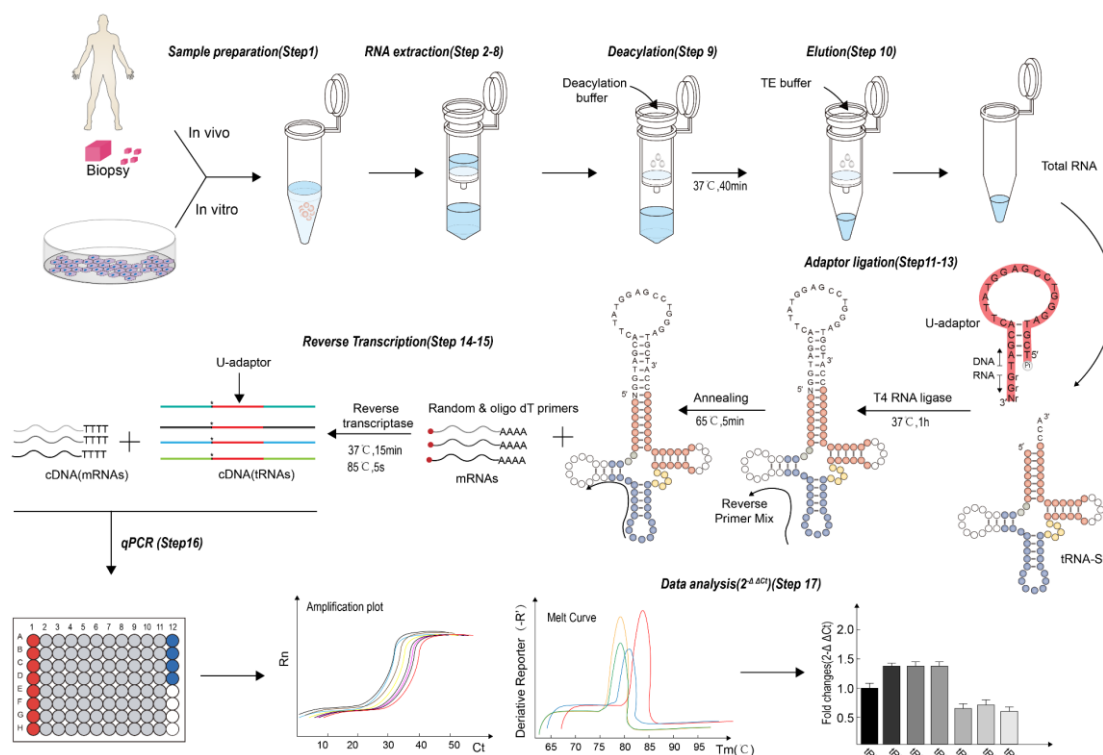


**Fig. 3. Workflow of quantifying tRNAome.**

First total RNA was extracted from the experimental systems involved according to a routine column-based RNA isolation protocol. Before elution the column is incubated with diacylation buffer at 37 °C for 40 min to remove acylating amino acids at tRNA CCA tail followed by elution with TE buffer. Subsequently, the tRNA and U-adaptor are linked by T4 RNA ligase followed by annealing with reverse primer mix. Finally, the cDNA of total mRNA and U-adaptor linked tRNAs are concurrently synthesized for qPCR amplification. The relative expression of tRNAs is calculated by  $2^{-\Delta\Delta C_t}$  method that can be normalized by housing keeping genes, such as GAPDH. The stepwise procedures are detailed by seventeen discrete steps in the Materials and Methods.

To this end, a mixture of tRNA specific reverse primers was used, which were designed to bind to the region between the anticodon loop and the D loop. A complication with regard to designing reverse primers for characterizing the tRNAome is that many iso-decoder tRNAs (i.e., tRNA with the same anticodon but vary in backbone) are responsible for decoding of the identical genetic codon [12]. We thus retrieved all 57-human genomic tRNA genes from the GtRNA 2.0 database and accordingly designed degenerate primers (**Table S2**). Using RNA obtained from Huh7 human liver cells, all primer pairs successfully amplified their iso-decoder tRNA molecules in qPCR reactions (**Fig. S2** and **Fig. S3**). We conclude that our approach employing the U-adaptor and degenerate primers allows easy quantification of cellular tRNA profiles.

**Normalization of tRNAome by reference gene**

In order to normalize tRNA level, tRNA specific reverse primers, random and oligo d(T) primers were concurrently used for reverse transcriptional reaction. *GAPDH*, a commonly accepted reference gene, is selected for tRNAome normalization [26]. tRNA-His-GUG is the only tRNA species capable of decoding Histidine codons (CAC & CAU), and thus we expect that its expression would be more stable. Indeed, we observed good correlation between levels of GAPDH mRNA and tRNA-His-GUG (**Fig. S4**). Comparing the U-adaptor and tRNA-histidine adaptor for ligation reaction, we found that the U-adaptor did not compromise the ligation efficiency as it caused only 0.11 variation calculated by  $\Delta C_t$  (**Table S1**). Efforts were made for further optimization of the protocol, for instance by combining steps involved annealing, but these efforts failed (**Fig. S5**). The final protocol (refer to Materials and methods) is organized in seventeen discrete steps and allows quantitative assessment of mature tRNAome.

**HEV infection provokes remodeling of mature tRNAome in host cells**

Although viruses are considered to adapt codon usage to their host [3,27], we observe that HEV is not subject to such adaptation. Hence, we decided to compare tRNAome composition in the presence and absence of HEV infection. To this end Huh7 cells were infected with full length HEV or exposed to vehicle control (**Fig. S4A**), and the levels of different tRNAs were determined (**Fig. S6A**). We observed a major effect on tRNAome remodeling by HEV infection. 29 out of 57 tRNA species showed significant upregulation. The most marked example is tRNA-Pro-GGG that shows 162 times higher expression in HEV-infected cells as compared to non-infected cells. tRNA-Gly-CCC was approximately 50 times and tRNA-Pro-UGG was about 35 times upregulated in HEV infected cells. Conversely, other tRNA species were downregulated following HEV infection. tRNA-Leu-UAG is most prominently downregulated by approximately 70 %. We conclude that HEV infection provokes major remodeling of the mature tRNAome in cells capable of sustaining its replication.

### **HEV infection triggered tRNAome remodeling is largely dependent on ORF2**

The capsid protein of HEV encoded by ORF2 features many  $\beta$ -sheets in its secondary structure [28] and consequently requires incorporation of a multitude of Proline and Glycine residues during synthesis. By far the most prominent effects of HEV infection on the tRNAome are the upregulation of tRNAs supporting Proline and Glycine decoding (tRNA-Pro-GGG, tRNA-Pro-UGG, and tRNA-Gly-CCC). Thus, we investigated the role of ORF2 in HEV-induced tRNA remodeling. We quantified tRNAome in cells carrying subgenomic HEV replicon with ORF2-deletion. This subgenomic HEV replicon contains a luciferase reporter and viral replication can be quantified by luciferase activity (**Fig. 4A**). Intriguingly, although effects on tRNAome composition were still observed in the subgenomic replicon (**Fig. S6B**), they are much moderate as compared to that in the full-length HEV model (**Fig. S6C**). Effects on tRNA-Pro-GGG, tRNA-Pro-UGG, and tRNA-Gly-CCC levels were not statistically significant in the subgenomic replicon.

Further insight came from unsupervised clustering analysis of the tRNAome profiles [29]. Three biologically independent experiments were performed with naïve Huh7 cells, Huh7 cells infected by HEV with the full-length genome and cells carrying the subgenomic replicon. The experimental conditions segregated the profiles generated. As expected, the effects on tRNAome provoked by infection of HEV with full-length genome were much more pronounced

as compared to those evoked by the subgenomic replicon (**Fig. 4B**). We thus conclude that ORF2 is essential for HEV-triggered tRNA remodelling.

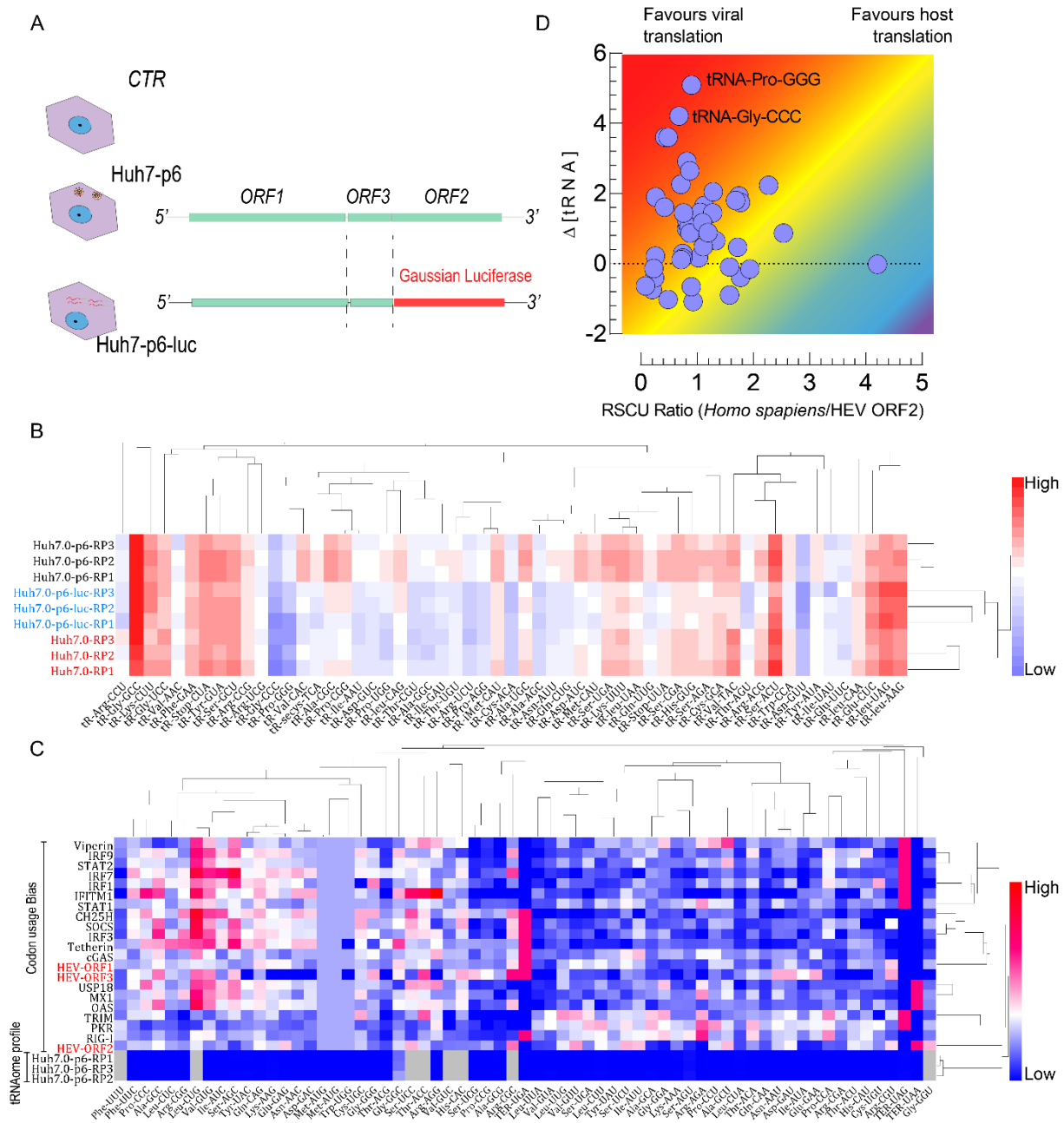


**Fig. 4. tRNAome remodeling following HEV infection favors viral translation.**

**A)** For profiling tRNAome, human hepatoma Huh7 cells harboring the infectious HEV clone with full-length genome (Huh7-p6), the subgenomic replicon lacking of ORF2 (Huh7-p6-luc), and naïve Huh7 cells were used (n = 3). **B)** Cluster analysis of the tRNAome profiles in the three cell models. **C)** Comparative analysis of the effects of HEV-induced tRNAome remodeling on codon usage of viral ORF (1-3) and a panel of antiviral interferon-stimulated genes (ISGs). **D)** Visualization of the effects of HEV infection on relative tRNA abundancies in relation to viral and host codon decoding. For each tRNA, the ratio of HEV codon usage over human codon usage is plotted on the X axis. A larger value indicates



that a tRNA is more often used for human decoding as compared to viral decoding. The effect of HEV infection on tRNA abundance is plotted on the Y axis. A positive value corresponds to upregulation of a tRNA following HEV infection.

### **HEV-induced tRNA remodelling may counteract decoding of interferon-stimulated genes**

Innate antiviral immunity, especially that mediated by the so-called interferon-stimulated genes (ISGs), is important for controlling HEV infection [30]. Interestingly, tRNAome remodeling by HEV mainly supported better decoding of ORF2 when compared to ORF1 and ORF3 (**Fig. 4C, D**). Hence, we analyzed the effects of tRNAome remodeling triggered by full-length infectious HEV on the decoding of essential ISGs. We selected a panel of ISGs known to inhibit HEV infection. We found that HEV-provoked tRNA remodeling is not correlated to the RSCU of these ISGs (**Fig. 4C** and **Table S5**), whereas viral ORF2 translation per se is related to the same changes (**Fig. 4C, D**). We thus conclude that HEV infection reprograms cellular tRNAome that is likely to facilitate viral translation but hamper cellular antiviral immunity.

5

## **Discussion**

The development of tRNA quantification methods has been greatly facilitated by the tRNAscan-SE program that allows accurate identification of genomic tRNA sequences. Earlier methods to detect tRNAs usually involve thin layer chromatography [31], liquid chromatography mass spectrometry [32], DNA arraying [33] and single tRNA-based qPCR [15]. Recently, quantification of the tRNAome at transcriptional level has become more efficient through high-throughput sequencing [14,34], but is dependent on programming and very specific reagents. In this study, we established a simplified qPCR method for rapid quantification of the mature tRNAome. This strategy is characterized by a length-extension step, a universally compatible adaptor and degenerate primers applicable for the entire mature tRNAome. The present study was only demonstrated in a human cell model, but we envision that it is applicable to other organisms by adjusting primer design.

As a proof-of-principle, this qPCR methodology was used for characterizing the effects of HEV infection on host tRNAome. We observed substantial remodeling of tRNA composition

following HEV infection. For example, the level of tRNA-Pro-GGG was increased by 162 times by HEV infection. Such regulations appear in a fashion that facilitates translation of viral proteins while simultaneously hampering the decoding of antiviral ISGs. Interestingly, these observed effects relate especially to HEV ORF2, which is the dominant ORF of this virus with respect to demands on the host translational machinery [35]. Our data suggest that counteracting HEV-dependent tRNA remodeling may constitute a novel avenue for supporting host defense in combating viral infection, but this will require further understanding of the molecular pathways involved.

It has been reported that codon usage bias of the zoonotic genotypes 3 and 4 of HEV is much weaker than that of the non-zoonotic genotypes 1 [19]. This indicates that less bias of HEV codon usage may be involved in zoonotic infection. Consistently, we found that genotype 3 HEV has not adapted codon usage to its human host. This suggests that an alternative pathway may be used by HEV to facilitate cross-species infection, such as remodeling of tRNA<sup>ome</sup>. It is well-known that viral infection can hijack host cell physiology for corrupting host defense and facilitating viral protein synthesis which is dependent on cellular mature tRNA<sup>ome</sup>.

Recent studies have indicated that tRNA<sup>ome</sup> disturbance has broad implications in many diseases, especially in cancer development and metastasis [23,36]. Further understanding the role of tRNAs in biology and pathogenesis requires easy techniques to detect and quantify these molecules. In this respect, the U-adapter strategy explored in the present study may provide new impetus and may form the basis of novel diagnostic possibilities. Hence, we envision that a convenient method, as the one presented in the current study, may prove instrumental for many aspects of contemporary biomedical research and practice with respect to tRNA biology.

## Supplementary information

## Supplementary Figures

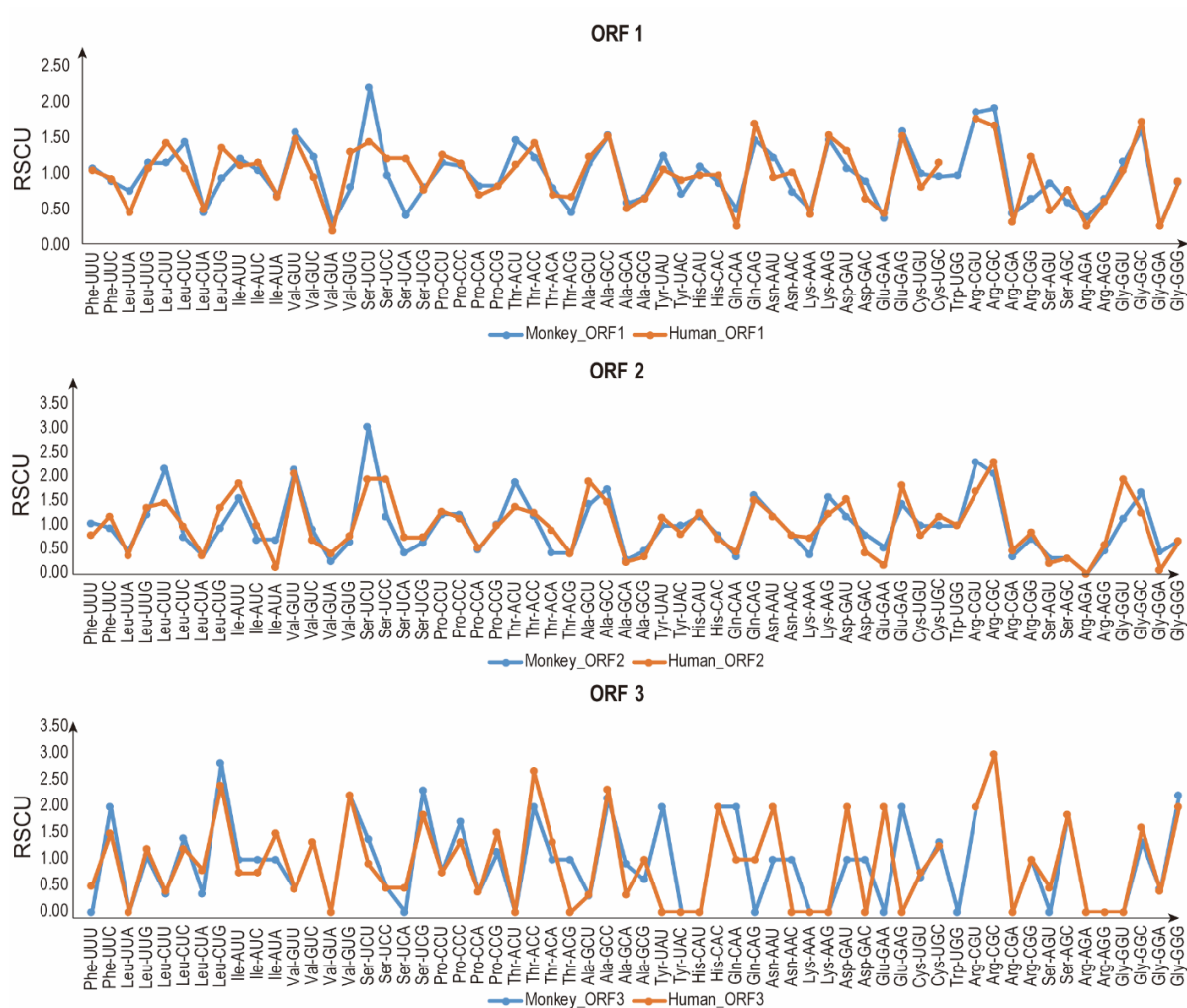


**Fig. S1. Comparative analysis of codon usage bias of HEV isolated from monkey and human.** ORF1, ORF2 and ORF3 of genotype 3 HEV isolated from monkey and human are compared. The majority of codon usage bias are similar between monkey and human according to the index of RSCU.

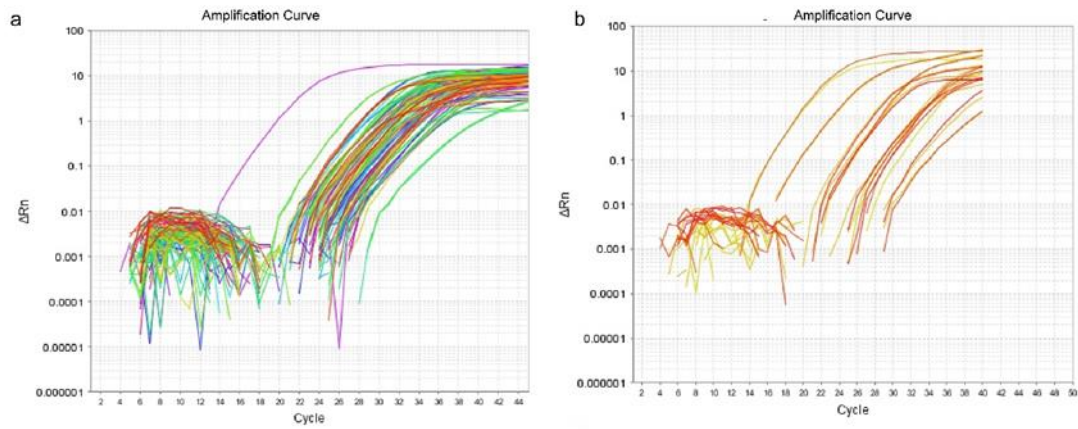


**Fig. S2. Usefulness of U-adaptor to detect 57 types of tRNA sets in human genome.** RNA was isolated from Huh7 cells, deaminacylated and ligated to the U-adaptor (see **Fig. 3**) before being subjected to PCR for specific tRNA species. A) Amplification of tRNA types 1-47 (see table S1). B) Amplification of tRNA type 48-57 (see table S1). The entire complement of 57 types of genomic tRNAs displayed Ct value less as 35 (threshold, 0.1) and we were able to calculate relative abundancy of the different tRNAs present in the RNA of Huh7 cells.

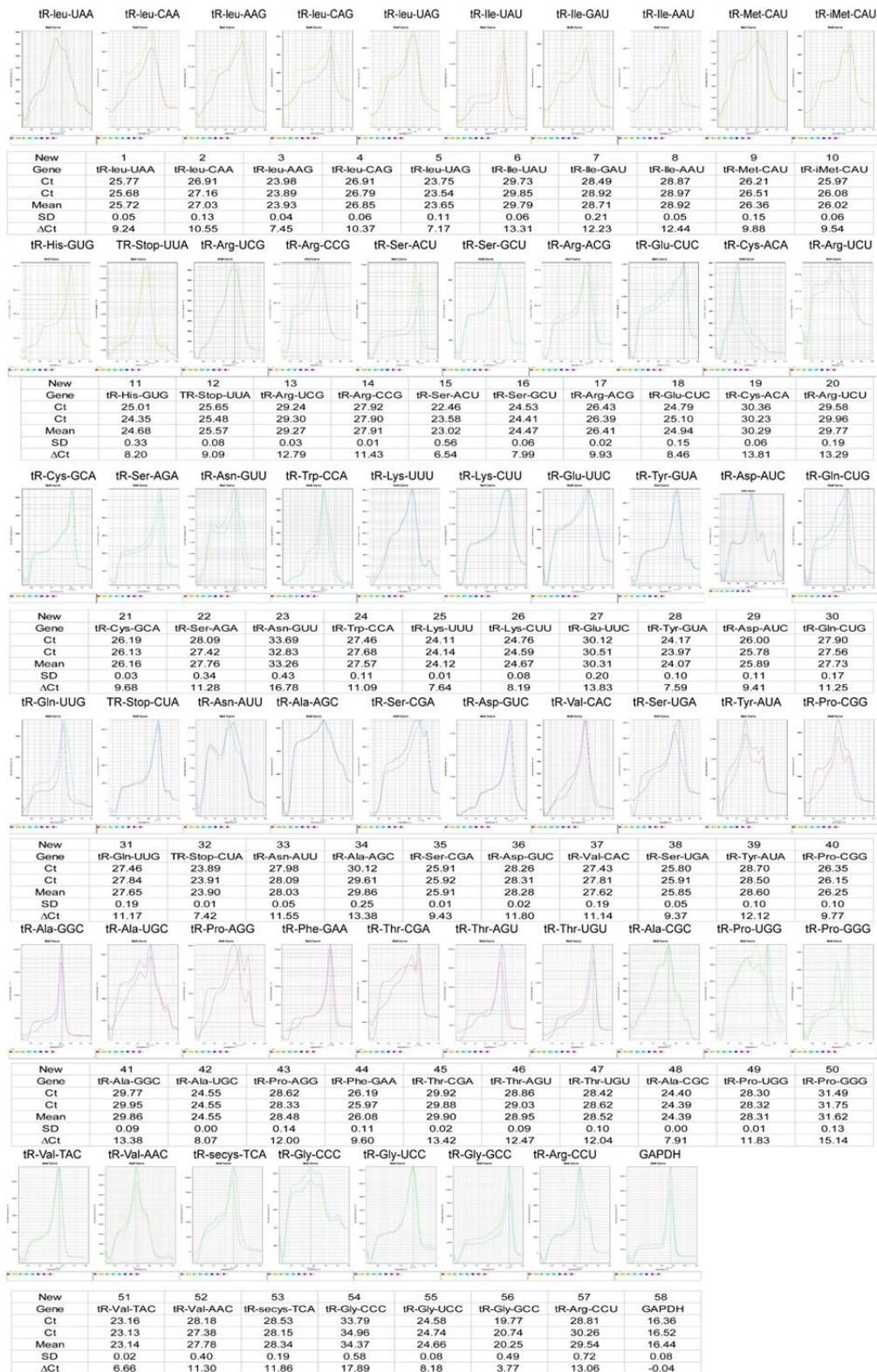
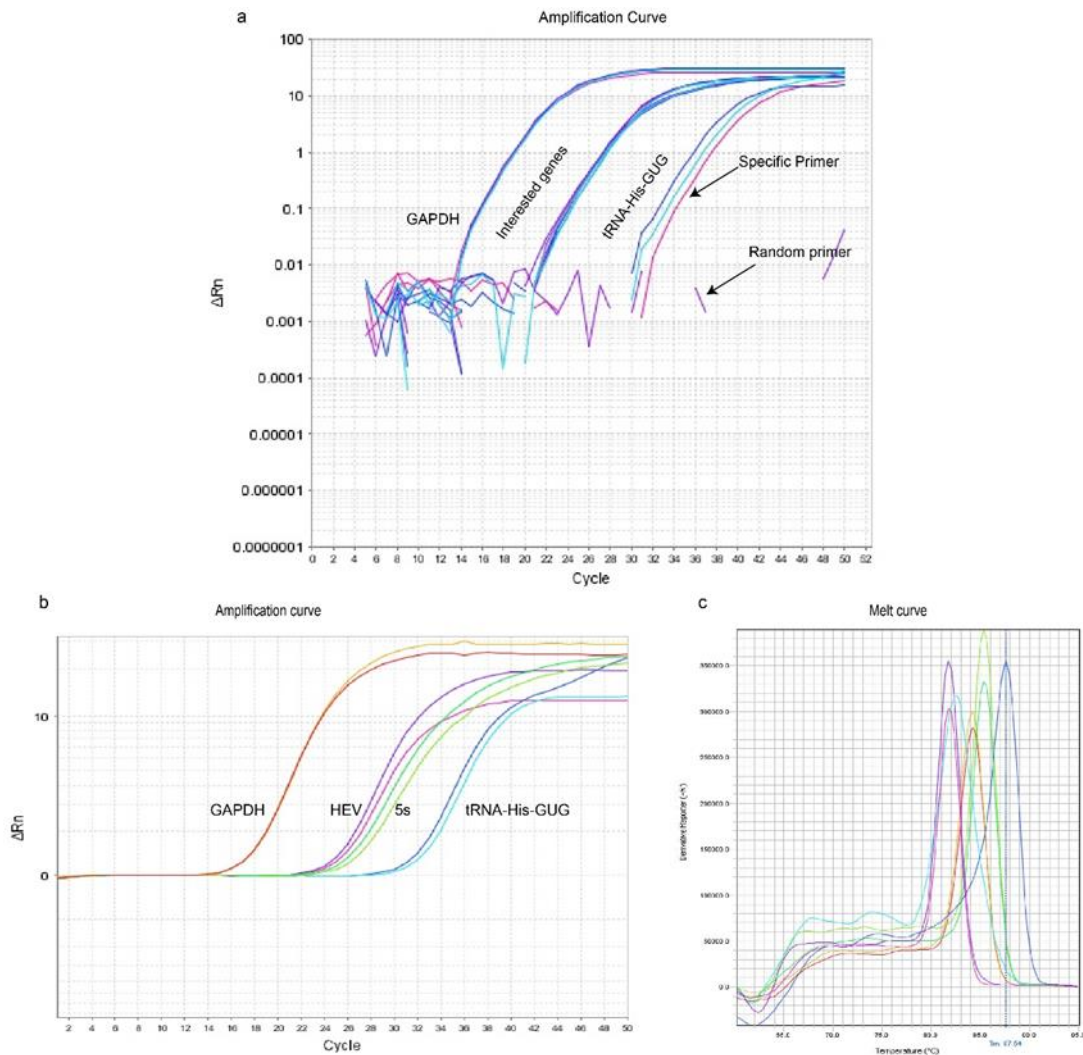
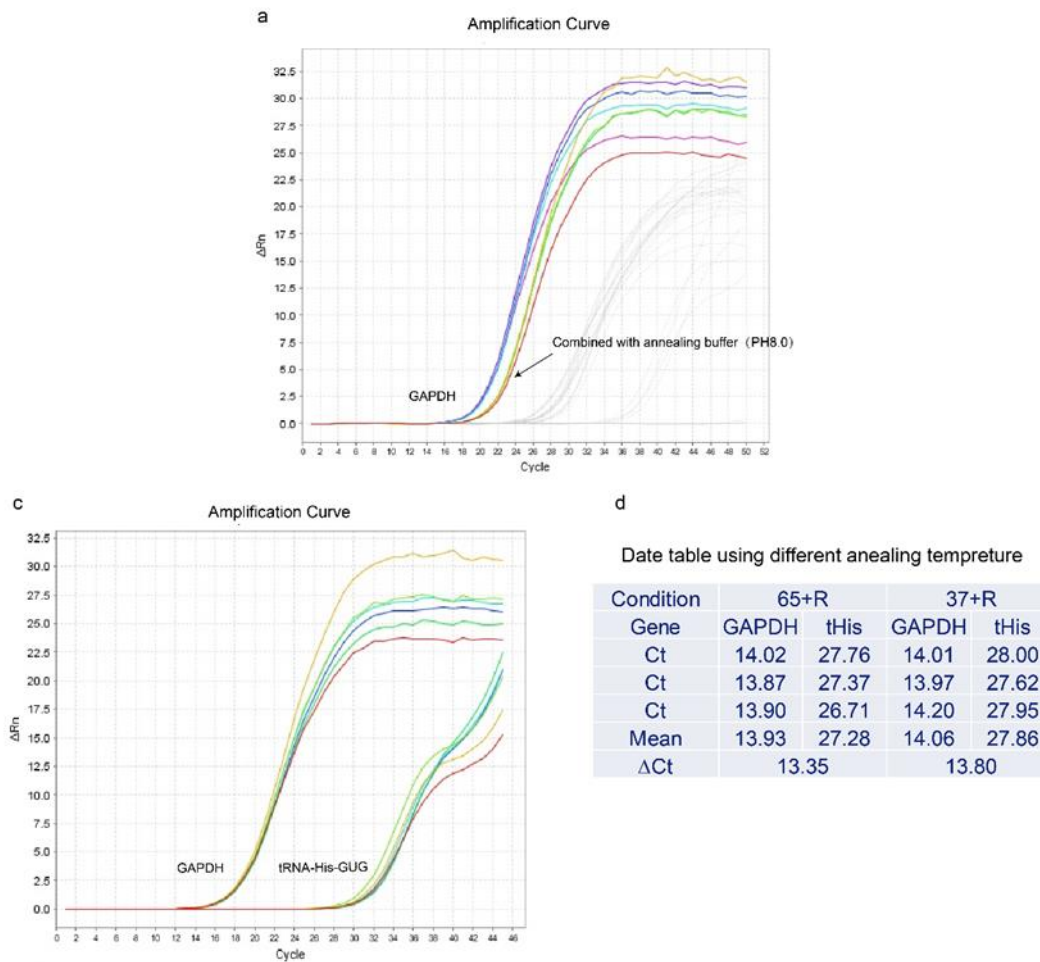


Fig. S3. Melt curves and variation analysis of 57 tRNA types. Amplicons of tRNA transcripts display single peaks and reproducible signals.



**Fig. S4. Specific and quantifiable expression of tRNAs that can be related to HEV infection levels.** Huh7 cells infected with HEV were subjected to the tRNAome detection protocol used in this study. A) Random primers do not allow amplification of products upon reverse transcription, suggesting that product formation is specific. Despite the deacylation, the RNA isolated allows following reverse transcription reproducible amplification of a GAPDH-specific product which allows normalization of samples based on mRNA levels. tRNA-His-GUG is the only tRNA species capable of decoding His-coding codons (CAA & CAU) and thus we considered its expression unlikely to be influenced by factors that would drive alternative expression of different tRNAs capable of decoding the same amino acid. The panel also shows reliable detection of this tRNA, which thus can serve for normalization purposes as well. B) HEV can also be detected in the same RNA preparation that allows detection of tRNA levels and GAPDH determinations and hence results can be linked to directly linked to HEV infection levels as well. C) The melt curves corresponding to the data presented in panel b shows the specific nature of the amplification involved.



**Fig. S5. Failed efforts aimed at protocol optimization.** A) Huh7 cells infected with HEV were subjected to the tRNAome determination, either by the original protocol or through a protocol in which step 11 and 12 were combined. The latter, however, increased mRNA degradation. B) Annealing temperature for reverse transcription has a slight impact on PCR efficiency. C) Comparative analysis of  $\Delta$ Ct values by using different annealing temperatures for linked tRNA and specific reverse primers (65 °C and 37 °C) had slight impact on PCR efficiency.

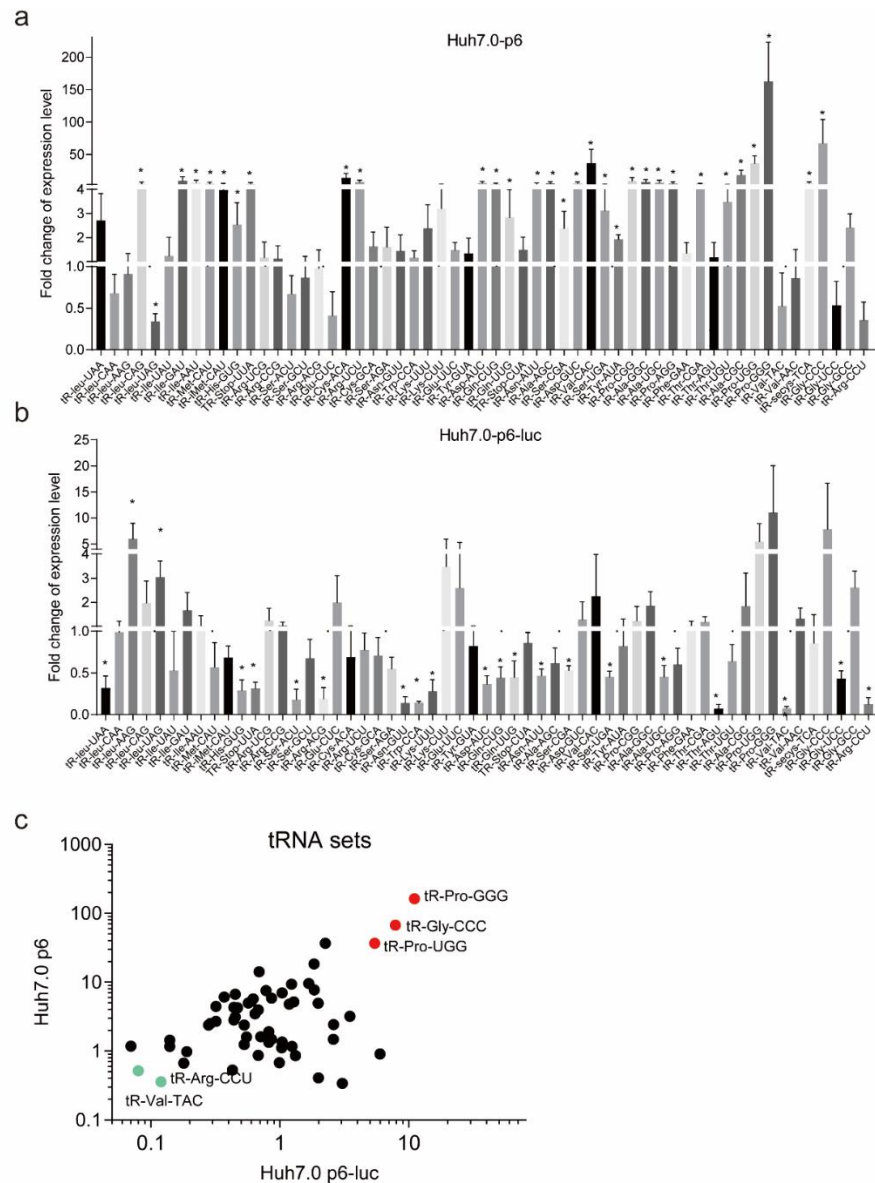


**Fig. S6. Relative transcription levels of 57 tRNA types following infection with either full length HEV or an ORF2-lacking subgenomic replicon.** In this figure a tRNA expression level of 1 indicates that levels following experimental intervention are unchanged as compared to uninfected Huh7 cells, a value between 0 and 1 indicates downregulation of tRNA levels following infection, whereas values in excess of 1 indicate upregulation of the specific tRNA species. A) Following infection with full length HEV (upper half of the panel) major and highly significant remodeling the tRNAome occurs (note that Y axis runs up to 200). B) Following infection with the HEV subgenomic replicon (Huh7-p6-Luc; lower half of the panel) remodeling is much less pronounced (Y axis runs to 20), but significant upregulation and downregulation of various tRNA types is still present. C) Compared to naïve Huh7 cells, tRNA-Gly-CCC, tRNA-Pro-GGG and tRNA-Pro-UGG are concurrently elevated while tRNA-Arg-CCU and tRNA-Val-TAC are concurrently downregulated following full-length and subgenomic HEV infection although magnitude of effects is substantially different. Statistical significance of differences observed was assessed by a Mann-Whitney U test (two tailed). \* $P \leq 0.05$  was indicated as significant.



## Supplementary Tables

Table S1. Key materials used in this study.

Reagent or Resource	Source	Identifier
NEB-5-alpha Competent E. coli	NEB	Cat#: C2987I
HEV Gt3 (Kernow-C1 P6 Clone)	National Institute of Allergy and Infectious Diseases, National Institutes of Health, USA	GenBank: JQ679013
HEV p6-luc (Gaussia luciferase reporter gene)	Wang et al., 2014	N/A
Tris-HCl	Sigma-Aldrich	Cat#10812846001
EDTA	Sigma-Aldrich	Cat#1233508
MgCl <sub>2</sub>	Sigma-Aldrich	Cat# M8266
RNA isolation kit (NucleoSpin@ RNA)	MACHEREY-NAGEL	Cat#740955.250
T4 RNA ligase (dsRNA ligase)	NEB	Cat#M0239L
Prime Script RT Master Mix	Takara	Cat#RR036Q
SYBR™ Green PCR Master Mix	Applied Biosystems™	Cat#4344463
Human: HuH7 (♂) Naïve Cell Line	This paper	N/A
HEV infectious HuH-7 (♂) Cell Line	This paper	N/A
HEV replicon HuH-7 (♂) Cell Line	This paper	N/A
Primers for reverse transcription, see Table S1	This paper	N/A
Primers for qPCR, see Table S1	This paper	N/A
U-adaptor: 5phos/TCGTAGGGTCCGAGGTATTCACGATGrN	Life technology	N/A
tRNA-histidine adaptor: 5phos/TCGTAGGGTCCGAGGTATTCACGATGrU	Life technology	N/A
CodonW	John Peden et al.	<a href="http://codonw.sourceforge.net/">http://codonw.sourceforge.net/</a>

HEMI	Department of Biomedical Engineering, Huazhong University of Science and Technology	<a href="http://hemi.biocuc.koo.org/">http://hemi.biocuc.koo.org/</a>
Python (Pandas, Seaborn, Matplot)	Guido van Rossum et al.	<a href="https://www.python.org/">https://www.python.org/</a>
2(-Delta Delta C(T)) Method	Livak et al.,2001	N/A
Deacylation buffer: 5 × Tris-HCl (100 mM, PH 9.0)	This paper	N/A

**Table S2. Primers used in mature tRNAome detection**

	# Genes	Forward primers (5'-3')	Reverse primer (5'-3')
1.	tRNA-Leu-UAA	RTRYCCGCGTGGGTTCGA	CTTAAGTCCAACGCCTTAACCACTC
2.	tRNA-Leu-CAA	TTCTGGTCTCCRBATGGAGGC	GAGTCTGGCGCCTTAGACCA
3.	tRNA-Leu-AAG	CTCCAGTCTCTTCGGRGGC	AATCCAGCGCCTTAGACCGCTCGGCC
4.	tRNA-Leu-UAG	GCTCCAGTCWYTTTCGRDGGCG	ATCCAGCGCCTTAGACCRCT
5.	tRNA-Leu-CAG	GGTCGCAGTCTCCCCTG	GAACGCAGCGCCTTAGACC
6.	tRNA-Ile-AAU	TAACGCCAAGGTCGYGGGT	TAGCACCACGCTCTRACCAACT
7.	tRNA-Ile-GAU	ATAACACCAAGGTCGCGGG	CAGCACCACGCTCTTACCAAC
8.	tRNA-Ile-UAU	YRATGCCGAGGTTGTGAGTTC	ATAAGTACCGCGCGCTAACC
9.	tRNA-iMet-CAU	ATAACCCAGAGGTCGATGGATCGAAAC	GGCCCAGCACGCTTCC
10.	tRNA-Met-CAU	ARACTGACGCGCTGCCHG	TAATCTGAARGTCSTGAGTTCRARCCTC
11.	tRNA-Stop-UUA	ATCAGAGGGTCCAGGGTTCAA	AGTCTGATGCTCTACCAACTGAACT
12.	tRNA-His-GUG	CAGCAACCTCGGTTCAATC	CGCAGAGTACTAACCACTATACGATC
13.	tRNA-Phe-GAA	AGATCTAAAGGTCCTGGTTCRATCC	CAGTCTAACGCTCTCCCAACTGA
14.	tRNA-Val-AAC	CACGCGAAAGGTCCCCG	TAGGCGAACGTGATAACCACTACAC
15.	tRNA-Val-UAC	CACGCGAAGGTCCTGGG	AAAGCAGAYGTGATAACCACTACTAT
16.	tRNA-Val-CAC	CACGCGAAAGGTCCCCG	TGAGGCGAACGTGATAACCACT
17.	tRNA-Ser-AGA	AGAAATCCATTGGGGTYTCCC	AGTCCATCGCCTTAACCACTCGGC
18.	tRNA-Ser-UGA	AATCCATTGGGGTYTCCCCG	AAGTCCAWCGCCTTAACCACTCG
19.	tRNA-Ser-CGA	AAATCCAATGGGGKYTCCCCG	GAGTCCAACRCCTTAACCACTC
20.	tRNA-Pro-AGG	GGTGCGAGAGGTCCCCG	TAAGCGAGAATCATACCCCTAGACCA
21.	tRNA-Pro-GGG	GGCTGCTGATCCCAGGC	CAGAGCGCACATTCTAACCACTATG
22.	tRNA-Pro-UGG	GTGCGAGAGGTCCCCGG	AAAGCGAGAATCATACCCCTAGACC
23.	tRNA-Pro-CGG	GGGTGYGAGAGGTCCCCG	AAGCGAGAATCATACCCCTAGACC

24.	tRNA-Thr-AGU	TAAACAGGAGATCCTGGGTTCAATC	CTAGACAGGCGCTTTAACCAGCTAA
25.	tRNA-Thr-UGU	TAAACCAGGGGTCGCGAGTT	CAAGACCAGYGCTCTAACCMCT
26.	tRNA-Thr-CGU	CGTAAACMGRAGATCVYGGGTTTC	AGACMGRRCGYTTAACMAACTRRG
27.	tRNA-Ala-CGC	ATGTRYGAGGYCCCGGGTTCR	AAGCATGCGCTCTACCACTG
28.	tRNA-Ala-GGC	CAAACAGGAGATGCTGGATTCAATCC	CAGACAAGTACTTTAACCCACAAAGCC
29.	tRNA-Ala-UGC	YGTRTGAGGYCYCGGGTTCR	AAGCATGCGCTCTACCACTG
30.	tRNA-Ala-AGC	CATGYAYGAGGYCCYGG	TAAGCAYGCGCTCYACCRCT
31.	tRNA-Tyr-AUA	AATCTAAAGACAGAGGTCAAGVYCT	ATAGTCTAATGCTTACTCAGCCATTTTACC
32.	tRNA-Tyr-GUA	CATCCTTAGGTCGCTGGTTCTGA	GTCCTCCGCTCTACCARCTGA
33.	tRNA-Stop-CUA	CATCCTTAGGTCGCTGGTTCTGA	GTCCTCCGCTCTACCARCTGA
34.	tRNA-Gln-UUG	ATCCAGCRATCCGAGTTCRAAT	AGTCCAGAGTGCTAACCACTACACC
35.	tRNA-Gln-CUG	ATCCAGCGATCCGAGTTCRART	AGTCCAGAGTGCTHACCATTACACC
36.	tRNA-Asn-AUU	AACCGAACGGTGAGTAGTTCAAGA	TAGCCGAACGCTCTGACCG
37.	tRNA-Asn-GUU	ACYGAAAGATTRGTGGTKCRAG	ACAGYCRAAYGCGCTAAC
38.	tRNA-Lys-UUU	TTAATCTGAGGGTCCRGGGTTTC	AGTCTGATGCTCTACCRCTGAG
39.	tRNA-Lys-CUU	TAATCYCAGGGTCGTGGGTTTCG	GAGTCYCATGCTCTACCGACTGAG
40.	tRNA-Asp-AUC	CACGAGGTCTTGGGCTGATTC	TGATAAGTACACTCTCTACCACTGAGCT
41.	tRNA-Asp-GUC	TCACGCGGGAGACCGG	AGGCGGGGATACTCACCCTA
42.	tRNA-Glu-UUC	TTCACCSMSGYGGCCCCG	ARCSMSGAACTCTARCCRCTAGAC
43.	tRNA-Glu-CUC	GATTCGGCGCTCTCACCG	CTAACCACTAGACCACCAGGGA
44.	tRNA-Cys-ACA	CTTTAAAGTCATATGTAGCTGGGTTCAA	GTTACATAGCTTATAGAGTTGCTTTTGA
45.	tRNA-Cys-GCA	GATCAAGAGGTCCCYGGTTCA	AGTCAAATGCTCTACCMCTGAGC
46.	tRNA-Trp-CCA	GATCAGAAGGTTGCGTGTTCAAATC	GGAGTCAGACGCGCTACC
47.	tRNA-Arg-ACG	GATCAGAAGATTCYAGTTTCGACTCC	AGTCAGACGCGTTATCCATTGC
48.	tRNA-Arg-UCG	GATCAGAAGATTGMRGGTTCGARTC	AGTCAGACGCCTTATCCATTAGGC
49.	tRNA-Arg-CCG	GAKCWGRRGATTGWGGGTTTCGAGTCC	ARKCWGAYGCCTTATCCATTAGGC
50.	tRNA-Ser-ACU	TAATGCCAGGGTCGAGGTTTCG	AGCAGCACGCTCTAACCAAC
51.	tRNA-Ser-GCU	AATCCATTGTGCTCTGCACGC	AGTCCATCGCCTTAACCACTCG
52.	tRNA-Arg-UCU	AATYCARAGGTTTCYGGGTTTCG	AAGTCCARYGCGCTCRCT
53.	tRNA-Arg-CCU	TAAGCCAGGGATTGTGGGTTTC	AGGCCARTGCCTTATCCATTAGG
54.	tRNA-Gly-GCC	ACGCRGGAGGCCCRGGT	CAGGCRAGAATTCTACCACTGAACC
55.	tRNA-Gly-UCC	CAAGCAGTTGACCCGGGTTTC	AAGGCAGCTATGCTHACCACTATAACC
56.	tRNA-Gly-CCC	CKKGMGMCCCGGGTTTCRA	ARKCKWGMATKMTACCACTRMACC
57.	tRNA-seCys-UCA	AAACCTGTAGCTGTCTAGYGACAGA	AAGCCTGCACCCCAGACC
	U-adaptor	5phos/TCGTAGGGTCCGAGGTATTCACGATGrGrN	

**Table S3. Preparation of qPCR mix.**

Component	Volume	Final amount
2×SYBR™ Green PCR Master Mix	5 µL	
tRNA-X-R/F	3 µL	0.25 pMol <i>per primer</i>
cDNA	2 µL	

**Table S4. Specifics of the qPCR analysis.**

Cycle	Denaturation	Annealing	Extension	Melt Curve
1	95 °C, 10 min			
2-51	95 °C, 10 s	58 °C, 30 s	72 °C, 40 s	
52	95 °C, 1 min			
53				65 °C, 1 min
≥54				+0.3 °C/cycle, 15 s

**Table S5. Interferon stimulated genes (ISGs) used in this study.**

Genes	GenBank #
CH25H	NM_003956
IFITM	NM_003641.4
TRIM	NM_016388.3
OAS/RNaseL	NM_022137.5
Viperin	AF442151.1
Tetherin	NM_003021.4
STAT1	NM_007315.3
STAT2	NM_005419.4
RIG-I	NM_014314.4
cGAS	NM_138441.3

PKR	NM_001135651.3
IRF1	NM_002198.3
IRF3	NM_001571.6
IRF7	NM_001572.5
IRF9	NM_006084.4
SOCS	NM_145071.2
USP18	NM_017414.3

---

## References

- [1] Stern-Ginossar, N. and Ingolia, N.T. (2015). Ribosome Profiling as a Tool to Decipher Viral Complexity. *Annual Review of Virology*, Vol 2 2, 335-349.
- [2] Novoa, E.M., Pavon-Eternod, M., Pan, T. and de Pouplana, L.R. (2012). A Role for tRNA Modifications in Genome Structure and Codon Usage. *Cell* 149, 202-213.
- [3] Ou, X.M., Cao, J.Y., Cheng, A.C., Peppelenbosch, M.P. and Pan, Q.W. (2019). Errors in translational decoding: tRNA wobbling or misincorporation? *Plos Genetics* 15
- [4] Coleman, J.R., Papamichail, D., Skiena, S., Futcher, B., Wimmer, E. and Mueller, S. (2008). Virus attenuation by genome-scale changes in codon pair bias. *Science* 320, 1784-7.
- [5] Lauring, A.S., Acevedo, A., Cooper, S.B. and Andino, R. (2012). Codon Usage Determines the Mutational Robustness, Evolutionary Capacity, and Virulence of an RNA Virus. *Cell Host & Microbe* 12, 623-632.
- [6] Shen, S.H. et al. (2015). Large-scale recoding of an arbovirus genome to rebalance its insect versus mammalian preference. *Proceedings of the National Academy of Sciences of the United States of America* 112, 4749-4754.
- [7] Eschke, K., Trimpert, J., Osterrieder, N. and Kunec, D. (2018). Attenuation of a very virulent Marek's disease herpesvirus (MDV) by codon pair bias deoptimization. *Plos Pathogens* 14
- [8] Li, Y., Qu, C., Yu, P., Ou, X., Pan, Q. and Wang, W. (2019). The Interplay between Host Innate Immunity and Hepatitis E Virus. *Viruses* 11
- [9] Li, M.Q. et al. (2012). Codon-usage-based inhibition of HIV protein synthesis by human schlafen 11. *Nature* 491, 125-145.
- [10] Smith, B.L., Chen, G.F., Wilke, C.O. and Krug, R.M. (2018). Avian Influenza Virus PB1 Gene in H3N2 Viruses Evolved in Humans To Reduce Interferon Inhibition by Skewing Codon Usage toward Interferon-Altered tRNA Pools. *Mbio* 9
- [11] Crick, F.H. (1958) On protein synthesis. In *Symp Soc Exp Biol ed. ^eds*), pp. 8
- [12] Chan, P.P. and Lowe, T.M. (2016). GtRNADB 2.0: an expanded database of transfer RNA genes identified in complete and draft genomes. *Nucleic Acids Research* 44, 184-189.
- [13] Kuhn, C.D., Wilusz, J.E., Zheng, Y.X., Beal, P.A. and Joshua-Tor, L. (2015). On-Enzyme Refolding Permits Small RNA and tRNA Surveillance by the CCA-Adding Enzyme. *Cell* 160, 644-658.
- [14] Zheng, G.Q., Qin, Y.D., Clark, W.C., Dai, Q., Yi, C.Q., He, C., Lambowitz, A.M. and Pan, T. (2015). Efficient and quantitative high-throughput tRNA sequencing. *Nature Methods* 12, 835-837.
- [15] Honda, S., Shigematsu, M., Morichika, K., Telonis, A.G. and Kirino, Y. (2015). Four-leaf clover qRT-PCR: A convenient method for selective quantification of mature tRNA. *Rna Biology* 12, 501-508.
- [16] Kamar, N., Izopet, J., Pavio, N., Aggarwal, R., Labrique, A., Wedemeyer, H. and Dalton, H.R. (2017). Hepatitis E virus infection. *Nature Reviews Disease Primers* 3, 17086.

- [17] Nimgaonkar, I., Ding, Q., Schwartz, R.E. and Ploss, A. (2018). Hepatitis E virus: advances and challenges. *Nature Reviews Gastroenterology & Hepatology* 15, 96-110.
- [18] Meng, X.J. (2016). Expanding Host Range and Cross-Species Infection of Hepatitis E Virus. *PLoS Pathog* 12, e1005695.
- [19] Zhou, J.-h., Li, X.-r., Lan, X., Han, S.-Y., Wang, Y.-n., Hu, Y. and Pan, Q. (2019). The genetic divergences of codon usage shed new lights on transmission of hepatitis E virus from swine to human. *Infection, Genetics and Evolution* 68, 23-29.
- [20] Shukla, P. et al. (2011). Cross-species infections of cultured cells by hepatitis E virus and discovery of an infectious virus-host recombinant. *Proceedings of the National Academy of Sciences of the United States of America* 108, 2438-2443.
- [21] Shukla, P., Nguyen, H.T., Faulk, K., Mather, K., Torian, U., Engle, R.E. and Emerson, S.U. (2012). Adaptation of a genotype 3 hepatitis E virus to efficient growth in cell culture depends on an inserted human gene segment acquired by recombination. *J Virol* 86, 5697-707.
- [22] Zhou, X.Y., Wang, Y.J., Metselaar, H.J., Janssen, H.L.A., Peppelenbosch, M.P. and Pan, Q.W. (2014). Rapamycin and everolimus facilitate hepatitis E virus replication: Revealing a basal defense mechanism of PI3K-PKB-mTOR pathway. *Journal of Hepatology* 61, 746-754.
- [23] Goodarzi, H., Nguyen, H.C.B., Zhang, S., Dill, B.D., Molina, H. and Tavazoie, S.F. (2016). Modulated Expression of Specific tRNAs Drives Gene Expression and Cancer Progression. *Cell* 165, 1416-1427.
- [24] Gamble, C.E., Brule, C.E., Dean, K.M., Fields, S. and Grayhack, E.J. (2016). Adjacent Codons Act in Concert to Modulate Translation Efficiency in Yeast. *Cell* 166, 679-690.
- [25] Coghlan, A. and Wolfe, K.H. (2000). Relationship of codon bias to mRNA concentration and protein length in *Saccharomyces cerevisiae*. 16, 1131-1145.
- [26] van de Moosdijk, A.A.A. and van Amerongen, R. (2016). Identification of reliable reference genes for qRT-PCR studies of the developing mouse mammary gland. *Scientific Reports* 6, 35595.
- [27] Berkhout, B. and van Hemert, F. (2015). On the biased nucleotide composition of the human coronavirus RNA genome. *Virus Research* 202, 41-47.
- [28] Guu, T.S.Y., Liu, Z., Ye, Q.Z., Mata, D.A., Li, K.P., Yin, C.C., Zhang, J.Q. and Tao, Y.J. (2009). Structure of the hepatitis E virus-like particle suggests mechanisms for virus assembly and receptor binding. *Proceedings of the National Academy of Sciences of the United States of America* 106, 12992-12997.
- [29] Johnson, S.C. (1967). Hierarchical clustering schemes. *Psychometrika* 32, 241-254.
- [30] Wang, W.S. et al. (2018). The RNA genome of hepatitis E virus robustly triggers an antiviral interferon response. *Hepatology* 67, 2096-2112.
- [31] Spears, J.L., Gaston, K.W. and Alfonzo, J.D. (2011) Analysis of tRNA editing in native and synthetic substrates. In *RNA and DNA Editing* ed. ^eds), pp. 209-226. Springer

- [32] Gaston, K.W. and Limbach, P.A. (2014). The identification and characterization of non-coding and coding RNAs and their modified nucleosides by mass spectrometry. *Rna Biology* 11, 1568-1585.
- [33] Grelet, S., McShane, A., Hok, E., Tomberlin, J., Howe, P.H. and Geslain, R. (2017). SPot: A novel and streamlined microarray platform for observing cellular tRNA levels. *Plos One* 12
- [34] Schwartz, M.H. et al. (2018). Microbiome characterization by high-throughput transfer RNA sequencing and modification analysis. *Nature Communications* 9, 5355.
- [35] Ankavay, M. et al. (2019). New insights into the ORF2 capsid protein, a key player of the hepatitis E virus lifecycle. *Scientific Reports* 9, 6243.
- [36] Grewal, S.S. (2015). Why should cancer biologists care about tRNAs? tRNA synthesis, mRNA translation and the control of growth. *Biochimica et Biophysica Acta (BBA)-Gene Regulatory Mechanisms* 1849, 898-907.



# Chapter 6

## The biological process of lysine-tRNA charging is therapeutically targetable in liver cancer

**Ruyi Zhang**<sup>1</sup>, Lisanne Noordam<sup>1</sup>, Xumin Ou<sup>1,2</sup>, Buyun Ma<sup>1</sup>, Yunlong Li<sup>1</sup>, Pronay Das<sup>3</sup>, Shaojun Shi<sup>1</sup>, Jiaye Liu<sup>1</sup>, Ling Wang<sup>1</sup>, Pengfei Li<sup>1</sup>, Monique MA Verstegen<sup>4</sup>, D Srinivasa Reddy<sup>3</sup>, Luc JW van Der Laan<sup>4</sup>, Maikel P Peppelenbosch<sup>1</sup>, Jaap Kwekkeboom<sup>1</sup>, Ron Smits<sup>1</sup>, Qiuwei Pan<sup>1</sup>

1. Department of Gastroenterology and Hepatology, Erasmus MC-University Medical Center, Rotterdam, The Netherlands.
2. Institute of Preventive Veterinary Medicine, Sichuan Agricultural University, Chengdu, China.
3. Organic Chemistry Division, CSIR-National Chemical Laboratory, Pune, India.
4. Department of Surgery, Erasmus MC-University Medical Center, Rotterdam, The Netherlands.

*Liver International*, 2021, 1(41): 206-219



## Abstract

**Background & Aims:** Mature transfer RNAs (tRNA) charged with amino acids decode mRNA to synthesize proteins. Dysregulation of translational machineries has a fundamental impact on cancer biology. This study aims to map the tRNAome landscape in liver cancer patients and to explore potential therapeutic targets at the interface of charging amino acid with tRNA.

**Methods:** Resected tumour and paired tumour-free (TFL) tissues from hepatocellular carcinoma (HCC) patients (n = 69), and healthy liver tissues from organ transplant donors (n = 21), HCC cell lines, and cholangiocarcinoma (CC) patient-derived tumour organoids were used.

**Results:** The expression levels of different mature tRNAs were highly correlated and closely clustered within individual tissues, suggesting that different members of the tRNAome function cooperatively in protein translation. Interestingly, high expression of tRNA-Lys-CUU in HCC tumours was associated with more tumour recurrence (HR 1.1; P = .022) and worse patient survival (HR 1.1; P = .0037). The expression of Lysyl-tRNA Synthetase (KARS), the enzyme catalysing the charge of lysine to tRNA<sup>Lys</sup>-CUU, was significantly upregulated in HCC tumour tissues compared to tumourfree liver tissues. In HCC cell lines, lysine deprivation, KARS knockdown or treatment with the KARS inhibitor cladosporin effectively inhibited overall cell growth, single cell-based colony formation and cell migration. This was mechanistically mediated by cell cycling arrest and induction of apoptosis. Finally, these inhibitory effects were confirmed in 3D cultured patient-derived CC organoids.

**Conclusions:** The biological process of charging tRNA-Lys-CUU with lysine sustains liver cancer cell growth and migration, and is clinically relevant in HCC patients. This process can be therapeutically targeted and represents an unexplored territory for developing novel treatment strategies against liver cancer.

**Keywords:** cladosporin, liver cancer, lysine, Lysyl-tRNA Synthetase, tRNA-Lys-CUU, tRNAome

This study was supported by the Dutch Cancer Society for funding a KWF Young Investigator Grant (10140) and the Netherlands Organization for Scientific Research (NWO) for a VIDI grant (No. 91719300) to Q. Pan and Science and Technology Program of Sichuan Province (2020YJ0396) to X. Ou, as well as the China Scholarship Council for funding PhD fellowship to R. Zhang (no. 201808530490), Y. Li (no. 201708530243), P. Li (no. 201808370170), J. Liu (no. 201606240079) and W. Ling (no. 201708530248).

## **Lay summary**

Dysregulation of the protein synthesis machinery in cancer has a major impact on pathophysiology, including cancer development and progression. This study found that the biological process of charging lysine to the corresponding tRNA is altered in liver cancer patients. This in turn can be explored for developing potential therapeutic strategies to treat liver cancer.

## Introduction

Translation, the synthesis of protein from mRNA, is a fundamental biological process required for virtually all cellular functions.<sup>1</sup> A key step in protein synthesis is the recognition of codons by the transfer RNAs (tRNA) charged with their corresponding amino acids.<sup>2,3</sup> tRNAs are transcribed from genomic DNA, have a length of typically 70-90 base pairs and are subjected to post-transcriptional modification. The addition of a common CCA ribonucleotide sequence to the 3' end of tRNA enables charging with an amino acid. Aminoacyl-tRNA synthetases (ARSs) catalyze the charging of amino acids to their cognate mature tRNAs, thereby providing the substrates for global protein synthesis.<sup>4</sup> Theoretically, 61 types of aminoacyl-tRNAs would be required for decoding the 61 triplet codons that specify 20 amino acids. However, the minimally required tRNA species for decoding in real life is usually less than the theoretically calculated number.<sup>5</sup> From the GtRNA 2.0 database, we have recently retrieved 57 human mature tRNA species constituting as the tRNAome.<sup>6</sup>

Dysregulation of gene translation has been well-recognized in cancer development and progression.<sup>7,8</sup> Involvement of tRNAs has been demonstrated in breast cancer, lung cancer and melanoma.<sup>9</sup> However, despite the biological importance of tRNA, it has hardly been investigated in depth, which includes the setting of cancer research. One of the main challenges is that tRNAs are technically difficult to be quantified due to redundancy in genomic copies, extremely short sequences, rigid secondary structure and post-transcriptional modifications. A recent study has analyzed the global expression landscape of tRNAs across 31 cancer types. They used the Cancer Genome Atlas database and analyzed tRNA profiles from miRNA-sequencing data, as an indirect interpretation of tRNA expression.<sup>10</sup> However, the functional forms are the mature tRNAs charged with amino acids. Based on these unique characteristics, we have developed a simplified qRT-PCR assay to quantify the mature tRNAome.<sup>6</sup>

Several enzymes participate in the modification and maturation of tRNAs. ARSs responsible for charging amino acids have evolutionarily conserved enzymatic properties. As protein synthesis is universally accelerated in proliferating malignant cells, the expression levels of many ARSs are increased.<sup>11</sup> In contrast to tRNAs, the functions of ARSs have been widely investigated and various therapeutic approaches have been explored, including the

development of pharmacological inhibitors targeting the catalytic sites.<sup>12</sup> This has provided new avenues for identifying unexplored therapeutic targets and developing effective anti-cancer therapeutics.

Primary liver cancer, mainly consisting of hepatocellular carcinoma (HCC) and cholangiocarcinoma (CC), is among the leading causes of cancer-related deaths with limited treatment options available. In this study, we aim to profile the tRNAome landscape in tumors of HCC patients using our recently developed mature tRNA quantification assay.<sup>6</sup> Secondly, we aim to assess the therapeutic potential of targeting the interface of amino acid charging to tRNA in experimental models of liver cancer.

## Patients, Materials and Methods

### Patient tissues and information

Fresh frozen tumor tissues and paired tumor-free liver (TFL) tissues, located at least 2 cm from the tumor, were collected after surgery or retrieved from the archives of the Department of Pathology, Erasmus Medical Center Rotterdam. The included patients underwent hepatic resection (n = 68) or liver transplantation (n = 1) for HCC at the Erasmus Medical Center between February 1995 and September 2017. Diagnosis of HCC was confirmed by histopathological examination and medical records were reviewed for clinicopathological characteristics including date of first recurrence, HCC-specific death, liver transplantation (if applicable), and last follow-up (**Table 1; Supplementary Table 1**). Tissue samples (n = 21) of healthy livers from organ donors that were used for liver transplantation were used as healthy controls. This study was approved by the Erasmus MC Medical Ethical Committee and adhered to the 1975 Declaration of Helsinki.

### Reagents

The natural product cladosporin was synthesized at the CSIR-National Chemical Laboratory, India, and the NMR data of cladosporin are shown in Supplementary Figure 1. It was dissolved in dimethyl sulfoxide (DMSO) at a stock concentration of 100 mM. L-Arginine, N-acetylcysteine, gastrin, nicotinamide and 3-(4, 5-dimethylthiazol-2-yl)-2, 5-diphenyltetrazolium bromide (MTT) were purchased from Sigma-Aldrich. Dulbecco's modified

Eagle's medium (DMEM, #41965039) and DMEM for SILAC (#88364) were purchased from Life Technologies Europe BV. Advanced DMEM/F-12 (#12634-010) and SILAC Advanced DMEM/F-12 Flex Media, no L-Lysine, no L-Arginine, no glucose, no phenol red (#A2494301) were purchased from Gibco Life Technologies. L-Lysine was purchased from Bio-Connect BV. Matrigel was purchased from BD Bioscience. Cytokines, B27 and N2 were purchased from Invitrogen. EGF, FGF10, and HGF were purchased from Peprotech Company.

### Cell culture and amino acid deprivation

HCC cell lines, including Huh6, Huh7, PLC/PRF/5, SNU398, SNU449, SNU182, Hep3B, HepG2, and human embryonic kidney epithelial cell line 293T (HEK293T) were grown in DMEM (GIBCO Life Technologies), supplemented with 10% (v/v) fetal bovine serum (Hyclone Technologies), 100 units/mL of penicillin and 100 µg/mL of streptomycin. To establish a lysine deprivation model, L-arginine (0.4 mM; the same concentration as in DMEM) was firstly added to "DMEM for SILAC" (L-lysine and L-arginine deficiency) medium, and then different concentrations of L-

Table 1. Patient characteristics	
Characteristics	HCC patients (n=69)
<b>Age at treatment (years)</b>	
Mean ± SD	60 ± 16
Median (range)	64 (11-82)
<b>Sex – no. (%)</b>	
Male	41 (59.4)
Female	28 (40.6)
<b>Race – no. (%)</b>	
White	58 (84.1)
African	6 (8.7)
Asian	4 (5.8)
Not reported	1 (1.4)
<b>Etiology – no. (%)</b>	
No known liver disease	20 (29.0)
Alcohol	16 (23.2)
NASH	8 (11.6)
Hepatitis B	8 (11.6)
Hepatitis C + Alcohol	5 (7.2)
Hepatitis B + Alc/HepC/HepD/NASH	4 (5.8)
Hepatitis C	4 (5.8)
Fibrolamellar HCC	3 (4.4)
Other	1 (1.5)
<b>Hepatitis status – no. (%)</b>	
Hepatitis B or C positive	21 (30.4)
Chronic Hepatitis B	12 (17.4)
Chronic Hepatitis C	10 (14.5)
<b>Cirrhosis – no. (%)</b>	
Yes	50 (72.5)
No	19 (27.5)
<b>Differentiation grade – no. (%)</b>	
Good	8 (11.6)

lysine were added. All the cells were incubated at 37°C in a humidified atmosphere containing 5% CO<sub>2</sub>. Authentication of all the cell lines was performed using the short tandem repeat genotyping assay at the Department of Pathology, Erasmus Medical Center Rotterdam. The mycoplasma-free status was regularly commercially checked and confirmed by GATC Biotech Konstanz, Germany.

To further test the deprivation of each of the nine essential amino acids, culture medium was prepared with Earle Balanced Salt Solution (H9269, Sigma-Aldrich), Glucose and MEM vitamin solution (100x) (M6895, Sigma-Aldrich). Different amino acids except for the deprived one were then added, according to the concentrations of amino acids in regular complete DMEM medium (#41965, Gibco) <sup>13,14</sup>

### **Organoid culture and lysine deprivation**

The establishment and maintenance of human normal liver and liver tumor organoids were performed as described.<sup>15</sup> Three batches of normal liver organoids (HLO-1, HLO-2, HLO-3) were derived from intrahepatic biliary epithelial progenitor cells. Three batches of liver tumor organoids (CCO-1, CCO-2, CCO-3) were derived from tumor tissue of CC patients. The use of human organoids was approved by the Erasmus MC Medical Ethical Committee. To establish a lysine deprivation model, L-Arginine (0.7 mM; the same concentration as in Advanced DMEM/F-12 DMEM) was firstly added to "Advanced DMEM/F-12 without L-Lysine, L-Arginine and no-phenol red" medium, and then different concentrations of L-Lysine were added. The culture medium for human normal liver organoids and liver tumor organoids was basic medium (Advanced/F12 DMEM with 1% penicillin/streptomycin, 1% L-Glutamine and 10 mM HEPES) supplemented with 1:50 B27 supplement (without vitamin A), 1:100 N2 supplement, 1 mM N-acetylcysteine, 10% (vol/vol) R-spondin 1 (conditioned medium), 10 mM nicotinamide, 10 nM recombinant human [Leu<sup>15</sup>]-gastrin I, 50 ng/ml recombinant human EGF, 100 ng/ml recombinant human FGF10, 25 ng/ml recombinant human HGF, 10 μM Forskolin and 5 μM A83-01. The medium was replaced every 3 days and passage was performed according to the growth of organoids.

### **Lentiviral shRNA packaging and transduction**

To perform gene knockdown, pLKO.1-based lentiviral vectors (Sigma-Aldrich) targeting KARS and a scrambled control vector (shCTR) were obtained from the Erasmus Medical Center



for Biomics. Lentiviral pseudoparticles were generated in HEK293T cells. After 2 days of transfection with the lentiviral particles, Huh7 and SNU398 cells were subsequently selected by 3 µg/mL puromycin (Sigma-Aldrich) for one week. The knockdown efficiency was confirmed by qRT-PCR and Western Blot. The target sequences of selected shRNAs are listed in Supplementary Table 2.

### RNA isolation and qRT-PCR

RNA was isolated by the NucleoSpin® RNA isolation kit of Macherey-Nagel (Dueren, Germany) and reverse-transcribed into cDNA using the PrimeScript™ RT Master Mix (Perfect Real Time, Takara, cat# RR036A), according to the manufacturer's instructions. mRNA quantification by qRT-PCR was performed using SYBR™ Green PCR Master Mix (ThermoFisher) in a StepOnePlus™ Real-Time PCR System (Applied Biosystems), using 12.5 ng cDNA per reaction, with the following conditions: 50°C for 2 min, 95°C for 2 min, then 38 cycles of 95°C for 15 s, 58°C for 15 s, 72°C for 1 min, followed by the Melt Curve stage of 95°C for 15 s, 60°C for 1 min and a 0.7°C step-wise increase until 95°C was reached. Means of technical replicates were used for calculation of gene expression by  $2^{-\Delta\Delta T}$  method. The geometric mean of three housekeeping genes (*HPRT1*, *GUSB*, *PMM1*) was used to normalize gene expression in patient samples. For experimental models, *GAPDH* was used as a reference gene to normalize target gene expression. Primer sequences used for qPCR of mRNA are included in Supplementary Table 3. For tRNA quantification, we used the isolation protocol and primer sequences that we previously described.<sup>6</sup>

### Western blotting

Cells were lysed in Laemmli sample buffer with 0.1 M DTT and heated for 5-10 min at 95°C, followed by loading and separation on an 8-15% sodium dodecyl sulphate-polyacrylamide gels. After 90 min running at 100V, proteins were electrophoretically transferred onto a polyvinylidene difluoride membrane (Invitrogen) for 1.5 h with an electric current of 250 mA. Subsequently, the membrane was blocked with blocking buffer (Li-COR, Lincoln, USA) mixed with PBST in the ratio of 1:1. This was followed by overnight incubation with rabbit anti-KARS (Sanbio BV, #14951-1-AP), anti-Cleaved-Caspase 3 (CST, #9664S), and mouse anti-β-actin (Santa Cruz, #SC-47778) at 4°C. The membrane was washed 3 times with PBST, which was followed by incubation for 1 h with anti-rabbit (1:10000) or anti-mouse

(1:5000) IRDye conjugated secondary antibodies (Li-COR, Lincoln, USA) at room temperature. Blots were assayed for actin content as standardization of sample loading and scanned and quantified by Odyssey infrared imaging (Li-COR, Lincoln, USA). The results were analyzed with Image Studio software.

### **Analysis of cell cycle**

Huh7 and SNU398 cells ( $5 \times 10^5$ /well) were plated in 6-well plates and incubated overnight to attach to the bottom, and then serial concentrations of Lysine were added. After incubated 3 days, cells were harvested and fixed in cold 70% ethanol for 2 h at 4°C. The cells were washed twice with PBS and incubated with 50  $\mu$ L RNase (100  $\mu$ g/ml) at 37°C for 30 min. Finally, cells were incubated with 250  $\mu$ L Propidium Iodide (PI, 50  $\mu$ g/ml) at room temperature for 5 min. The samples were analyzed immediately by flow cytometry using a FACS Canto (BD Biosciences), and the cell cycle was analyzed by using FlowJo\_V10 software.

### **Colony and organoid formation assay**

For colony formation assay, HCC cells were harvested and suspended in medium, then seeded into 6-well plates (1000 cells/well) and the medium was refreshed every 4 days. After two weeks of culture, formed colonies were washed with PBS and fixed by 70% ethanol, followed by counterstaining with crystal violet (Sigma-Aldrich) and washed with PBS. Colony sizes were measured microscopically by digital image analysis.

For the organoid formation assay, intact organoids were first digested into single cells, and then seeded into 48-well plates (3000-5000 cells/well). After two weeks, the sizes and numbers of formed organoids were calculated.

### **MTT and Alamar Blue assays**

HCC cells were seeded in 96-well plates at a concentration of  $3 \times 10^3$  cells/well in 100  $\mu$ L medium. Upon indicated treatment, cell viability was analyzed by adding 5 mg/mL MTT for 4 h. After discarding the cell supernatant, 100  $\mu$ L DMSO was added followed by 10 min shaking. Absorbance was determined using the microplate absorbance reader (Bio-Rad, Hercules, CA, USA) at a wavelength of 490 nm.

Organoids were split in the ratio of 1:10 for daily culture and seeded in 24-well plates. On the third or seventh day of indicated treatment, organoids were incubated with Alamar

Blue (Invitrogen, 1:20 in Advanced/F12 DMEM) for 4 h, and the medium was collected for measurement of the metabolic activity of the organoids. Absorbance was determined by a fluorescence plate reader (CytoFluor® Series 4000, Perseptive Biosystems) at the excitation of 530/25 nm and emission of 590/35 nm.

### Cell migration assay

Cells ( $5 \times 10^5$ /well) were collected and suspended in 300  $\mu$ L of serum-free medium after the indicated treatment for 48 h. Cells were placed into the upper chamber of a 24-transwell (8- $\mu$ m pore size; Corning, #353097), and 700  $\mu$ L of DMEM containing 20% FBS was added into the lower chamber. Cells were allowed to migrate to the bottom chamber for 24 h. Next, cells that remained on the apical side of the chamber were gently scraped off using wetted cotton swabs. Subsequently, cells were fixed with 4 % paraformaldehyde solution for 30 min and stained with 0.1% crystal violet for 30-60 min. Finally, the cells were observed with a microscope, and images were obtained.

### Statistics

All statistical analyses were performed using Graphpad (Version 5 for Windows, San Diego, CA) and R Statistical software (Version 3.6.1 for Windows, Foundation for Statistical Computing, Vienna, Austria). The expression level of genes between HCC and TFL patient tissues were compared using the Wilcoxon matched pairs test. For functional experiments, potential differences between the experimental groups were analyzed using the Mann-Whitney test. The correlation analysis was performed in RStudio with the “corplot” package, using Spearman’s correlation coefficient. For creating heatmaps, RStudio was used with the “gplots” and “pheatmap” packages. Survival analysis was performed by the Kaplan-Meier method and the Cox proportional hazards model. Time to the event, either HCC-specific death or HCC-recurrence, was calculated from the day of surgery. If the event of interest did not occur, data were censored at the time of the last follow-up, or if a patient underwent liver transplantation, at the time of liver transplantation. Used statistical tests are indicated in the figures. P-values < 0.05 were considered significant, and indicated with a single asterisk. P-values < 0.01 were indicated with double asterisks and P-values < 0.001 were indicated with triple asterisks.

## Results

### Profiling the tRNAome landscape in patient HCC tumors identified the potential clinical significance of tRNA-Lys-CUU

Mature tRNAs with a CCA tail are charged with amino acids to elongate protein synthesis and are thus biologically most relevant. To focus on this functional species of tRNAs, we recently developed a specific qRT-PCR quantification assay involving the removal of attached amino acids and a universal adaptor ligated to the CCA tail.<sup>6</sup> We profiled the tRNAome consisting of 57 mature tRNA species in 69 pairs of tumors and matched TFL tissues of HCC patients. The heatmap depicted in **Figure 1A** shows the relative expression levels of 57 mature tRNAs in 69 pairs of tumors and TFL tissues. Significantly differentially expressed tRNAs between tumor and TFL tissues were listed in Supplementary Table 4, showing that many tRNAs were down-regulated in tumors. Interestingly, the patterns of tRNA expression were closely clustered and correlated based on the individual tissues (**Supplementary Figure 2A**), suggesting that different members of the tRNAome function cooperatively in protein translation. Next, the expression of each individual tRNA in tumor tissues was further analyzed to identify potential associations with clinical features. We found that tRNA-Lys-CUU has potential clinical relevance. Kaplan–Meier analysis showed that high expression of tRNA-Lys-CUU in tumor appears to associate with more tumor recurrence (**Figure 1B**) and worse patient survival late after tumor resection (**Figure 1C**), although not statistically significant. Interestingly, univariate Cox regression analysis indicated that high levels of tRNA-Lys-CUU in tumor were significantly associated with increased rates of tumor recurrence (HR 1.1;  $p = 0.022$ ) and HCC-specific death (HR 1.1;  $p = 0.0037$ ) (**Figure 1B, C**; lower panels). In multivariate analysis together with clinicopathological characteristics, tRNA-Lys-CUU expression in tumor was an independent negative prognostic factor for both HCC-specific survival and HCC recurrence (**Supplementary Figure 2B**). As TFL tissues from HCC patients often show various signs of liver pathology, we also included healthy controls of liver tissues obtained from organ donor livers. The expression of tRNA-Lys-CUU was significantly higher in HCC tumor tissues compared with the healthy liver tissues (**Supplementary Figure 2C**).

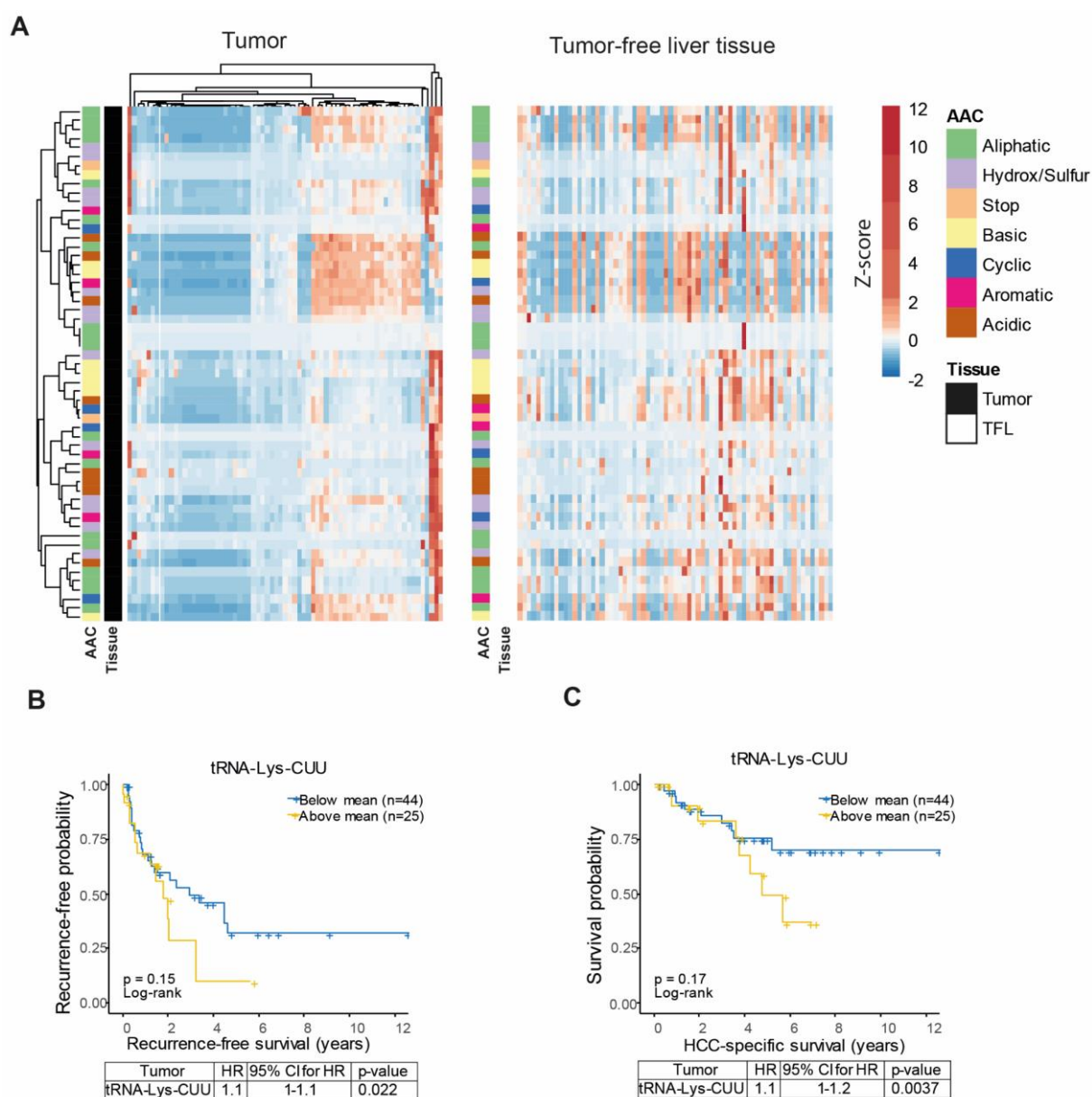


**Figure 1 Profiling tRNAome in HCC patients identified tRNA-Lys-CUU having potential clinical significance.**

(A) Heatmap showing the mean expression (z-score normalized per tRNA species, represented in color, as indicated in the legend) of 57 tRNA in tumor and TFL tissues, respectively. Both rows (tRNA) and columns (patient samples) of tRNAs expressed in tumors (left panel) are hierarchically clustered using correlation distance and complete linkage. Rows and columns of tRNAs expressed in TFL (right panel) were ordered according to the rows and columns in the tumor heatmap. (B-C) Kaplan Meier analysis and Cox regression analysis of tumor recurrence (B) and HCC-specific survival (C) in relation to tRNA-Lys-CUU expression. The panels below the survival graphs show the results of univariate Cox regression analysis. HR: Hazard Ratio; AAC: amino acid class. HCC: hepatocellular carcinoma; TFL: tumor free liver; CI: confidence interval.

## Elevated expression of Lysyl-tRNA synthetase in patient HCC tissues

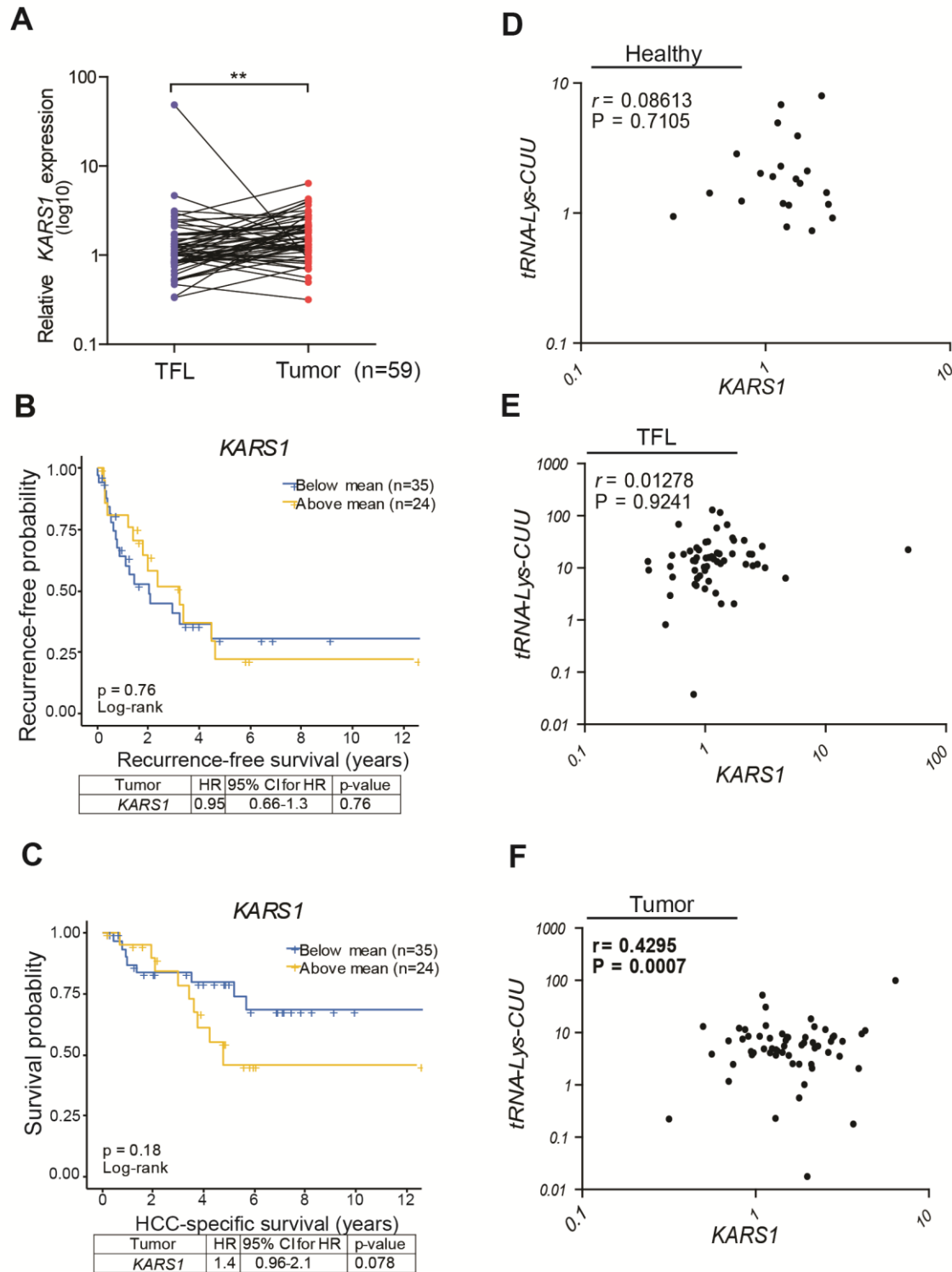
Lysyl-tRNA synthetase (KARS), encoded by *KARS1*, catalyzes the charging of lysine to tRNA-Lys-CUU and tRNA-Lys-UUU.<sup>16</sup> We found that mRNA expression levels of *KARS1* were significantly higher in HCC tumor tissues compared with paired TFL tissues (n = 59) (**Figure 2A**; **Supplementary Figure 3A**), and this was further confirmed by analysis of the publically available GEPIA database (**Supplementary Figure 3B**). When analyzing the association with clinical outcomes, we found no evidence for a relation with tumor recurrence (**Figure 2B**). However, there was a trend of association with patient survival. In univariate Cox regression analysis patients with high *KARS1* expression seemed to have an increased death rate (HR 1.4; **Figure 2C**), although statistically not significant ( $p = 0.078$ ). Importantly, multivariate analysis revealed a significantly increased risk of death for high *KARS1* expressers (HR 1.66;  $p=0.021$ ) (**Supplementary Figure 3C**). Altogether, these associations between the expression levels of tRNA-Lys-CUU and *KARS1* in tumor tissues and prognosis of HCC patients indicate a potential clinical relevance for the interface of charging lysine with its tRNA in liver cancer. In addition, we found a significant positive correlation of tRNA-Lys-CUU and *KARS1* in tumor tissues (**Figure 2F**), but not in healthy liver tissues or TFL tissues (**Figure 2D, E**). This promoted us to further explore their functions in experimental models.

---

### Figure 2 KARS1 expression and clinical relevance in HCC patients.

(A) mRNA expression of *KARS1* in HCC tumors compared to paired TFL tissues (n = 59). (B-C) Kaplan Meier analysis of tumor recurrence (B) and HCC-specific survival (C) in relation to *KARS1* expression in tumors. The panels below the survival graphs show the results of univariate Cox regression analysis. (D-F) Correlation analysis between the expression levels of tRNA-Lys-CUU and *KARS1* in healthy organ donor liver tissues (D, n = 21), TFL (E) and paired HCC tissues (F, n = 59), respectively. \*\* $P < 0.01$ , by the Wilcoxon matched pairs test. *KARS1*: Lysyl-tRNA Synthetase; HCC: hepatocellular carcinoma; TFL: tumor free liver; HR: Hazard Ratio; CI: confidence interval.

Figure 2



6

## Knockdown of KARS inhibits HCC cell growth

To study the functionality of KARS in liver cancer cells, we first examined *KARS1* expression at mRNA and protein levels (**Figure 3A, B**), and tRNA-Lys-CUU expression across eight HCC cell lines (**Supplementary Figure 4A**). All HCC cell lines expressed higher *KARS1* RNA levels, and all except one expressed higher levels of tRNA-Lys-CUU than healthy liver organoids. Huh7 and SNU398 cell lines with high levels of *KARS1* and tRNA-Lys-CUU expression were selected for further experimentation. We used the lentiviral RNA interference approach to investigate the effects of silencing KARS on HCC cells, and selected the two shRNAs with optimal efficiency for KARS knockdown (**Supplementary Figure 4B,C; Figure 3C,D**). KARS knockdown attenuated the overall growth of Huh7 and SNU398 cells (**Figure 3E**), and dramatically inhibited single cell-based colony formation (**Figure 3F**). Silencing of KARS arrested cell cycling at the G0/G1 phase (**Figure 3G**) and induced cell apoptosis as indicated by drastically increased levels of cleaved-Caspase 3 protein (**Figure 3C**).

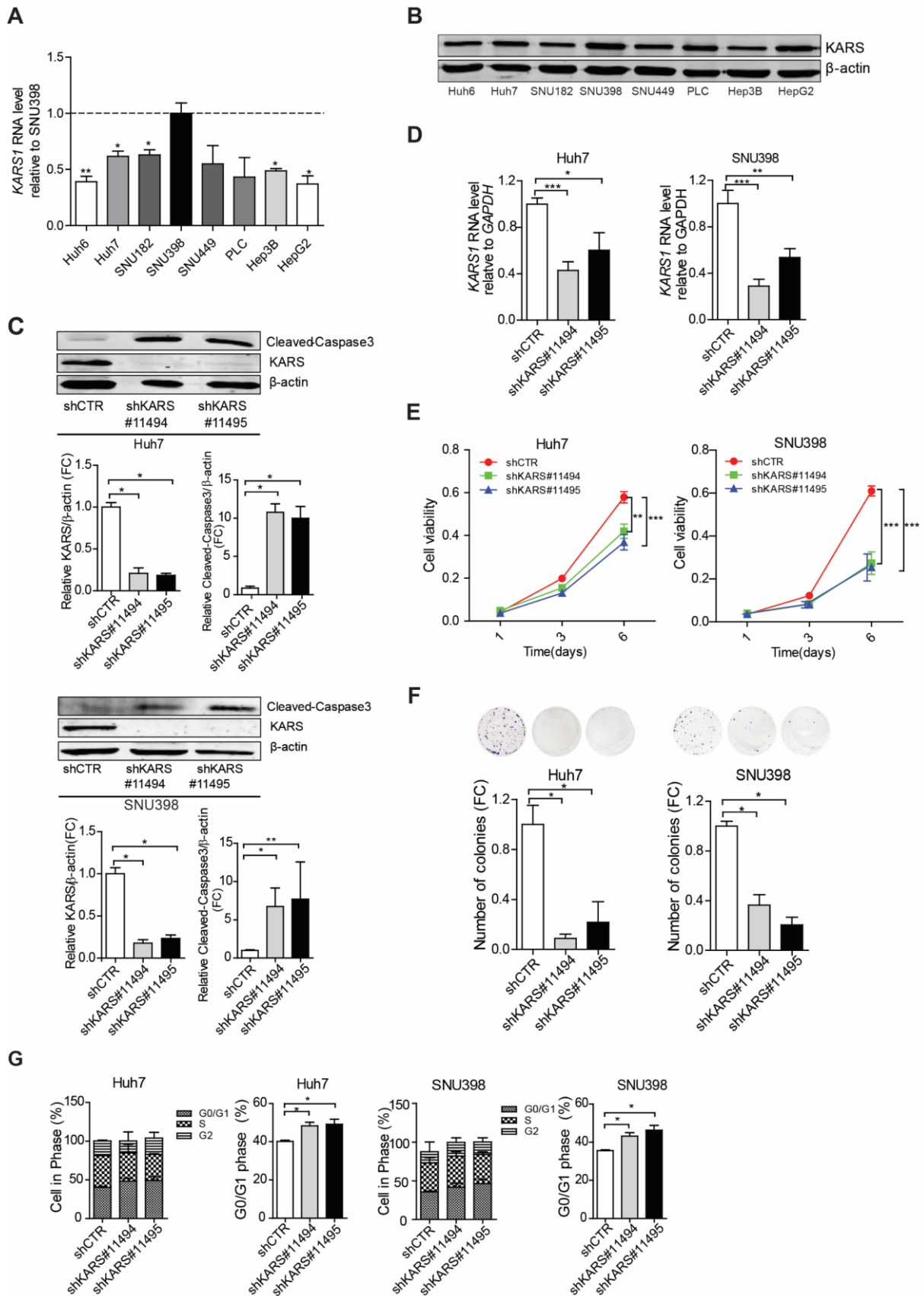
---

### Figure 3 The effects of KARS knockdown on HCC cell lines.

(A) Relative expression of *KARS1* mRNA in HCC cell lines compared to SNU398 (n = 4-6). (B) KARS protein expression in HCC cell lines. (C) Protein expression levels of KARS and cleaved-Caspase 3 in Huh7 and SNU398 HCC cells following shRNA mediated knockdown of KARS. The intensity was quantified relative to  $\beta$ -actin (n = 4-8). (D) *KARS1* mRNA expression following shRNA mediated knockdown quantified by qRT-PCR (n= 4-10). (E) Effects of KARS knockdown on cell growth measured by MTT assay following 1, 3 and 6 days of culture (n = 11, 22). (F) KARS knockdown affects the number of single cell formed colonies as assayed 2 weeks following seeding (n = 5). (G) The effect of KARS knockdown on cell cycling was measured by Propidium Iodide staining, and the fraction of cells in G0/G1 was quantified (n = 4-6). Quantification of C, D, and F data of knockdown groups were relative to the shCTR group. Data are presented as mean  $\pm$  SEM. \**P* < 0.05; \*\**P* < 0.01; \*\*\**P* < 0.001, by the Mann-Whitney test. HLO: healthy liver organoids; HCC: hepatocellular carcinoma; FC: fold change; *KARS1*: Lysyl-tRNA Synthetase.

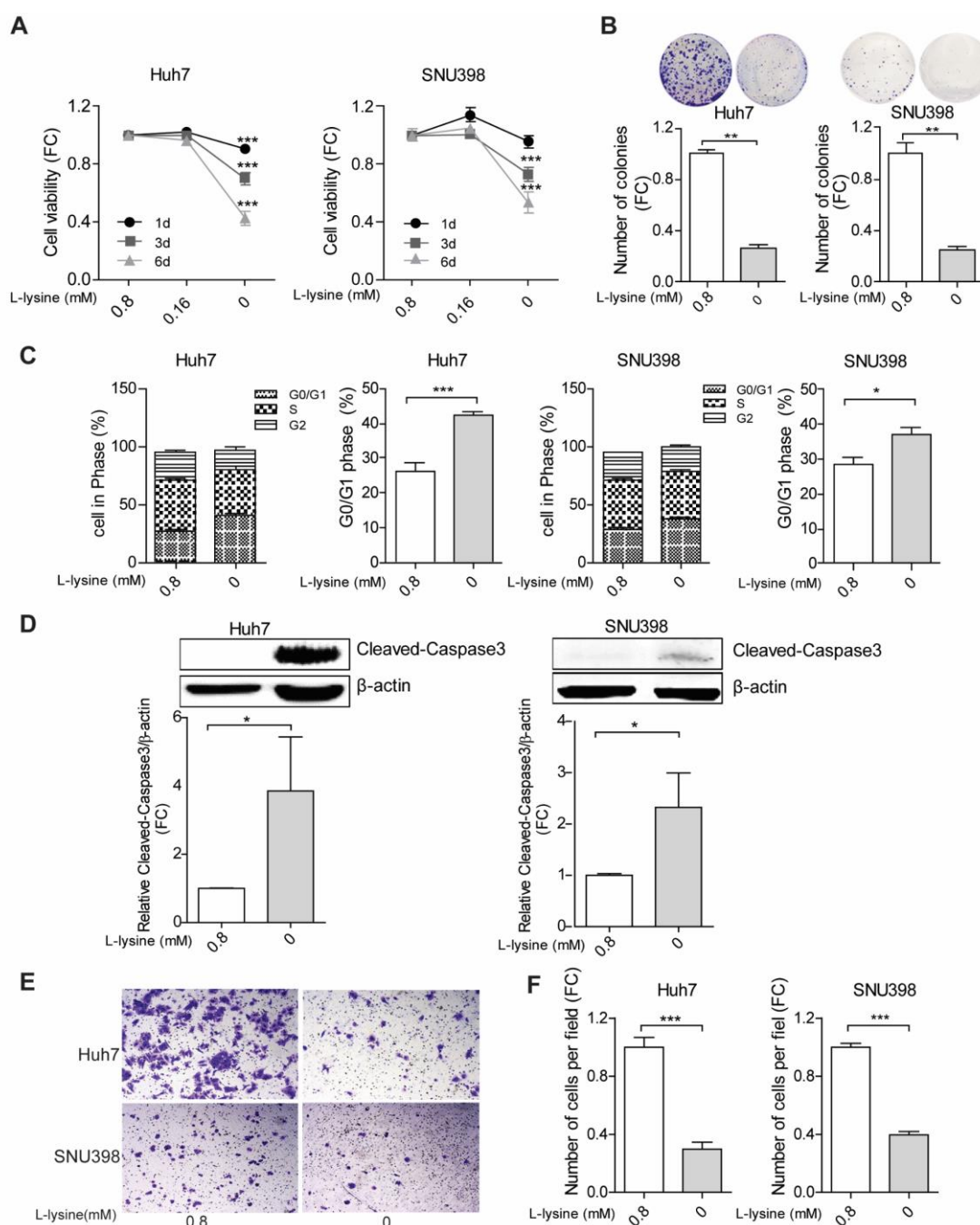


Figure 3



## Lysine deprivation inhibits HCC cell growth and migration

Lysine is the substrate which is ligated by KARS to tRNA-Lys-CUU. We first examined the effects of complete deprivation of each of the nine essential amino acids in SNU398 cells. We found that deprivation of any of the nine amino acids had some effects on cell growth, but lysine deprivation exerted the strongest inhibitory effect (**Supplementary Figure 5A**). In single cell-based colony formation assay, deprivation of lysine, methionine or valine but not any of the other six amino acids had significant inhibition, and lysine deprivation again exerted the strongest effect (**Supplementary Figure 5B**). These results collectively indicated lysine is most essentially required. Next, compared to the normal concentration (0.8 mM) of lysine in cell culture medium, lowering the concentration to 0.16 mM had minimal effects on HCC cell growth (**Figure 4A**). However, complete deprivation of lysine dramatically inhibited overall cell growth (**Figure 4A**) and single cell-based colony formation (**Figure 4B**). This was associated with increased G0/G1 cell cycle arrest (**Figure 4C**), and increased cell apoptosis indicated by the dramatic increase of Caspase 3 cleavage (**Figure 4D**). Interestingly, lysine deprivation also attenuated HCC cell migration in the transwell system, an assay recapitulating some features of cancer cell invasion and metastasis (**Figure 4E, F**).



**Figure 4** The effects of lysine on HCC cell lines.

(A) The effects of lysine on cell growth measured by MTT assay following 1, 3 and 6 days of culture ( $n = 20$ ). (B) Lysine affects the number of single cell-derived colonies as assayed 2 weeks following seeding ( $n = 6$ ). (C) The effects of lysine on cell cycling were measured by Propidium Iodide staining, and the fraction of cells in G0/G1 was quantified ( $n = 6-9$ ). (D) Protein expression levels of cleaved-Caspase 3 in Huh7 and SNU398 HCC cells. The intensity was quantified relative to  $\beta$ -actin ( $n = 5$ ). Huh7 and SNU398 cells were cultured with or without lysine for 3 days. (E) Representative images of migrating cells with or without lysine and (F) quantification of the number of migrating cells ( $n = 10-20$ ). Quantification of A, B, D and F data without lysine groups were relative to with lysine group. Data are presented as mean  $\pm$  SEM. \* $P < 0.05$ ; \*\* $P < 0.01$ ; \*\*\* $P < 0.001$ , by the Mann-Whitney test. HCC: hepatocellular carcinoma; FC: fold change.

## **Cladosporin, a pharmacological inhibitor of KARS, inhibits HCC cell growth and migration**

As the biological process of charging lysine with tRNA sustains HCC cells, we next examined whether this can be therapeutically targeted. We evaluated the effects of the well-established KARS pharmacological inhibitor cladosporin, an antifungal antibiotic isolated from *Cladosporium cladosporioides* and *Aspergillus flavus*. Recently we accomplished a scalable synthesis of the active natural product cladosporin, producing more than 2 grams of the compound.<sup>17</sup> We found the 50% inhibitory concentrations of cladosporin to be 104  $\mu$ M and 70  $\mu$ M in Huh7 and SNU398 cells, respectively (**Supplementary Figure 6**). Treatment with different concentrations of cladosporin (0-200  $\mu$ M) dose-dependently inhibited Huh7 and SNU398 cell growth (**Figure 5A**). Consistently, cladosporin significantly inhibited single cell-based colony formation (**Figure 5B**), induced Caspase 3 cleavage (**Figure 5C**), and affected cell migration (**Figure 5D, E**). Combination of cladosporin treatment and *KARS1* gene silencing further augmented the inhibitory effects (**Supplementary Figure 7A, B**).

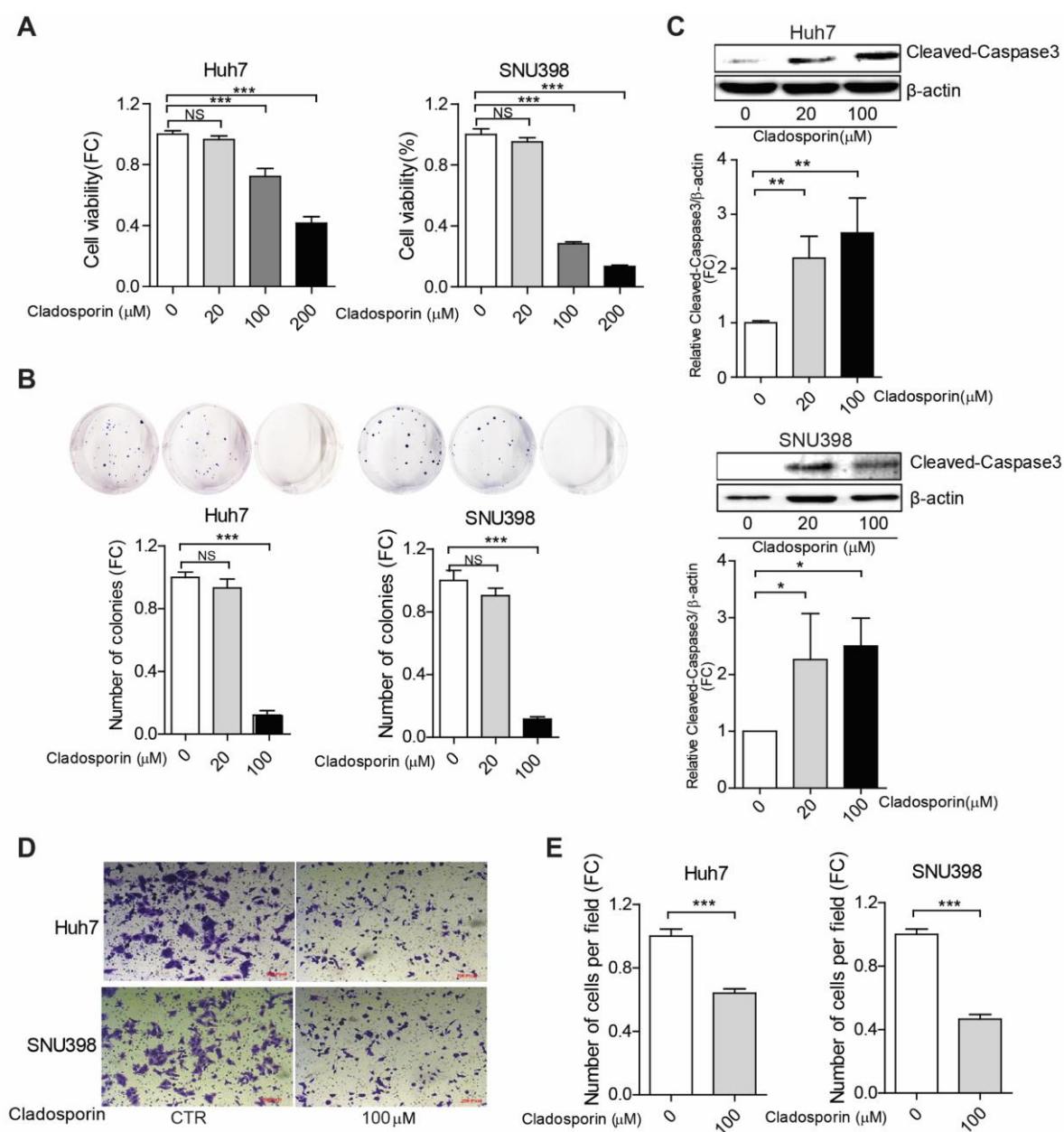


**Figure 5** The effects of cladosporin treatment on HCC cell lines.

(A) Huh7 and SNU398 cells were treated with different concentrations of cladosporin for 3 days. Cell viability was measured by MTT assay ( $n = 12$ ). (B) Cladosporin affects the number of single cell-derived colonies as assayed 2 weeks following seeding ( $n = 6-8$ ). (C) Protein expression levels of cleaved-Caspase 3 in Huh7 and SNU398 cells, and the intensity was quantified relative to  $\beta$ -actin ( $n = 5$ ). Huh7 and SNU398 were treated with cladosporin for 3 days. (D) Representative images of migrating cells with cladosporin and (E) quantification of the number of migrating cells ( $n = 20-25$ ). Quantification of all data were relative to the negative control group. Data are presented as mean  $\pm$  SEM. \* $P < 0.05$ ; \*\* $P < 0.01$ ; \*\*\* $P < 0.001$ , by the Mann-Whitney test. HCC: hepatocellular carcinoma; FC: fold change.

## **Clinical relevance of KARS expression in CC patients and inhibition of patient CC organoids growth by lysine deprivation or treatment with cladosporin**

We have included three batches of healthy human liver organoids and three batches of CC organoids. Because organoids are very difficult to be cultured from HCC tissues, we used liver tumor organoids cultured from CC patients,<sup>18</sup> of which the *KARS1* expression levels were shown in **Figure 6A**. Importantly, similar to what we found in HCC patients, *KARS1* expression was significantly higher in patient CC tumor tissues based on the GEPIA database. However, in this small CC cohort, *KARS1* expression was not significantly associated with patient's prognosis (**Supplementary Figure 8**). Thus, we tested the effects of lysine deprivation or cladosporin on patient-derived CC organoids in 3D culture. We found significant growth inhibition of three independent batches of CC organoids, with the effects being more robust after 7 days of treatment (**Figure 6B, C; Supplementary Figure 9A, B**). In parallel, we examined the effects on three independent batches of healthy human liver organoids. Although lysine deprivation or cladosporin treatment also inhibited growth of the healthy liver organoids, the effects were significantly stronger on the CC organoids (**Figure 6D, E; Supplementary Figure 9C, D**). Next, we tested the effects on organoid initiation. Lysine deprivation or cladosporin treatment significantly inhibited the number and the size of initiated CC organoids from single cells (**Figure 6F, G; Supplementary Figure 9E-H**). Interestingly, the responsiveness varies among organoids derived from different patients (**Figure 6**). Taken together, the biological process of charging tRNA with lysine sustains HCC cell growth and can be therapeutically targeted as demonstrated in cell culture and patient organoid models.

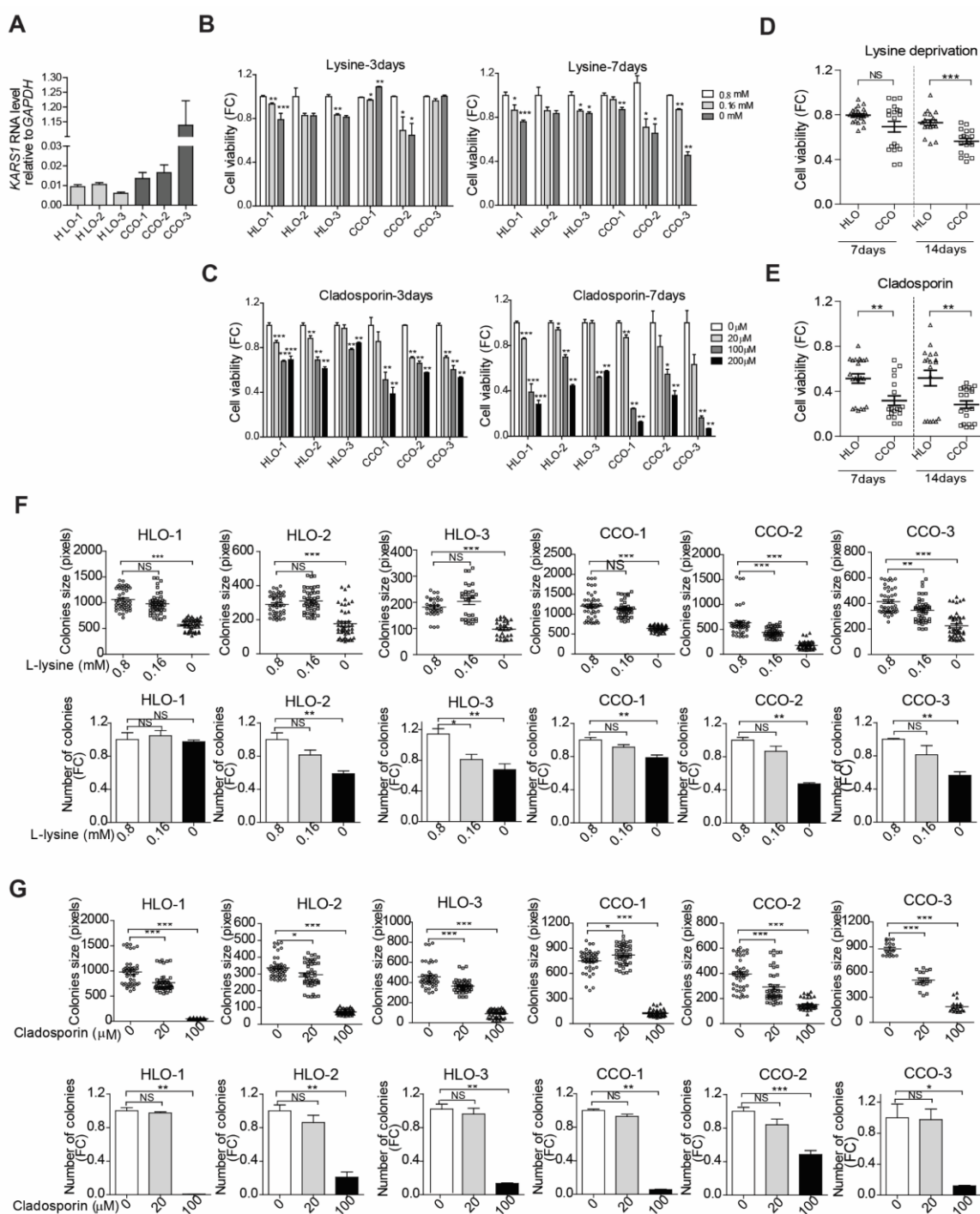


**Figure 6** Lysine deprivation or treatment with cladosporin affects the growth of patient-derived CC organoids.

(A) Relative expression of KARS1 mRNA in patient CC organoids and human healthy liver organoids (HLO) ( $n = 5-11$ ). Effects of (B) lysine deprivation or (C) cladosporin treatment on cell viability were measured by Alamar blue assay after culturing 3 or 7 days ( $n = 4-12$ ). Organoids were treated with (D) lysine deprivation or (E) cladosporin ( $100 \mu\text{M}$ ) for 7 or 14 days. The results depicts the mean viability of CC organoids (CCO-1, CCO-2, CCO-3) compared with the mean viability of healthy liver organoids (HLO-1, HLO-2, HLO-3) ( $n = 18-24$ ). (F) Lysine deprivation or (G) cladosporin treatment affects organoid initiation as assayed 2 weeks following seeding. The number ( $n = 4-10$ ) and size ( $n = 18-45$ ) of organoids

after culturing for 14 days were calculated. Quantification of the data target groups were relative to the negative control group. Data are presented as mean  $\pm$  SEM and dots represent individual organoid cultures. \* $P < 0.05$ , \*\* $P < 0.01$ , \*\*\* $P < 0.001$ , by the Mann-Whitney test. CCO: cholangiocarcinoma organoid; HLO: human liver healthy organoid; FC: fold change.

## Discussion

tRNAs perform central functions in protein synthesis. Intuitively, dysregulation of tRNA expression is expected to associate with pathogenesis, such as cancer development.<sup>19-21</sup> However, due to the intrinsic complexity and lack of easy techniques for quantification, the role of tRNAs in cancer has rarely been studied. The recently launched tRNAscan-SE program that can accurately identify genomic tRNA sequences has facilitated the development of tRNA-based quantification methods.<sup>22</sup> High-throughput sequencing techniques have been used to quantify the tRNAome at transcriptional level,<sup>23</sup> but they are highly dependent on programming and very specialized reagents. We have recently developed a novel qPCR method that specifically quantifies mature tRNAs.<sup>6</sup> We think this form of tRNAs is functionally most relevant as these mature tRNAs are directly charged with amino acids and thus facilitate protein synthesis.

In this study, we first profiled the tRNAome consisting of 57 mature tRNA species in 69 pairs of tumors and matched TFL tissues of HCC patients. We surprisingly observed that many tRNAs are down-regulated in HCC tumor compared to TFL. This is different from previous studies comparing tRNA expression between cancer cell lines and noncancerous cell lines or human cancer and healthy non-cancer tissues.<sup>21</sup> Of note, TFL tissues represent a unique intermediate state between healthy liver tissue and tumor tissue. In many HCC patients, TFL is chronically inflamed and cirrhotic (**Table 1**). Indeed, expression levels of tRNA-Lys-CUU in both tumors and tumor-free liver tissues of HCC patients were significantly enhanced compared to healthy livers. Interestingly, we found that the expression patterns of tRNAs were closely clustered and correlated within individual tissues, suggesting that they function cooperatively and collectively in protein synthesis. Among these tRNAs, we found that high expression of tRNA-Lys-CUU in HCC tissue appears to associate with poor clinical outcomes, although the effects were moderate and our cohort is too small to draw firm conclusions.



Recently, amino acid deprivation therapy has been widely explored as potential anti-cancer strategy. Among different approaches in interrupting amino acid metabolism in cancer cells, enzymatic depletion is the most promising strategy. This results in deprivation of these exogenously supplied nutrients, and thus inhibits tumor growth.<sup>24</sup> Deprivation of amino acids including asparagine,<sup>25</sup> arginine,<sup>26</sup> glutamine,<sup>27</sup> methionine,<sup>28,29</sup> and phenylalanine<sup>30</sup> has been tested for cancer treatment in experimental models. As we have observed that high expression levels of tRNA-Lys-CUU potentially associates with poor outcomes in HCC patients, we tested whether deprivation of the substrate lysine functionally affects HCC cells in experimental models. Lysine deprivation inhibited overall cell growth, migration and single cell-based colony formation, and induced cell cycling arrest and cell apoptosis in two HCC cell line models. These effects were further confirmed in 3D cultured patient CC organoids. Importantly, we found HCC cells are more sensitive to deprivation of lysine compared to other essential amino acids. Our findings together with those of previous studies<sup>13,31</sup> suggest the potential of developing anti-cancer strategies based on amino acid deprivation. However, the dependency of particular amino acid varies among different cancer types, and normal cells also require these amino acids to survive. Therefore, which amino acid to be targeted and which therapeutic modality to be used should be further studied.<sup>32</sup>

The structures and functions of ARSs that catalyze the charging of amino acids to cognate tRNAs have been widely studied. A systematic analysis of the expression of ARSs has identified that many of them are highly expressed in tumors and form networks with cancer-associated genes. This also supports the fact that protein synthesis is universally accelerated in proliferating malignant cells.<sup>33,34</sup> We found that the expression of *KARS1* was significantly upregulated in HCC compared to TFL tissues. Similar results were also observed in CC patients. We postulate that the abundance of KARS will enhance the efficiency of catalyzing lysine to charge the tRNAs including tRNA-Lys-CUU. This will accelerate protein translation of genes enriched with cognate codons, therefore promoting cancer cell growth. This hypothesis is supported by our findings in two HCC cell lines that knockdown of KARS inhibited cell growth, migration and colony formation, and induced cell cycle arrest and apoptosis.

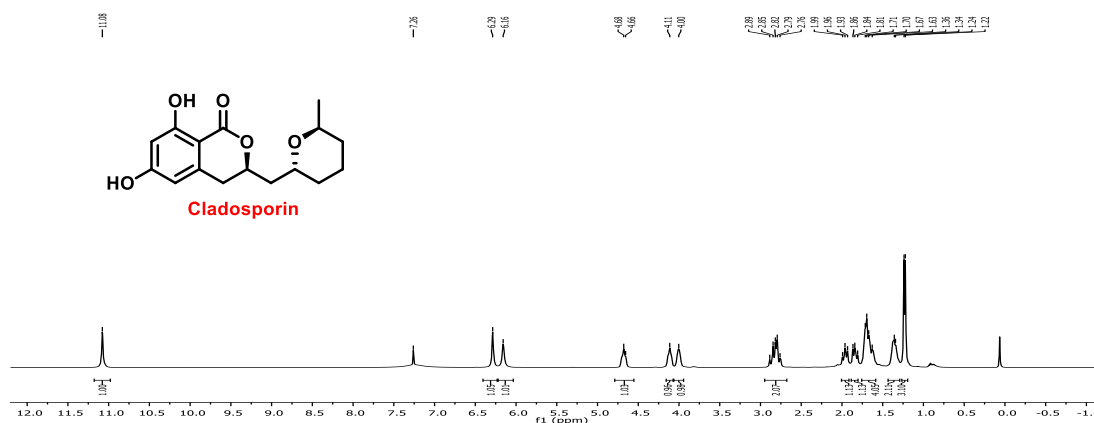
ARSs targeted drug development has mainly been examined in the field of infectious diseases by exploiting species-specific structural diversity and catalytic activity.<sup>35</sup> For example, ARS-inhibitors mupirocin and AN2690 are FDA-approved for treatment of gram-positive

bacterial skin infections and fungal nail infections, respectively.<sup>12</sup> With respect to oncology, ARSs represent overlooked targets for therapeutic development against cancer.<sup>34</sup> In this study, we tested a specific pharmacological KARS inhibitor cladosporin, an antifungal antibiotic isolated from *Cladosporium cladosporioides* and *Aspergillus flavus*.<sup>36,37</sup> We found that cladosporin can effectively inhibit the growth of HCC cell lines and CC organoids, consistent with the results from KARS knockdown and lysine deprivation. Interestingly, the responsiveness to lysine deprivation or cladosporin varies among CC organoids derived from different patients. However, the activity of cladosporin towards human KARS is 100-fold lower than towards KARS of the malaria parasite.<sup>38-40</sup> Cladosporin is currently explored as a potential treatment for malaria, but whether it is also applicable for treating cancer remains uncertain.<sup>17</sup> Another important consideration is that ARSs are essentially required for maintaining the physiological functions of normal cells. Targeting human ARSs for treating cancer is expected to cause substantial side effects. Indeed, in healthy human liver organoids, we observed that both lysine deprivation and cladosporin treatment resulted in notable inhibitory effects, although to a lesser extent than those in CC organoids. Based on our HCC cell lines and CC organoids, cells expressing higher level of KARS appear to be more sensitive to KARS or lysine targeted inhibition. Collectively, our results support the notion that ARSs are viable targets for anti-cancer drug development, but this is just the start in unveiling their biological functions in cancer and exploring possible therapeutic modalities.

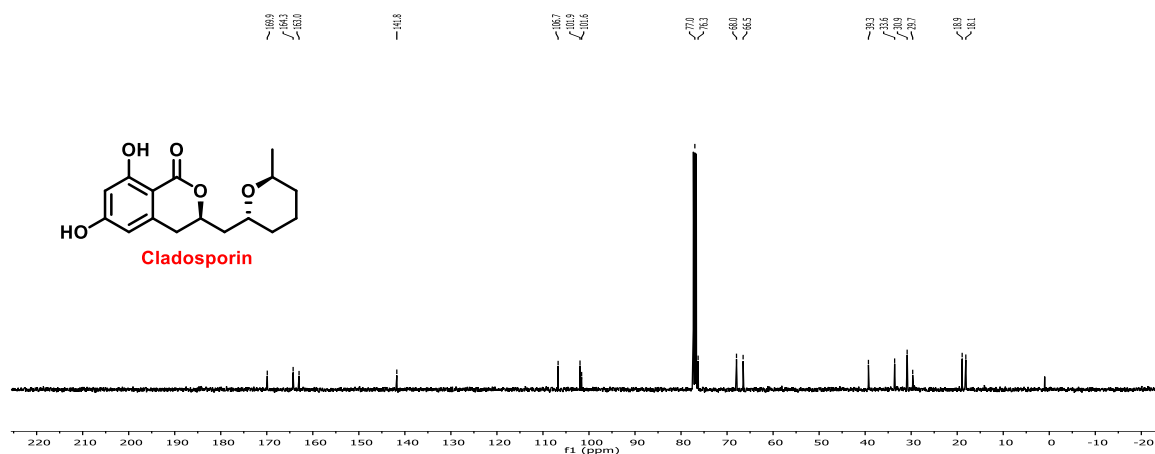
In summary, we have profiled the tRNAome landscape in human HCC tumors and identified that high expression of tRNA-Lys-CUU in tumor is potentially associated with poor clinical outcomes. KARS expression is upregulated in both patient HCC and CC tumor tissues. In experimental models of HCC cell lines and CC patient-derived organoids, biological or pharmacological targeting the interface of charging lysine to tRNA-Lys-CUU inhibits cancer cell growth and migration. These findings bear important implications of exploring such unexplored territories for developing novel therapeutics against liver cancer.

## Supplementary information

## Supplementary Figures

<sup>1</sup>H NMR of Cladosporin in 400 MHz

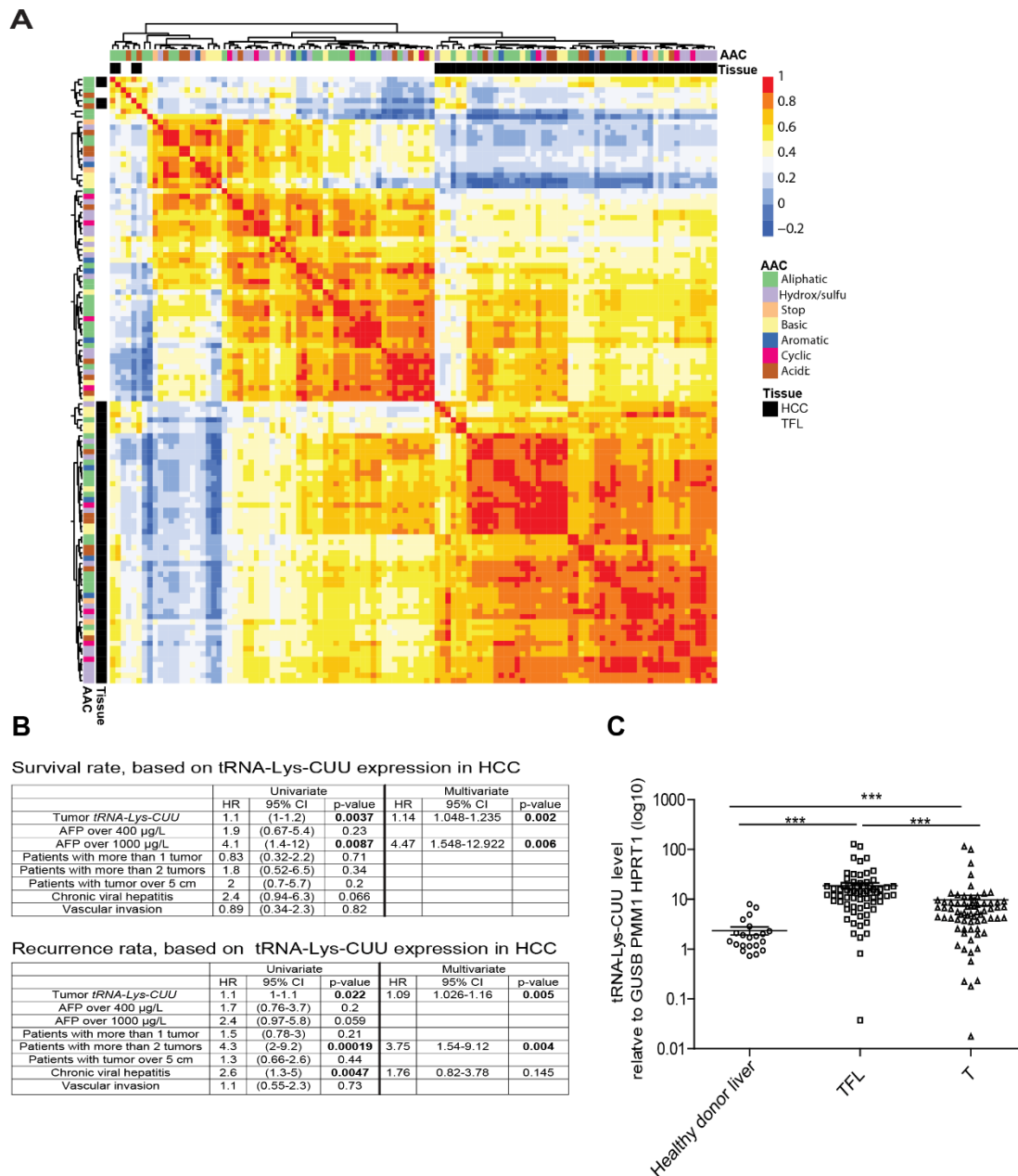
<sup>1</sup>H NMR (400 MHz, CDCl<sub>3</sub>) δ 11.08 (s, 1H), 6.29 (s, 1H), 6.16 (s, 1H), 4.68-4.66 (m, 1H), 4.11 (s, 1H), 4.00 (s, 1H), 2.89 – 2.76 (m, 2H), 1.90 (dt, *J* = 23.0, 12.8 Hz, 2H), 1.68 (dd, *J* = 21.9, 12.2 Hz, 4H), 1.36 -1.34 (m, 2H), 1.23 (d, *J* = 6.4 Hz, 3H).

<sup>13</sup>C NMR of Cladosporin in 100 MHz

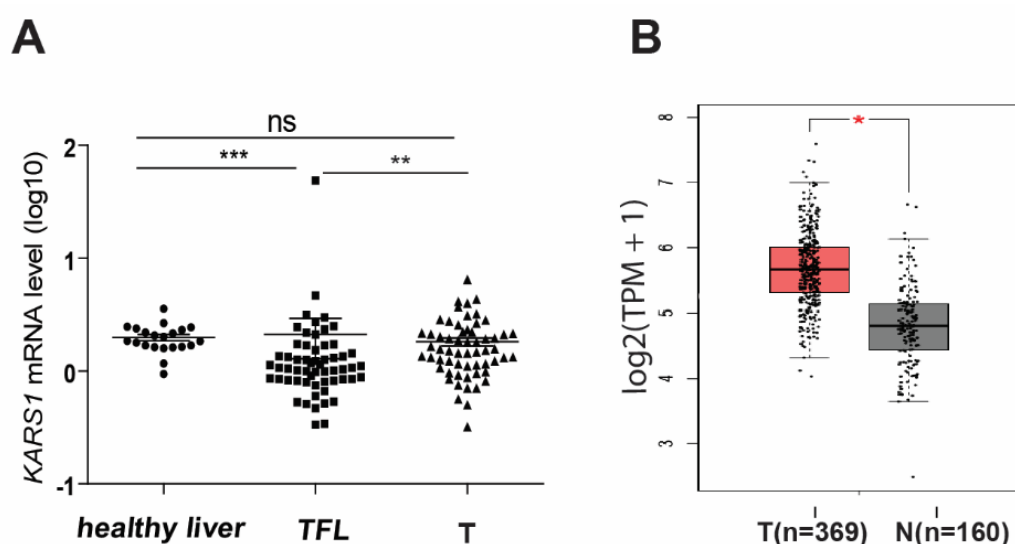
<sup>13</sup>C NMR (100 MHz, CDCl<sub>3</sub>) δ 169.9, 164.3, 163.0, 141.8, 106.7, 102.0, 101.6, 76.3, 68.0, 66.5, 39.3, 33.6, 30.9, 29.7, 18.9, 18.1

Supplementary Figure 1. NMR for Cladosporin.

6



**Supplementary Figure 2.** (A) Heatmap showing the correlation patterns of 57 tRNA species in 69 pairs of human HCC and TFL tissues. (B) The expression of tRNA-Lys-CUU in organ donor liver tissues (n = 21), TFL and paired HCC tissues (n = 69), respectively. (C) Univariate and multivariate analysis of associations between clinicopathological risk factors and tRNA-Lys-CUU expression in tumor tissue and HCC-specific patient survival rate and cancer recurrence rate (n=69) in our HCC patient cohort. \*\*\*P <0.001, by the Mann-Whitney test. TFL: tumor free liver; T: HCC tumor.



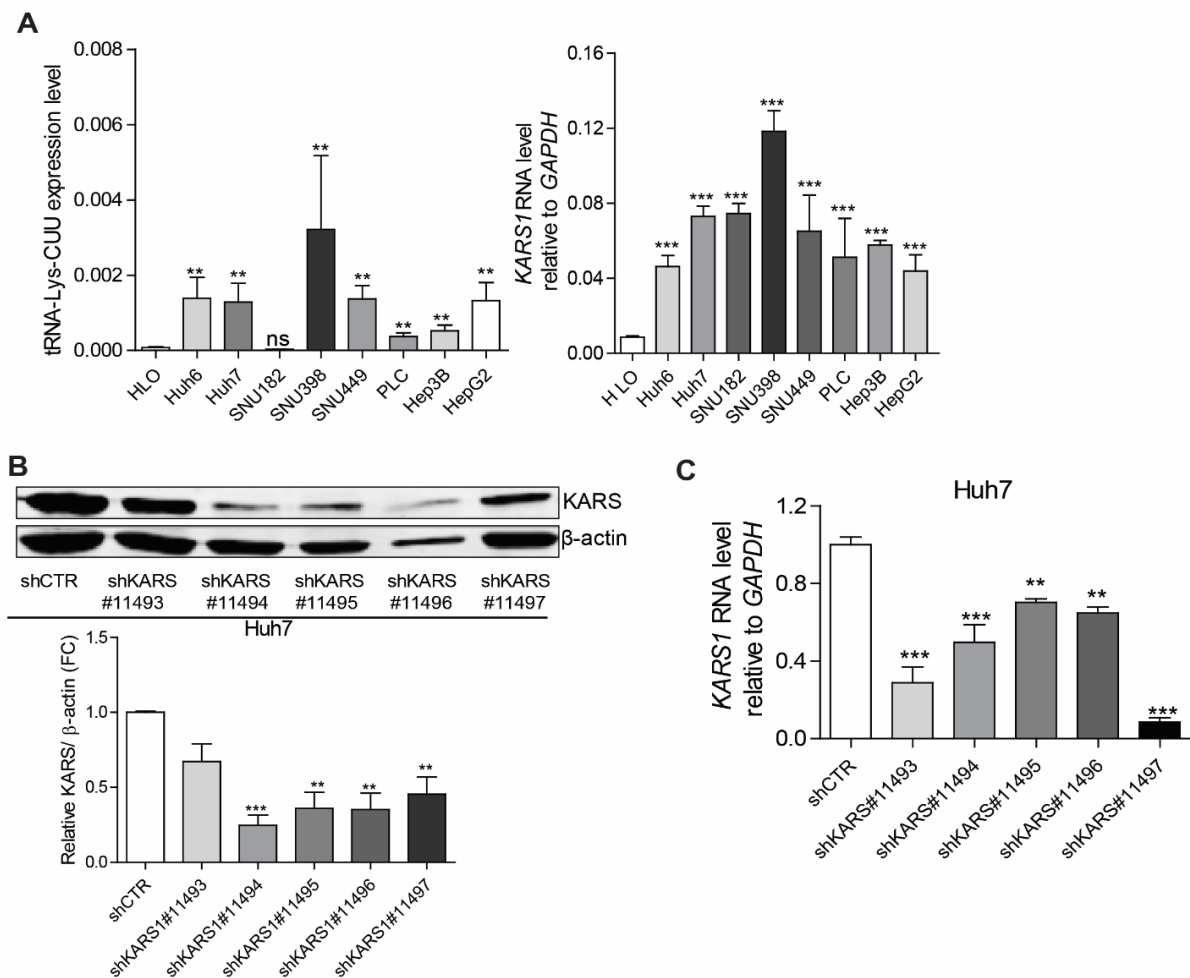
**C** Survival rate, based on *KARS1* expression in HCC

	Univariate			Multivariate		
	HR	95% CI	p-value	HR	95% CI	p-value
Tumor <i>KARS1</i>	1.4	0.96-2.1	<b>0.078</b>	<b>1.66</b>	1.08-2.55	<b>0.021</b>
AFP over 400 µg/L	1.9	(0.67-5.4)	0.23			
AFP over 1000 µg/L	4.1	1.4-12	<b>0.008</b>	5.77	1.86-17.94	<b>0.002</b>
Patients with more than 1 tumor	0.78	(0.3-2.1)	0.62			
Patients with more than 2 tumors	1.8	(0.5-6.3)	0.38			
Patients with tumor over 5 cm	2.1	(0.74-6)	0.16			
Chronic viral hepatitis	2.4	(0.92-6.2)	0.073			
Vascular invasion	1.2	(0.48-3.2)	0.66			

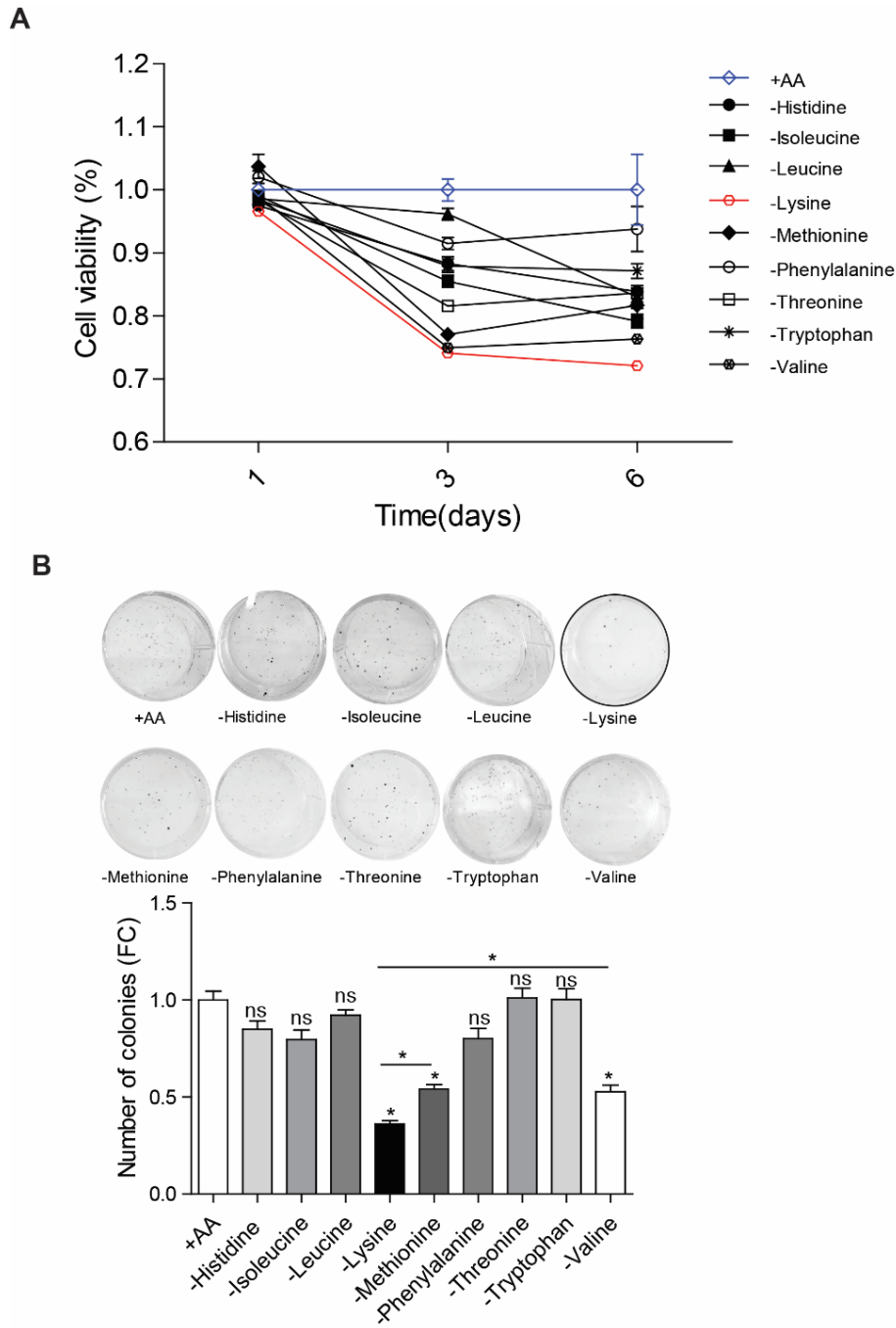
Recurrence rate, based on *KARS1* expression in HCC

	Univariate		
	HR	95% CI	p-value
Tumor <i>KARS1</i>	0.95	(0.66-1.3)	0.76
AFP over 400 µg/L	1.6	(0.7-3.8)	0.26
AFP over 1000 µg/L	2.3	(0.88-6.1)	0.09
Patients with more than 1 tumor	1.4	(0.68-2.8)	0.38
Patients with more than 2 tumors	3.6	(1.6-8.3)	<b>0.0025</b>
Patients with tumor over 5 cm	1.4	(0.68-2.9)	0.37
Chronic viral hepatitis	2.5	(1.2-5)	0.011
Vascular invasion	0.97	(0.48-2)	0.94

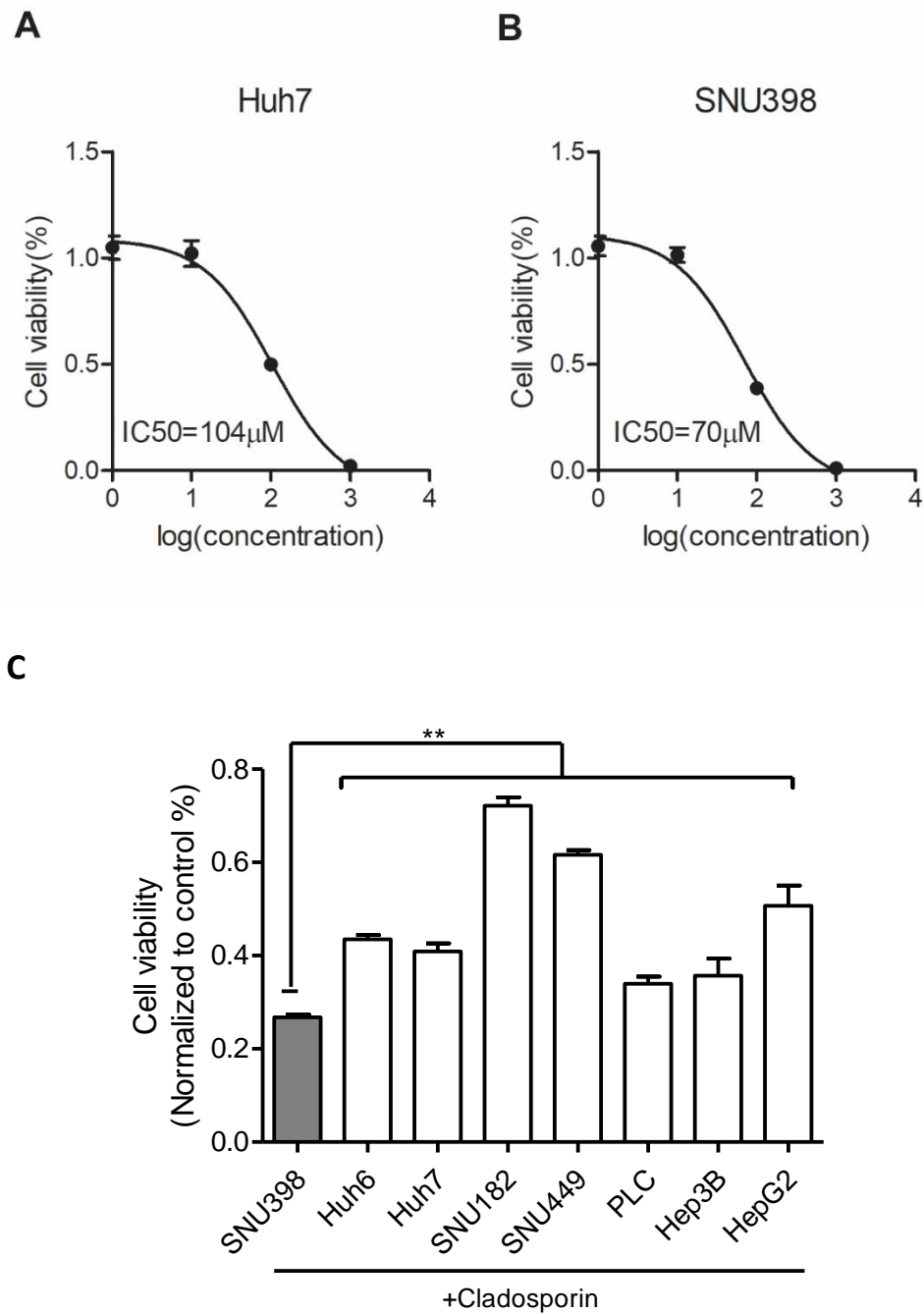
**Supplementary Figure 3 The mRNA expression levels of *KARS1*, and their relation with clinical outcomes.** (A) The mRNA expression levels of *KARS1* in organ donor liver tissues (n = 21), TFL and paired HCC tissues (n = 59). (B) The mRNA expression data of *KARS1* from GEPIA database, and red boxplot showed HCC tumor samples (n = 369), black boxplot showed Normal healthy liver samples (n = 160). (C) Univariate and multivariate analysis of associations between clinicopathological risk factors and *KARS1* expression in tumor tissue and HCC-specific patient survival rate and cancer recurrence rate (n=59) in our HCC patient cohort. \* $P < 0.05$ ; \*\* $P < 0.01$ ; \*\*\* $P < 0.001$ , by the Mann-Whitney test. TFL: tumor free liver; T:HCC tumor.



**Supplementary Figure 4 The expression level of tRNA-Lys-CUU and *KARS1*, and *KARS* knockdown efficiency.** (A) The expression level of tRNA-Lys-CUU (left graph) and *KARS1* (right graph) respectively, relative to GAPDH in HCC cell lines compared to normal healthy liver organoids (n = 4-7). (B-C) Knockdown in Huh7 and SNU398 was analyzed in (B) by western blot (upper graph), and the intensity was quantified relative to  $\beta$ -actin (lower graph) by image studio software. In (C) the expression of *KARS1* mRNA upon knockdown was determined by qRT-PCR (mean  $\pm$  SEM, n = 4-9). \*\* $P < 0.01$ ; \*\*\* $P < 0.001$ , by Mann-Whitney test. HLO: healthy liver organoids.

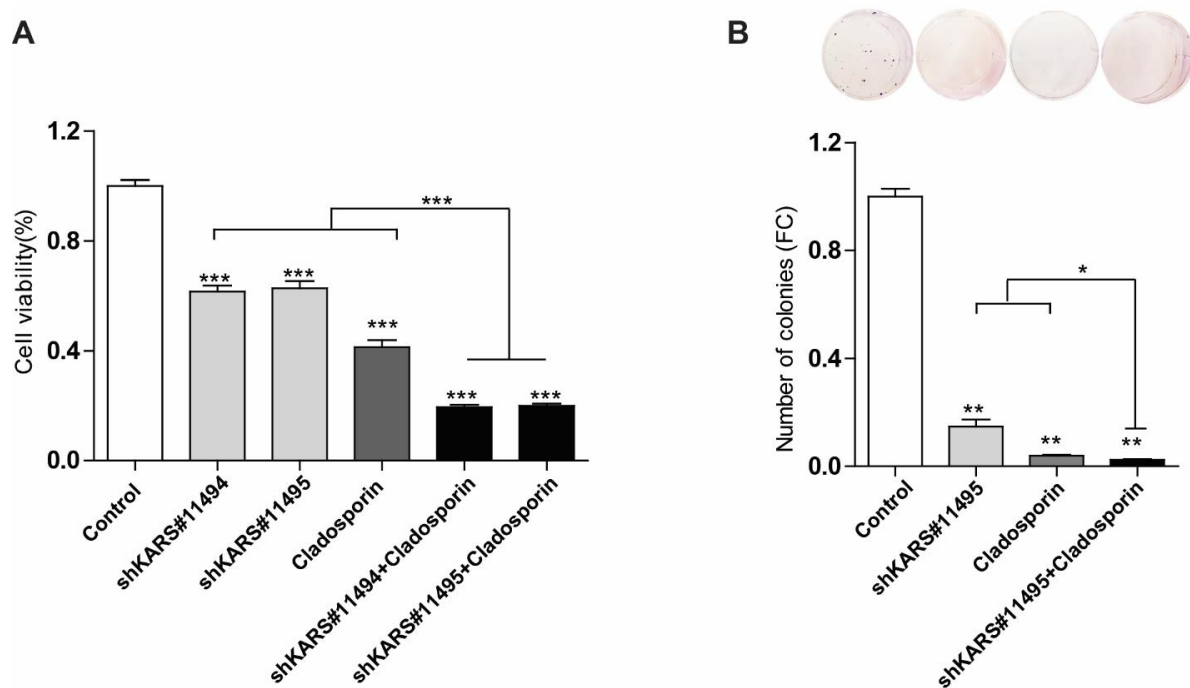


**Supplementary Figure 5 Lysine deprivation exerts the strongest inhibitory effects on HCC cell lin growth.** (A) The effects of nine essential amino acid deprivation on SNU398 cell growth measured by MTT assay following 1, 3 and 6 days of culture (n = 8). (B) The effects of amino acid deprivation in SNU398 single cell-derived colony formation as assayed 2 weeks after seeding (n = 4). \* $P < 0.05$ , by the Mann-Whitney test. AA: amino acid; "-" means deprivation.

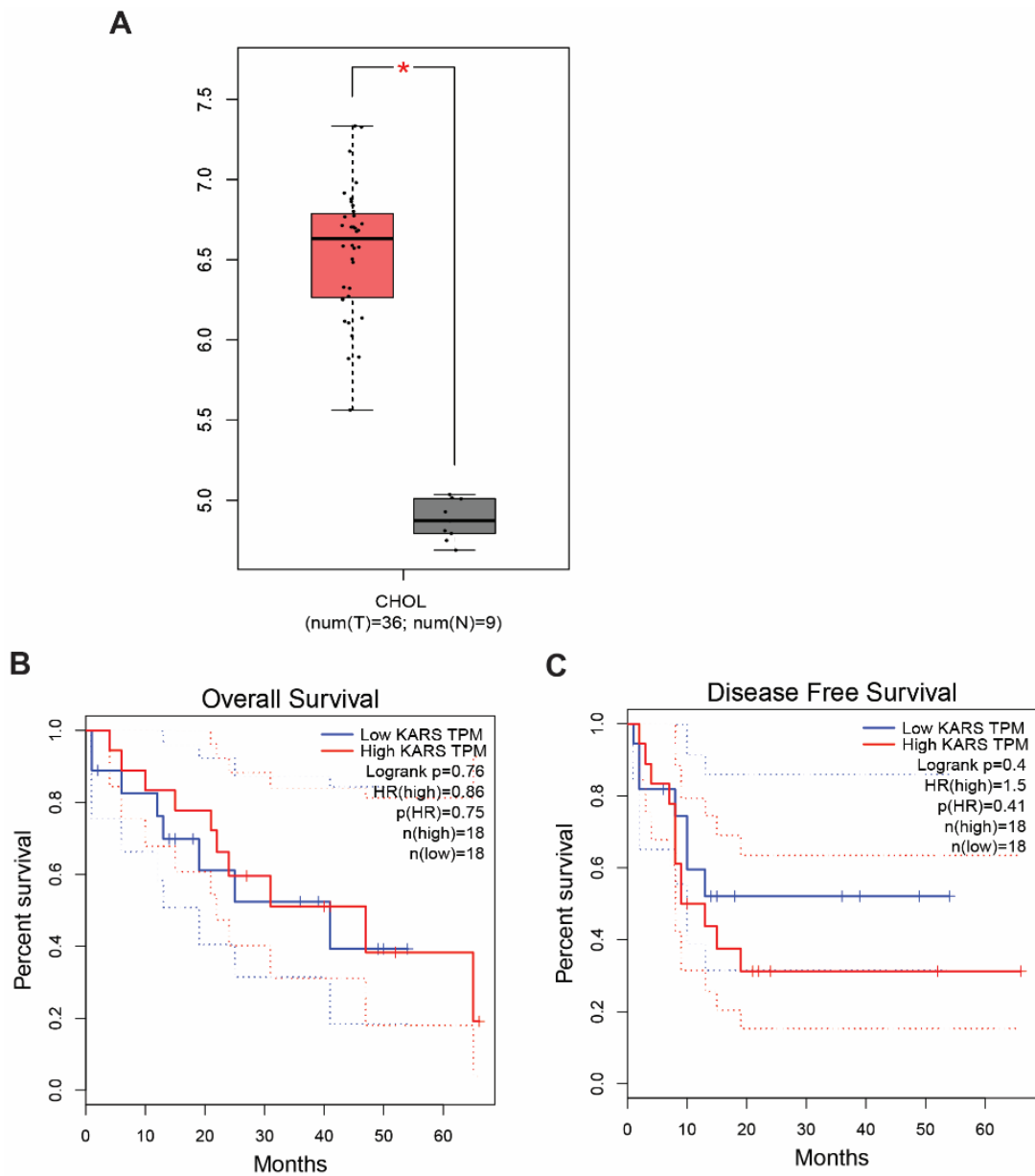


**Supplementary Figure 6** The 50% inhibitory concentration of cladosporin was determined by MTT for Huh7 (A) and SNU398 (B) cells following 3 days of treatment. The drug concentrations were 1, 10, 100 and 1000  $\mu$ M. Data are presented as mean  $\pm$  SEM. (C) SNU398 cells are more sensitive than other HCC cell lines to treatment of 100  $\mu$ M cladosporin (n = 6). \*\* $P$  < 0.01, by the Mann-Whitney test.

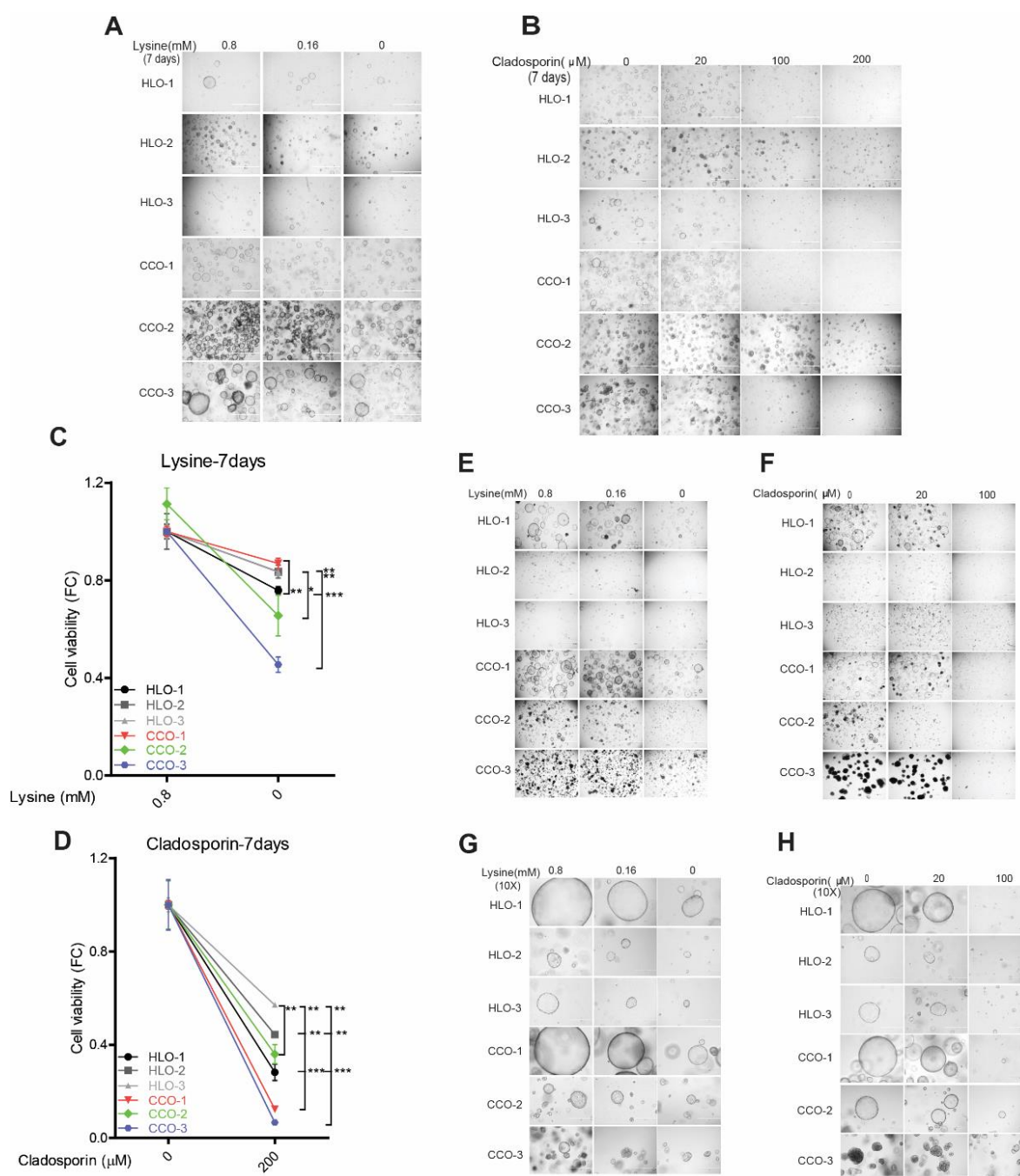




**Supplementary Figure 7** The effects of combining cladosporin treatment with KARS silencing in SNU398 cells. Cell viability (A) and single-colony formation (B) were quantified when combining *KARS1* knockdown and cladosporin treatment (n = 4 -16). \* $P < 0.05$ ; \*\* $P < 0.01$ ; \*\*\* $P < 0.001$ , by the Mann-Whitney test.



**Supplementary Figure 8** The expression level of *KARS1* and association with patient survival in cholangiocarcinoma from the GEPIA database. (A) The boxplot shows expression level of KARS in CHOL (red color, n = 36). (B) and (C) indicated overall survival and disease free survival in CHOL, respectively. \* $P < 0.05$ ; CHOL: cholangiocarcinoma.



6

**Supplementary Figure 9 Lysine deprivation or treatment with cladospirin affects the growth of patient CC organoids.** (A-B) Images of organoids were treated with different concentrations of lysine (A) or cladospirin (B) for 7 days. (C-D) For cell viability of HLOs and CCOs were treated with lysine deprivation (C) or cladospirin 200  $\mu$ M (D), high expression of *KARS1*, CCO-3 more sensitive. (E-H) Images were taken after 14 days of culture. (G) and (H) show a 10x magnification highlighting the reduced organoid size after prolonged culture with lysine deprivation or cladospirin. CCO: cholangiocarcinoma organoid; HLO: human liver healthy organoid. \* $P$ <0.05; \*\* $P$ <0.01; \*\*\* $P$ <0.001, by the Mann-Whitney test.

## Supplementary Tables

<b>Supplementary Table 1 Patient characteristics</b>		
<b>Characteristic</b>	<b>HCC patients (n=69)</b>	<b>Healthy controls (n=21)</b>
<b>Age at treatment (years)</b>		
Mean $\pm$ SD	60 $\pm$ 16	51 $\pm$ 16.2
Median (range)	64 (11-82)	52 (13-88)
<b>Sex – no. (%)</b>		
Male	41 (59.4)	12 (57.1)
Female	28 (40.6)	9 (42.9)
<b>Race – no. (%)</b>		
White	58 (84.1)	-
African	6 (8.7)	-
Asian	4 (5.8)	-
Not reported	1 (1.4)	21 (100)
<b>Etiology – no. (%)</b>		
No known liver disease	20 (29.0)	NA
Alcohol	16 (23.2)	NA
NASH	8 (11.6)	NA
Hepatitis B	8 (11.6)	NA
Hepatitis C + Alcohol	5 (7.2)	NA
Hepatitis B + Alc/HepC/HepD/NASH	4 (5.8)	NA
Hepatitis C	4 (5.8)	NA
Fibrolamellar HCC	3 (4.4)	NA
Other	1 (1.5)	NA
<b>Hepatitis status – no. (%)</b>		
Hepatitis B or C positive	21 (30.4)	0 (0)
Chronic Hepatitis B	12 (17.4)	0 (0)

Chronic Hepatitis C	10 (14.5)	0 (0)
<b>Cirrhosis – no. (%)</b>		
Yes	50 (72.5)	0 (0)
No	19 (27.5)	21 (100)
<b>Differentiation grade – no. (%)</b>		
Good	8 (11.6)	NA
Moderate	35 (50.7)	NA
Poor	14 (20.3)	NA
Unknown	12 (17.4)	NA
<b>Number of lesions – no. (%)</b>		
1	38 (55.1)	NA
>1	31 (44.9)	NA
Median (range)	1 (1-11)	NA
<b>Size of largest lesion (cm)</b>		
Mean ± SD	7.5 ± 5.1	NA
Median (range)	6.2 (1-24)	NA
<b>AFP level before resection (ug/l)</b>		
Mean ± SD	46679.2 ± 375310.5	NA
Median (range)	9 (1-3118700)	NA

Supplementary Table 2 shRNA target sequences of lysyl-tRNA synthetase.

targetSeq	Oligoseq	Gene ID	Clone name	Vector
CGGCGAATCAA CATGGTAGAA	CCGGCGGCGAATCAACATGGTAGAACTCG AGTTCTACCATGTTGATTCGCCGTTTTTG	NM_005548.1	1214s1c1	pLKO.1
GCCTTTCATCAC TTATCACAA	CCGGGCCTTTCATCACTTATCACAACCTCGA GTTGTGATAAGTGATGAAAGGCTTTTTG	NM_005548.1	883s1c1	pLKO.1
CCTGGAAGTGA CTTGATCAA	CCGGCCTGGAAGTGACTTGCATCAACTCGA GTAGTATTGATTTGGGTCCACGTTTTTG	NM_005548.1	1393s1c1	pLKO.1
CGTGGACCCAAT CAA4TACTA	CCGGCGTGGACCCAATCAATACTACTCGA GTAGTATTGATTTGGGTCCACGTTTTTG	NM_005548.1	250s1c1	pLKO.1
CCAGAGATACTT GGACTTGAT	CCGGCCAGAGATACTTGGACTTGATCTCGA GATCAAGTCCAAGTATCTCTGTTTTTG	NM_005548.1	724s1c1	pLKO.1

Supplementary Table 3 Primer sequences

Genes	Forward primers (5'-3')	Reverse primer (5'-3')
<i>KARS1</i>	GACGCACAATCCTGAGTTCACC	AGGTGACCTTGTAAGTGCCTGTA
<i>GUSB</i>	CAGGTGATGGAAGAAGTGG	GTTGCTCACAAAGGTCACAG
<i>HPRT1</i>	GCTATAAATCTTTGCTGACCTGCTG	AATTACTTTTATGTCCCCTGTTGACTGG
<i>PMM1</i>	CGAGTTCTCCGAACTGGAC	CTGTTTTTCAGGGCTTCCAC
<i>GAPDH</i>	GTCTCCTCTGACTTCAACAGCG	ACCACCCTGTTGCTGTAGCCAA

Supplementary Table 4 List of tRNA expression comparison.

Differences of tRNA expression between tumor and TFL patient tissues (n=69) were analyzed using the Wilcoxon matched pairs test. \* $P < 0.05$ , \*\* $P < 0.01$ , \*\*\* $P < 0.001$ . TFL:tumor-free liver. Red: significant up-regulation in tumor; Green: significant down-regulation in tumor; Black: no significant difference.

Gene	Mean		Wilcoxon matched pairs test	Gene	Mean		Wilcoxon matched pairs test
	TFL	Tumor			TFL	Tumor	
tRNA-Leu-CAA	1.522	1.277	***	tRNA-Gly-GCC	197.2	603.3	***
tRNA-Leu-CAG	5.106	3.551	***	tRNA-Ser-AGA	2.547	2.894	***
tRNA-Ile-AAU	1.37	1.254	***	tRNA-Leu-AAG	6.162	8.093	**
tRNA-Ile-GAU	1.076	0.8677	***	tRNA-Leu-UAG	8.082	8.548	**
tRNA-iMet-CAU	13.49	12.49	***	tRNA-Pro-UGG	3.571	3.923	**
tRNA-Met-CAU	6.762	5.325	***	tRNA-Trp-CCA	4.311	5.186	**
tRNA-Stop-UUA	5.32	4.172	***	tRNA-Glu-CUC	2.303	3.733	*
tRNA-His-GUG	16.01	13.99	***	tRNA-Gly-UCC	1.371	3.731	*
tRNA-Phe-GAA	1.095	0.801	***	tRNA-Leu-UAA	4.735	5.492	ns
tRNA-Val-AAC	1.8	0.6382	***	tRNA-Ser-UGA	4.997	5.848	ns
tRNA-Val-CAC	2.248	0.7724	***	tRNA-Ser-GCU	3.642	4.028	ns
tRNA-Pro-GGG	0.6167	0.4805	***	tRNA-Arg-CCU	1.474	1.573	ns
tRNA-Pro-CGG	4.063	3.23	***				
tRNA-Thr-AGU	0.748	0.5531	***				
tRNA-Thr-UGU	2.64	1.922	***				
tRNA-Thr-CGU	1.107	0.7374	***				
tRNA-Ala-CGC	10.14	4.745	***				
tRNA-Ala-GGC	3.448	1.932	***				
tRNA-Ala-UGC	8.042	4.49	***				
tRNA-Ala-AGC	1.779	1.098	***				
tRNA-Tyr-AUA	1.429	1.227	***				
tRNA-Tyr-GUA	5.609	2.763	***				
tRNA-Stop-CUA	5.562	2.651	***				
tRNA-Asn-AUU	2.535	1.669	***				
tRNA-Lys-UUU	18.79	9.738	***				
<b>tRNA-Lys-CUU</b>	<b>6.867</b>	<b>3.389</b>	<b>***</b>				
tRNA-Asp-AUC	4.942	2.412	***				
tRNA-Asp-GUC	0.8559	0.6074	***				
tRNA-Glu-UUC	0.9868	0.753	***				
tRNA-Cys-GCA	4.178	3.506	***				
tRNA-Arg-ACG	0.8352	0.6351	***				
tRNA-Arg-CCG	2.109	1.783	***				
tRNA-Ser-ACU	1.497	1.283	***				
tRNA-seCys-UCA	3.942	3.471	***				
tRNA-Val-UAC	1.783	0.4871	**				
tRNA-Ser-CGA	5.424	5.389	**				
tRNA-Pro-AGG	1.317	1.246	**				
tRNA-Gln-CUG	18.07	12.53	**				
tRNA-Cys-ACA	0.8275	0.4544	**				
tRNA-Arg-UCG	0.682	0.5212	**				
tRNA-Ile-UAU	2.046	1.529	ns				
tRNA-Gln-UUG	18.85	14.06	ns				
tRNA-Asn-GUU	0.4828	0.3918	ns				
tRNA-Arg-UCU	0.7006	0.6279	ns				
tRNA-Gly-CCC	0.4193	0.3827	ns				

## References

1. Gingold H, Pilpel Y. Determinants of translation efficiency and accuracy. *Mol Syst Biol.* 2011;7:481.
2. Wu Q, Medina SG, Kushawah G, et al. Translation affects mRNA stability in a codon dependent manner in human cells. *Elife.* 2019;8.
3. Chatterjee S, Yadav S. The Origin of Prebiotic Information System in the Peptide/RNA World: A Simulation Model of the Evolution of Translation and the Genetic Code. *Life (Basel).* 2019;9(1):25.
4. Yao P, Fox PL. Aminoacyl-tRNA synthetases in medicine and disease. *EMBO Mol Med.* 2013;5(3):332-343.
5. Ou X, Cao J, Cheng A, Peppelenbosch MP, Pan Q. Errors in translational decoding: tRNA wobbling or misincorporation? *PLoS Genet.* 2019;15(3):e1008017.
6. Ou X, Ma B, Zhang R, et al. A simplified qPCR method revealing tRNAome remodeling upon infection by genotype 3 hepatitis E virus. *FEBS Lett.* 2020.
7. Hernandez-Alias X, Benisty H, Schaefer MH, Serrano L. Translational efficiency across healthy and tumor tissues is proliferation-related. *bioRxiv.* 2019:782227.
8. Goodarzi H. Charting the "unknown unknowns" of cancer progression. *Sci Transl Med.* 2017;9(400).
9. Huang SQ, Sun B, Xiong ZP, et al. The dysregulation of tRNAs and tRNA derivatives in cancer. *J Exp Clin Cancer Res.* 2018;37(1):101.
10. Zhang Z, Ye Y, Gong J, et al. Global analysis of tRNA and translation factor expression reveals a dynamic landscape of translational regulation in human cancers. *Commun Biol.* 2018;1:234.
11. Musier-Forsyth K. Aminoacyl-tRNA synthetases and tRNAs in human disease: an introduction to the JBC Reviews thematic series. *J Biol Chem.* 2019;294(14):5292-5293.
12. Kwon NH, Fox PL, Kim S. Aminoacyl-tRNA synthetases as therapeutic targets. *Nat Rev Drug Discov.* 2019.
13. Tang X, Wu J, Ding CK, et al. Cystine Deprivation Triggers Programmed Necrosis in VHL-Deficient Renal Cell Carcinomas. *Cancer Res.* 2016;76(7):1892-1903.
14. Campisano S, Bertran E, Caballero-Díaz D, La Colla A, Fabregat I, Chisari AN. Paradoxical role of the NADPH oxidase NOX4 in early preneoplastic stages of hepatocytes induced by amino acid deprivation. *Biochim Biophys Acta Gen Subj.* 2019;1863(4):714-722.
15. Broutier L, Andersson-Rolf A, Hindley CJ, et al. Culture and establishment of self-renewing human and mouse adult liver and pancreas 3D organoids and their genetic manipulation. *Nat Protoc.* 2016;11(9):1724-1743.
16. Melnikov SV, Soll D. Aminoacyl-tRNA Synthetases and tRNAs for an Expanded Genetic Code: What Makes them Orthogonal? *Int J Mol Sci.* 2019;20(8).

17. Das P, Mankad Y, Reddy DS. Scalable synthesis of cladosporin. *Tetrahedron Letters*. 2019;60(12):831-833.
18. Li M, Wang L, Wang Y, et al. Mitochondrial Fusion Via OPA1 and MFN1 Supports Liver Tumor Cell Metabolism and Growth. *Cells*. 2020;9(1):121.
19. Sulima SO, Hofman IJF, De Keersmaecker K, Dinman JD. How Ribosomes Translate Cancer. *Cancer Discov*. 2017;7(10):1069-1087.
20. Truitt ML, Ruggero D. New frontiers in translational control of the cancer genome. *Nat Rev Cancer*. 2016;16(5):288-304.
21. Santos M, Fidalgo A, Varanda AS, Oliveira C, Santos MAS. tRNA Deregulation and Its Consequences in Cancer. *Trends Mol Med*. 2019.
22. Chan PP, Lowe TM. tRNAscan-SE: Searching for tRNA Genes in Genomic Sequences. *Methods Mol Biol*. 2019;1962:1-14.
23. Schwartz MH, Wang H, Pan JN, et al. Microbiome characterization by high-throughput transfer RNA sequencing and modification analysis. *Nature Communications*. 2018;9(1):5353.
24. Dhankhar R, Gupta V, Kumar S, Kapoor RK, Gulati P. Microbial enzymes for deprivation of amino acid metabolism in malignant cells: biological strategy for cancer treatment. *Appl Microbiol Biotechnol*. 2020;104(7):2857-2869.
25. Fernandes HS, Silva Teixeira CS, Fernandes PA, Ramos MJ, Cerqueira NM. Amino acid deprivation using enzymes as a targeted therapy for cancer and viral infections. *Expert Opin Ther Pat*. 2017;27(3):283-297.
26. Zou S, Wang X, Liu P, Ke C, Xu S. Arginine metabolism and deprivation in cancer therapy. *Biomed Pharmacother*. 2019;118:109210.
27. Gwangwa MV, Joubert AM, Visagie MH. Effects of glutamine deprivation on oxidative stress and cell survival in breast cell lines. *Biol Res*. 2019;52(1):15.
28. Jeon H, Kim JH, Lee E, et al. Methionine deprivation suppresses triple-negative breast cancer metastasis in vitro and in vivo. *Oncotarget*. 2016;7(41):67223-67234.
29. Chaturvedi S, Hoffman RM, Bertino JR. Exploiting methionine restriction for cancer treatment. *Biochem Pharmacol*. 2018;154:170-173.
30. Yang J, Tao R, Wang L, et al. Thermosensitive Micelles Encapsulating Phenylalanine Ammonia Lyase Act as a Sustained and Efficacious Therapy Against Colorectal Cancer. *J Biomed Nanotechnol*. 2019;15(4):717-727.
31. Fernandes HS, Silva Teixeira CS, Fernandes PA, Ramos MJ, Cerqueira NMFS. Amino acid deprivation using enzymes as a targeted therapy for cancer and viral infections. *Expert Opinion on Therapeutic Patents*. 2017;27(3):283-297.
32. Fung MKL, Chan GC. Drug-induced amino acid deprivation as strategy for cancer therapy. *J Hematol Oncol*. 2017;10(1):144.
33. Hyeon DY, Kim JH, Ahn TJ, Cho Y, Hwang D, Kim S. Evolution of the multi-tRNA synthetase complex and its role in cancer. *The Journal of biological chemistry*. 2019;294(14):5340-5351.



34. Kim S, You S, Hwang D. Aminoacyl-tRNA synthetases and tumorigenesis: more than housekeeping. *Nat Rev Cancer*. 2011;11(10):708-718.
35. Francklyn CS, Mullen P. Progress and challenges in aminoacyl-tRNA synthetase-based therapeutics. *The Journal of biological chemistry*. 2019;294(14):5365-5385.
36. Baragana B, Forte B, Choi R, et al. Lysyl-tRNA synthetase as a drug target in malaria and cryptosporidiosis. *Proc Natl Acad Sci U S A*. 2019;116(14):7015-7020.
37. Wang X, Wedge DE, Cutler SJ. Chemical and Biological Study of Cladosporin, an Antimicrobial Inhibitor: A Review. *Natural Product Communications*. 2016;11(10):1934578X1601101039.
38. Hoepfner D, McNamara Case W, Lim Chek S, et al. Selective and Specific Inhibition of the Plasmodium falciparum Lysyl-tRNA Synthetase by the Fungal Secondary Metabolite Cladosporin. *Cell Host & Microbe*. 2012;11(6):654-663.
39. Khan S, Garg A, Camacho N, et al. Structural analysis of malaria-parasite lysyl-tRNA synthetase provides a platform for drug development. *Acta Crystallogr D Biol Crystallogr*. 2013;69(Pt 5):785-795.
40. Khan S, Sharma A, Belrhali H, Yogavel M, Sharma A. Structural basis of malaria parasite lysyl-tRNA synthetase inhibition by cladosporin. *J Struct Funct Genomics*. 2014;15(2):63-71.



# Chapter 7

## Summary



## The Wnt/ $\beta$ -catenin signaling pathway in liver cancer

Hepatocellular carcinoma (HCC) represents the most common form of liver cancer. HCC tumorigenesis is strongly associated with gene mutations that lead to abnormal activation of the Wnt/ $\beta$ -catenin signaling pathway<sup>1-3</sup>. Mutations in AXIN1, a scaffold protein in the destruction complex that degrades Wnt/ $\beta$ -catenin, have often been observed in HCC (8-10%), but are also frequently observed in several other types of cancers, including those of the skin, uterus, and gastrointestinal tract<sup>4-7</sup>. In this thesis, we first aim to determine which AXIN1 functional domains are most likely to impact  $\beta$ -catenin signaling when deleted, and to identify which specific tumor-associated amino acid alterations and truncations may be driver mutations that increase  $\beta$ -catenin signaling. Next, I describe the generation of five AXIN1-repaired HCC cell lines and their functional analysis with respect to  $\beta$ -catenin signaling, growth characteristics and other genes/pathways that may be affected. In the following chapter, we present the quality analysis of four commonly used RNF43 antibodies. Finally, in the last two chapters, I describe a novel method to detect levels of tRNA expression, and use this novel method to analyze which tRNAs may be differentially regulated in liver cancer.

In **Chapter 2**, we show that the majority of AXIN1 mutations in cancer, including missense and truncated mutations, are evenly distributed throughout the coding region of the protein. First, we identified which functional domains of the protein had the biggest impact on  $\beta$ -catenin signaling when removed from an AXIN1 expression construct. Deletion of either the GSK3 $\beta$  or  $\beta$ -catenin interaction domains strongly affected signaling, followed by deletion of the RGS/APC interaction region. The relevance of these domains was confirmed by gene editing in cell lines. Next, we retrieved tumor-associated missense variants observed in these domains from the cBioPortal and COSMIC databases. Among 18 tested variants in the GSK3 $\beta$  interaction domain, only the R395P variant strongly affected signaling. Of 15 variants tested in the  $\beta$ -catenin domain, 4 affected  $\beta$ -catenin regulation of which the V478G variant showed the biggest impact on signaling. Most of these variations also resulted in reduced or lost binding to their corresponding interaction partner.

Out of 37 tested variants within the RGS/APC interaction domain, 13 resulted in increased  $\beta$ -catenin signaling. At large, we observed two classes of variants. The first one either directly affected the interaction with APC, or indirectly by being located in adjacent

structures that support the AXIN1 interface with APC. The second class of variants occurred within the hydrophobic core of the RGS/APC structure and are predicted to destabilize the entire RGS/APC domain. A common feature of both classes is the loss of APC binding, which likely explains their failure to efficiently form cytoplasmic puncta in cells. These puncta are so-called degradasomes in which proteins from the breakdown complex cluster to efficiently degrade  $\beta$ -catenin. In addition to losing APC binding, some hydrophobic core variants have been reported to induce the formation of nanoaggregates that affect  $\beta$ -catenin signaling in a dominant-negative manner by binding to a new repertoire of proteins<sup>8</sup>. Accordingly, these variants (e.g., L106R, C121F) show a stronger defect in  $\beta$ -catenin regulation than the ones merely losing APC binding. However, in a direct side-by-side comparison even these stronger RGS/APC mutants retained more functionality than the defective GSK3 $\beta$  or  $\beta$ -catenin domain variants.

In all, we identified 18 missense variants out of a total of 80 tested, which affected  $\beta$ -catenin signaling. The observed effects on  $\beta$ -catenin signaling overlapped mostly with the predicted consequences of a comprehensive protein structure analysis.

In this chapter, we also determined the functional consequences of AXIN1 truncating mutations. In HCC, these are the most common type of AXIN1 mutations observed. In total, we generated five Crispr-cas9 mediated HEK293T clones carrying AXIN1 truncations with sequential loss of C-terminal domains. All investigated truncating variants, including one that only lost the last 22 C-terminal amino acids, showed loss of  $\beta$ -catenin regulatory function. Importantly, loss of function appears to be inversely correlated to the length of the truncated AXIN1 protein, with longer proteins retaining more functionality. Thus, our analyses suggest that all truncating mutations at least partially affect  $\beta$ -catenin regulation, while this is only the case for a subset of missense mutations. In support of the latter, most colorectal and liver cancers carrying missense variants, acquire mutations in other  $\beta$ -catenin regulatory genes such as *APC* and *CTNNB1*. These results will aid the functional annotation of AXIN1 mutations identified in large scale sequencing efforts or those from individual patients. In addition, they lead to a better understanding how the AXIN1 protein is involved in properly regulating  $\beta$ -catenin signaling.

The analyses described above, all focus on AXIN1's role in  $\beta$ -catenin regulation. However, with respect to HCC several reports have suggested that AXIN1 mutation does not

lead to increased  $\beta$ -catenin signaling and that this pathway is not relevant for AXIN1-driven tumorigenesis. This assumption is largely based on lack of nuclear  $\beta$ -catenin accumulation in AXIN1-mutant cancers and low/no activation of  $\beta$ -catenin target genes. As outlined extensively in my thesis discussion, these arguments by themselves are insufficient to exclude an important role for  $\beta$ -catenin. In support of this Qiao et al. showed that AXIN1-driven HCC development in mice is almost entirely dependent on functional  $\beta$ -catenin<sup>9</sup>. To address this controversy, we used the CRISPR/Cas9 genome editing technique to repair the AXIN1 truncating mutation present in five HCC cell lines, described in **Chapter 3**. In total we obtained 14 successfully repaired clones (2-4 per cell line) that all showed reduced  $\beta$ -catenin signaling. In combination with other published data, this firmly shows that AXIN1 truncation in HCC leads to increased signaling, albeit modest compared with e.g.,  $\beta$ -catenin mutant cancers. A second observation was that all AXIN1-repaired clones showed reduced growth characteristics, demonstrated using a colony formation and MTT assay. At first sight, this seems to lead to the straightforward conclusion in which the reduced growth can be explained by the reduced level of  $\beta$ -catenin signaling. However, restoring  $\beta$ -catenin signaling to the original mutant level by supplementing the cells with exogenous WNT3a ligand, failed to revive the growth of these clones.

As reduced  $\beta$ -catenin signaling could not solely explain the altered growth characteristics of AXIN1-repaired cells, we explored other genes or signaling pathways that may be affected by AXIN1. To this aim, we used RNA sequencing combined with a detailed investigation of specific genes/pathways. We identified between 37-283 significantly up- or downregulated genes per cell line. However, comparing differentially expressed genes between cell lines shows little consistency in the identified genes or pathways that may be affected. With respect to  $\beta$ -catenin signaling only a small number of the more responsive target genes (*AXIN2*, *NKD1*, *NOTUM*) were altered in expression in most clones, while other supposed target genes showed more variability.

More recently, it was suggested that AXIN1 also directly regulates YAP/TAZ protein levels and signaling in HCC cells<sup>10</sup>. Hippo-YAP/TAZ signaling is an important pathway to control organ size and tissue growth, and is increased in activity in most HCCs, especially in AXIN1-mutant tumors. However, our YAP/TAZ immunoblot and target gene analysis fails to find any correlation between AXIN1 mutation status and YAP/TAZ signaling, questioning the published

link between AXIN1 and YAP/TAZ. Likewise, we failed to find a correlation with Notch signaling, which has also been reported to be increased in many AXIN1-mutant HCCs. Taken together, in this chapter we show that AXIN1 mutation increases both HCC cell fitness and  $\beta$ -catenin signaling, but we do not find a solid functional correlation between both traits, nor with other genes/pathways that may be affected by AXIN1-mutation status.

In **Chapter 4**, we describe the quality analysis of four commonly used RNF43 antibodies. RNF43, like its homologue ZNRF3, is an important regulator of Wnt signaling by reducing the amount of Wnt-receptor that is available on the plasma membrane of cells. Mutations are observed in many cancer types, especially those of the gastrointestinal tract, and lead to aberrantly high levels of  $\beta$ -catenin signaling when cells are exposed to Wnt ligands. Based on this function, its presumed functional location is at the cell membrane. However, several reports have postulated additional nuclear functions for RNF43. These observations are supported by showing clear nuclear staining patterns using RNF43 antibodies. We have generated a cell line that entirely lacks two exons encoding the epitopes recognized by these antibodies. In addition, we use several cell lines that are expected to express no RNF43 or truncated variants thereof. Using these four commonly used RNF43 antibodies on this cell line panel, we can only observe non-specific signals using western blotting, immunofluorescence or immunohistochemistry. In other words, they cannot reliably detect endogenous RNF43. Our results suggest that the nuclear staining patterns are an antibody artifact and that RNF43 is unlikely to localize within the nucleus. More generally, reports using RNF43 antibodies should be interpreted with caution, at least for the RNF43 protein aspects described in these papers.



## Role of the tRNA decoding system in liver cancer development

tRNAs play a crucial role in the synthesis of proteins from amino acids during translation, based on the genetic code. Abnormalities in the tRNA pool have been linked to the development of cancer, as they can contribute to the transformation of normal cells into cancer cells. Changes in tRNA abundance or modification patterns can lead to the increased production of oncogene encoded proteins or reduced generation of tumor suppressor proteins, both of which can contribute to cancer development<sup>11-13</sup>. Additionally, dysregulation of tRNA processing and modification enzymes have been linked to the development and progression of certain types of cancer<sup>14,15</sup>.

Currently, it is challenging to detect and quantify tRNA at the transcriptional level due to redundancy in genomic copies, extremely short sequences, rigid secondary structure and post-transcriptional modifications. This makes it difficult to accurately determine the levels of mature (functional) tRNAs. In **Chapter 5**, we developed a simple tRNA detection approach using qPCR. This method involves a length-extension step, a universally compatible adaptor, and degenerate primers that can be used for the entire mature tRNAome. By applying this method, I found that HEV infection significantly alters the hepatic tRNAome, potentially favoring the translation of viral capsid-encoding genes over host antiviral genes like interferon stimulating genes. This reprogramming of the tRNAome is likely to aid in the replication of the virus.

In **Chapter 6**, the aim of our study was to investigate the role of tRNA in the development of liver cancer (HCC) and identify potential tRNA-related targets for therapy. Our analysis of the tRNAome in HCC tumors and adjacent normal liver tissue revealed that a higher expression of tRNA-Lys-CUU associated with increased tumor recurrence and worse patient survival. We also observed significant upregulation of Lysyl-tRNA Synthetase (KARS), the enzyme responsible for attaching lysine to tRNA-Lys-CUU, in HCC tumors compared to normal liver tissue. To further explore the functions of tRNA-Lys-CUU and KARS in HCC, we conducted experiments using HCC cell lines and patient-derived organoids. Our results showed that lysine deprivation, KARS knockdown, or treatment with the KARS inhibitor cladosporin effectively inhibited cell growth, colony formation, and migration, through mechanisms involving cell

cycle arrest and apoptosis. Our study highlights the potential of tRNA molecules and KARS as therapeutic targets for HCC treatment.

## Reference

- 1 Parsons, M. J., Tammela, T. & Dow, L. E. WNT as a Driver and Dependency in Cancer. *Cancer Discov* **11**, 2413-2429 (2021).
- 2 Perugorria, M. J. *et al.* Wnt- $\beta$ -catenin signalling in liver development, health and disease. *Nat Rev Gastroenterol Hepatol* **16**, 121-136 (2019).
- 3 Xu, C. *et al.*  $\beta$ -Catenin signaling in hepatocellular carcinoma. *J Clin Invest* **132** (2022).
- 4 Timbergen, M. J. M. *et al.* Activated Signaling Pathways and Targeted Therapies in Desmoid-Type Fibromatosis: A Literature Review. *Front Oncol* **9**, 397 (2019).
- 5 Zucman-Rossi, J., Villanueva, A., Nault, J. C. & Llovet, J. M. Genetic Landscape and Biomarkers of Hepatocellular Carcinoma. *Gastroenterology* **149**, 1226-1239 e1224 (2015).
- 6 Ledinek, Ž., Sobočan, M. & Knez, J. The Role of CTNNB1 in Endometrial Cancer. *Dis Markers* **2022**, 1442441 (2022).
- 7 Bugter, J. M., Fenderico, N. & Maurice, M. M. Mutations and mechanisms of WNT pathway tumour suppressors in cancer. *Nature Reviews Cancer* **21**, 5-21, doi:10.1038/s41568-020-00307-z (2021).
- 8 Anvarian, Z. *et al.* Axin cancer mutants form nanoaggregates to rewire the Wnt signaling network. *Nature Structural & Molecular Biology* **23**, 324-332, doi:10.1038/nsmb.3191 (2016).
- 9 Qiao, Y. *et al.* Axis inhibition protein 1 (Axin1) Deletion-Induced Hepatocarcinogenesis Requires Intact  $\beta$ -Catenin but Not Notch Cascade in Mice. *Hepatology* **70**, 2003-2017 (2019).
- 10 Liang, B. *et al.* Differential requirement of Hippo cascade during CTNNB1 or AXIN1 mutation-driven hepatocarcinogenesis. *Hepatology* **n/a**, doi:10.1002/hep.32693 (2022).
- 11 Dai, Z. *et al.* N(7)-Methylguanosine tRNA modification enhances oncogenic mRNA translation and promotes intrahepatic cholangiocarcinoma progression. *Mol Cell* **81**, 3339-3355 e3338 (2021).
- 12 Passarelli, M. C. *et al.* Leucyl-tRNA synthetase is a tumour suppressor in breast cancer and regulates codon-dependent translation dynamics. *Nat Cell Biol* **24**, 307-315 (2022).
- 13 Orellana, E. A. *et al.* METTL1-mediated m(7)G modification of Arg-TCT tRNA drives oncogenic transformation. *Mol Cell* **81**, 3323-3338 e3314 (2021).
- 14 Goodarzi, H. *et al.* Modulated Expression of Specific tRNAs Drives Gene Expression and Cancer Progression. *Cell* **165**, 1416-1427 (2016).
- 15 Huang, S. Q. *et al.* The dysregulation of tRNAs and tRNA derivatives in cancer. *J Exp Clin Cancer Res* **37**, 101 (2018).

# Chapter 8

## Discussion



Liver cancer, particularly Hepatocellular Carcinoma (HCC), remains the leading cause of malignancy-related deaths worldwide. HCC development is a complex and long-term process, characterized by a multifaceted interaction between the tumor microenvironment, the accumulation of genetic mutations, and the dysregulation of associated signaling pathways within tumor cells. Among the significant oncogenic pathways implicated in HCC, the Wnt/ $\beta$ -catenin pathway plays a crucial role. Therefore, understanding the pathological significance of this pathway, including the role of key proteins such as AXIN1, is of utmost importance. In my thesis, I aim to investigate the diverse types of AXIN1 mutations and their impact on the tumorigenesis of HCC. Additionally, I will explore the involvement of tRNA biology in HCC development.

### **Unraveling dysregulated Wnt/ $\beta$ -catenin signaling in HCC tumorigenesis**

The Wnt/ $\beta$ -catenin signaling pathway is a vital player in the development and progression of various cancer types, including liver cancer. Abnormal activation of this pathway leads to uncontrolled cell proliferation, migration, and invasion - all hallmark features of cancer<sup>1,2</sup>. In HCC, somatic mutation of the *CTNNB1* gene (about 25%) is primarily responsible for aberrantly activating  $\beta$ -catenin signaling<sup>3</sup>. Another frequently observed mutation affecting approximately 8-10% of HCC cases is that of *AXIN1*<sup>3</sup>, encoding a scaffold protein that plays a crucial role in bringing together other proteins involved in the pathway to effectively regulate nuclear  $\beta$ -catenin. In my study, we conducted a systematic exploration of the structural domains of the AXIN1 protein and their relationship to AXIN1 alterations, with a focus on how they induce  $\beta$ -catenin signaling. Furthermore, we conducted an investigation into the role of endogenous truncating mutations of AXIN1 within the context of HCC and their involvement in this signaling pathway and potentially other tumor-associated mechanisms.

The Wnt/ $\beta$ -catenin pathway is often affected by gain-of-function (GOF) mutations in the *CTNNB1* gene, primarily found in exon 3. These mutations specifically affect the S/T phosphorylation residues and the  $\beta$ -TrCP binding motif (residues S33-S45). More recent findings indicate that missense mutations within armadillo repeats 5 and 6, which are located at the binding interface with APC, have emerged as novel tumorigenic alterations<sup>4,5</sup>. Both type of mutations contributes to the stabilization and accumulation of  $\beta$ -catenin protein within cells, consequently leading to the activation and dysregulation of  $\beta$ -catenin regulated gene

expression<sup>4,6</sup>. In addition to *CTNNB1*, mutations in other genes that regulate the Wnt/ $\beta$ -catenin pathway, such as *APC*, *RNF43/ZNRF3*, *AXIN1* and *AXIN2*, are also commonly found in cancer<sup>3,7,8</sup>. From the perspective of the destruction complex regarding the degradation of  $\beta$ -catenin, *AXIN1* and *AXIN2* are proteins that function as scaffolds and recruit members of the degradation complex, thereby assisting in the regulation of  $\beta$ -catenin stability. Consequently, they are believed to play a role in maintaining proper cell signaling and preventing cancer. *AXIN2* expression levels are typically low under normal physiological conditions but increase in response to Wnt/ $\beta$ -catenin signaling activation. This upregulation serves as a negative feedback mechanism, controlling the intensity and duration of the pathway<sup>9</sup>.

### Truncating *AXIN1* variants in cancer

Besides oncogenic  $\beta$ -catenin mutations, loss of function (LOF) mutations in the *AXIN1* gene are the second most common type of mutation found in HCC (about 8-10%) linked to  $\beta$ -catenin signaling<sup>3</sup>. *AXIN1* is a tumor suppressor gene, meaning that both copies need to acquire inactivating mutations, and its alterations can involve deletions, missense, nonsense, and frameshift mutations distributed throughout the entire gene<sup>10</sup>. In **Chapter 2** we describe the functional consequences on  $\beta$ -catenin signaling for various truncating and missense mutations, which are the most common type of genetic *AXIN1* alterations observed in cancers. In HCC, it is mainly truncating *AXIN1* mutations that are observed. Our analysis shows that all *AXIN1* truncations, including the ones that only lose a small part of the C-terminal domain, demonstrate at least a partial loss of  $\beta$ -catenin regulatory activity. However, we also observed that the shorter variants of *AXIN1* exhibited a stronger loss of function, primarily resulting from the elimination of important functional domains, while longer truncations retain more function. The latter may explain why only few truncating mutations are being identified in the most C-terminal domain of *AXIN1* in HCC (**Figure 1**). In addition to liver cancer, *AXIN1* truncating mutations have also been identified in other tissues, particularly in the colon<sup>7</sup>. However, it is noteworthy that in intestinal tumors, *AXIN1* mutations are predominantly observed in tumors characterized by a defect in the DNA mismatch repair system. This repair system recognizes mistakes in both the number and type of nucleotides being incorporated during DNA replication<sup>11</sup>. When defective, it results in the accumulation of mutations at the nucleotide level, especially at repetitive sequences, which are more prone to mutation. This

likely explains the presence of two mutational hotspots observed in intestinal cancer that occur at AXIN1 codons G265 (GCTCCCCCGGA) or G508 (GCACTGGGGGT) (**Figure 1**).

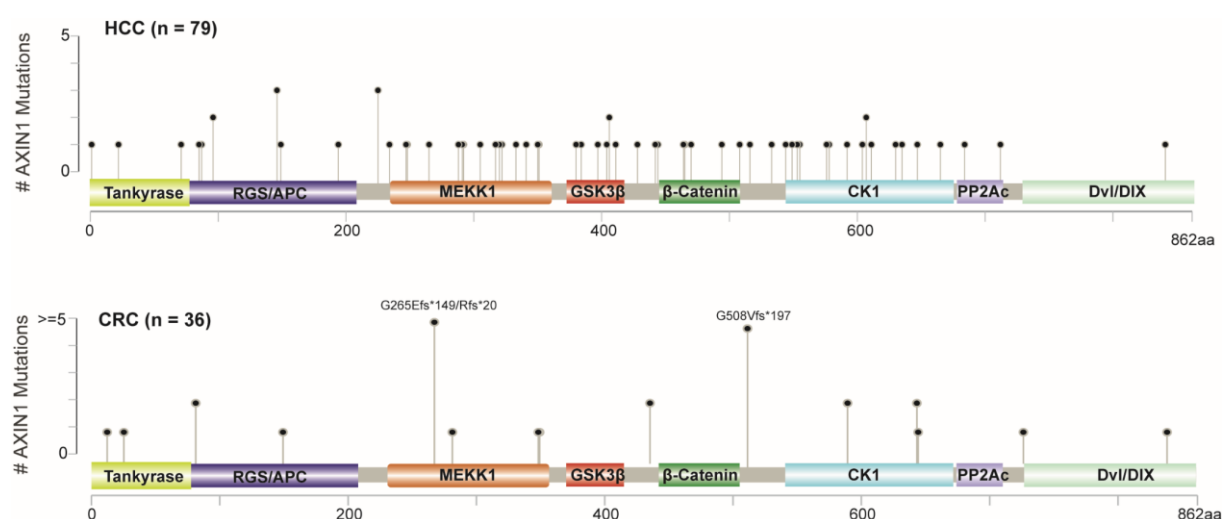


**Figure 1** Distribution of truncating AXIN1 mutations in Hepatocellular carcinoma (HCC) and Colorectal cancer (CRC), as reported in cBioPortal March, 2023.

The truncating AXIN1 mutations observed in HCC are mostly the only alterations observed in genes related to  $\beta$ -catenin signaling, whereas the AXIN1-mutant CRCs also carry mutations in other genes that are expected to lead to a modest further increase in signaling (**Figure 8 in Chapter 2**). Additional mutations rarely involve the genes classically linked to  $\beta$ -catenin signaling, that is *APC* and *CTNNB1*, but more often involve *AXIN2*, *ZNRF3* or *RNF43*. The *RNF43* mutations are mainly at the mismatch repair deficient G659 mutational hotspot leading to a truncated protein that retains substantial residual function<sup>12</sup>. The need for additional mutations in  $\beta$ -catenin related genes in CRC can possibly be explained by a requirement for higher  $\beta$ -catenin signaling levels to successfully support tumor growth compared with HCC, as outlined in more detail below.

### Missense AXIN1 variants in cancer

As more tumor samples are sequenced, an increasing number of genetic variants are being identified, including variants of uncertain significance (VUS) in the *AXIN1* gene<sup>10</sup>. Understanding the role of these VUS in HCC and other tumor types is important to understand whether and how they contribute to the tumorigenic process. In **Chapter 2**, our observations indicate that the majority of AXIN1 missense variants (n=62/80) that we studied, exhibit a behavior similar to wild-type AXIN1 when overexpressed in vitro. However, a subset of

variants (n=18/80) affects the normal function of AXIN1 leading to increased  $\beta$ -catenin signaling. These variants were identified in the domains through which AXIN1 interacts with APC, GSK3 $\beta$  and  $\beta$ -catenin. Especially, small deletions or missense variants (e.g., R395P) that lead to loss of GSK3 $\beta$  binding have a big impact on  $\beta$ -catenin signaling. This is not entirely surprising, as GSK3 $\beta$  is not only responsible for directly phosphorylating the S/T residues of  $\beta$ -catenin leading to its breakdown, but also to enhance the stability of the entire destruction complex by phosphorylating APC and AXIN1/2<sup>13</sup>. The second biggest impact had deletions/variants in the  $\beta$ -catenin domain followed by those in the RGS/APC-binding domain.

We tested those missense variants using overexpression in HEK293T cells. Unpublished qPCR experiments suggest that this leads to a more than 5000-fold overexpression on RNA level. Assuming that this also translates into a similar overexpression on protein level, it means that basically all AXIN1 protein incorporated into the breakdown complex is represented by the missense variants that we transfected. If that AXIN1 variant cannot bind to GSK3 $\beta$ , it strongly interferes with  $\beta$ -catenin regulation through the mechanism described above. Variants that lose APC binding have a more modest effect, most likely because APC can also be incorporated into the breakdown complex indirectly by binding to  $\beta$ -catenin, albeit it less efficiently. The same holds true for  $\beta$ -catenin that can also be introduced into the breakdown complex by binding to APC.

Taken together, our analysis of truncating and missense AXIN1 variants has identified which mutations affect  $\beta$ -catenin regulation. Longer truncating variants retain more function than shorter ones that in addition lose the GSK3 $\beta$  and  $\beta$ -catenin interaction domains. These latter domains are also the ones in which we identified selected missense mutations that strongly impair function. In addition, we identified several missense mutations in the RGS/APC binding domain that led to partial loss of function.

### **The relevance of $\beta$ -catenin signaling dosage**

AXIN1-mutant hepatocellular carcinomas rarely show features clearly associated with increased  $\beta$ -catenin signaling. First,  $\beta$ -catenin immunohistochemistry (IHC) fails to show a clear accumulation of nuclear  $\beta$ -catenin in this subset of cancers<sup>14-17</sup>, often regarded as the hallmark of active signaling. Second, expression profiling reveals no or at most a modest increase in expression of  $\beta$ -catenin target genes<sup>16</sup>. Below I discuss why these observations by



themselves are not sufficient to conclude that  $\beta$ -catenin signaling is not relevant for AXIN1-driven HCC tumorigenesis.

The identification of nuclear localized  $\beta$ -catenin using antibodies, is a good indicator that  $\beta$ -catenin is actively signaling. However, as we and others have outlined previously, its absence does not rule out that a low level of signaling may be active<sup>18</sup>. We believe it merely to be a technical shortcoming of  $\beta$ -catenin IHC to detect low levels of nuclear  $\beta$ -catenin above background levels. Previously, we have shown that atypical  $\beta$ -catenin mutations present in armadillo repeats 5 and 6, result in loss of APC binding leading to a modest induction of  $\beta$ -catenin signaling<sup>4</sup>. Hydrodynamic transfection of these variants in mice led to a robust induction of liver cancers, associated with increased expression of  $\beta$ -catenin target genes. However,  $\beta$ -catenin IHC uncovered mainly a membranous and a slightly increased cytoplasmic staining pattern in the great majority of tumor cells. Similar observations have been made for human liver cancers carrying these armadillos' repeat mutations, and even for tumors with mutation of the S45 phosphorylation site of  $\beta$ -catenin<sup>5</sup>. Regarding these S45 mutations, there is little doubt that they lead to increased  $\beta$ -catenin signaling, even though nowadays they are known to be less potent in inducing  $\beta$ -catenin signaling compared with other S/T variants of  $\beta$ -catenin<sup>5</sup>. All these examples show that weak  $\beta$ -catenin mutants can significantly induce signaling without accumulating IHC-detectable nuclear levels. AXIN1-mutant HCCs also show no clear nuclear  $\beta$ -catenin accumulation<sup>14-16</sup>. In accordance, the same has been observed in Axin1-mutant mouse liver tumors<sup>17,19</sup>. As outlined above, this is no direct proof that these tumors lack increased  $\beta$ -catenin signaling.

The second suggestion that activation of  $\beta$ -catenin target genes is too low or absent in AXIN1-mutant cancers to support tumor growth, is based on the misconception that high signaling levels are strongly favored during tumorigenesis. However, as we and others have already shown extensively during the last two decades, tumors select for  $\beta$ -catenin signaling levels that are sufficiently high to provide some growth advantage compared with wild-type neighboring cells, but are not that high that they induce an apoptotic process<sup>11</sup>. According to this "just-right" signaling model each tissue type shows an optimal level of signaling that best supports tumor formation. Tumors of the distal colon prefer rather high signaling levels, which is best accomplished by APC mutations that remove more of the  $\beta$ -catenin breakdown activity, while more proximal CRCs select for mutations that lead to somewhat lower signaling levels.

The latter is reflected in the selection of *APC* mutations that retain more breakdown activity, oncogenic  $\beta$ -catenin mutations, *RNF43/ZNRF3* mutations, *AXIN1/AXIN2* mutations, or combinations thereof (several weak mutations combined can also provide the optimal level of signaling for a given tumor type). Liver tumors seem to prefer even lower levels of signaling. Among others, this was shown by Buchert et al. who showed that late-onset hepatocellular tumors were present in all mice carrying a hypomorphic *Apc* mutation associated with just a modest increase in  $\beta$ -catenin signaling, while tumor formation was strongly reduced both with slightly increased or decreased signaling levels<sup>6</sup>. This may explain why *APC* mutations are rarely observed in HCC as most of them are expected to activate  $\beta$ -catenin signaling too strongly. Instead, they acquire more frequently  $\beta$ -catenin mutations, which leads to a robust but generally lower activation of  $\beta$ -catenin signaling than full-blown *APC* mutations<sup>11</sup>.

Along the same line of reasoning, the low/modest increase of  $\beta$ -catenin signaling associated with *AXIN1* mutations, may be sufficient or even optimal to contribute to HCC formation. As described above, several reports have suggested that *AXIN1*-mutant HCCs do not show increased  $\beta$ -catenin signaling based on lack of nuclear staining and no obvious induction of target genes. However, our analysis of five *AXIN1*-mutant HCC cell lines and their *AXIN1*-repaired counterparts described in **Chapter 3**, shows that in all cases  $\beta$ -catenin signaling is increased through *AXIN1* mutation measured using two sensitive methods, that is a  $\beta$ -catenin reporter assay and *AXIN2* qPCR. In addition, we have repaired the *AXIN1* mutation in the SNU449 HCC cell line previously<sup>20</sup>. This cell line expresses an *AXIN1* protein truncated at R712 that retains the domains that can bind to  $\beta$ -catenin and GSK3 $\beta$ , for which we have shown in **Chapter 2** that it retains residual breakdown activity. This likely explains why repair of this *AXIN1* mutation leads to minor alterations in growth and RNA expression, but importantly, it shows a consistent reduction of *AXIN2/AXIN2* expression in all repaired clones. In further support, we and others have shown that *AXIN1* knockdown in non-mutant HCC cell lines in all cases leads to increased signaling<sup>16,17,20</sup>. In conclusion, we feel that it is convincingly shown that *AXIN1* mutation leads to increased  $\beta$ -catenin signaling in HCC, albeit modest in many occasions.

## Does increased $\beta$ -catenin signaling associated with AXIN1 mutation, contribute to improved growth characteristics?

Despite having shown that AXIN1 mutation leads to increased  $\beta$ -catenin signaling, this does not prove that this modest increase is also relevant for liver tumorigenesis. Abitbol and coworkers have argued this not to be the case, based on the lack of nuclear  $\beta$ -catenin and no/low induction of target genes<sup>16</sup>, but as outlined above, this does not convincingly prove that  $\beta$ -catenin is not involved. More recently, Qiao et al showed that AXIN1-driven HCC development in mice is almost entirely dependent on functional  $\beta$ -catenin<sup>17</sup>, but as argued by others this experiment was performed with simultaneous overexpression of MET, which may have biased the result<sup>21,22</sup>. Hence, it is still unclear if and to what extent the modest increased  $\beta$ -catenin signaling contributes to AXIN1-driven HCC development.

We decided to address this question using AXIN1-mutant HCC cell lines, despite that organoid models are emerging as promising models for exploring cancer development due to their ability to more closely mimic the cancer environment in the body. However, in the context of liver cancer, there are significant limitations to the applicability of organoids. First, HCCs have a low success rate to become established as long-term organoid models<sup>23-25</sup> compared to other cancers such as those of the prostate<sup>26</sup>, colorectal tract<sup>27</sup> and breast<sup>28</sup>. In addition, to the best of our knowledge, currently no organoid models exists that are derived from an AXIN1-mutant HCC. Second, it remains technically challenging to genetically modify organoids, especially when the desired modification does not provide a selective growth advantage, which would favor the selection of modified clones. Third, most organoids require a continuous exposure to reagents, such as Wnt and R-Spondin ligands, that maintain sufficient  $\beta$ -catenin signaling for supporting their growth. This may obscure the requirement for low level  $\beta$ -catenin signaling imposed by AXIN1 mutations that we wish to investigate. Moreover, HCC cell lines may represent better models of primary liver cancer than often appreciated. A team led by Dr. Sandra Rebouissou analyzed 34 liver cancer cell lines and demonstrated that their genetic, RNA and protein expression profiles were comparable to the more aggressive forms of HCC<sup>29</sup>. Using these cell lines, they tested 31 anticancer agents for their effectiveness in reducing cell viability and identified markers that associated with the response to selected therapeutics.

From this collection of liver cancer cell lines, we used five AXIN1-mutant HCC cell lines, representative of both hepatoblast- and mesenchymal-like subclasses. As shown in **Chapter 3**, we successfully obtained 14 AXIN1-repaired clones (2-4 per cell line) that were all characterized by reduced  $\beta$ -catenin signaling and reduced growth characteristics. At first glance this seems to prove that AXIN1 mutation contributes to HCC growth by modestly increasing  $\beta$ -catenin signaling. However, when we tried to rescue the growth of these repaired clones by increasing  $\beta$ -catenin signaling through WNT3a addition, we failed to revive the growth of these clones. In theory it may be that merely adding exogenous WNT3a does not entirely recapitulate the mechanism through which AXIN1 mutation induces  $\beta$ -catenin signaling. WNT3a is added at one specific time point, initially leading to a burst of  $\beta$ -catenin signaling, which may then subsequently decrease by the activation of negative feedback mechanisms in the cell, until WNT3a is refreshed several days later. This pattern of  $\beta$ -catenin activation is likely different from that present in the original AXIN1 mutant cell lines and may influence the growth characteristics of the repaired clones. Alternatively, the modestly increased  $\beta$ -catenin signaling is merely a bystander effect of AXIN1 mutation, while other cellular features affected by AXIN1 mutation are more relevant for tumorigenesis (see below). In support of this, RNA sequencing and qPCR analysis reveals only significant alterations in a small number of  $\beta$ -catenin target genes. Besides the well-established target gene *AXIN2*, we only see a consistent alteration in *NOTUM* and *NKD1* expression, while several other generic or liver-specific target genes are altered only in selected cell lines, or occasionally even show opposite trends. Whether these small changes in  $\beta$ -catenin related gene expression are sufficient to explain the altered growth characteristics remains uncertain at present.

If these observations indeed indicate that increased  $\beta$ -catenin signaling is not responsible for a more robust growth of AXIN1-mutant HCC cell lines, which alternative scenarios can be envisaged? First,  $\beta$ -catenin signaling may require cooperation with other cellular features affected by AXIN1. Mostly in a small number of publications, AXIN1 has been linked to various other proteins and signaling pathways, such as MYC, SMAD3, TP53, and YAP/TAZ signaling<sup>19,30-34</sup>. Possibly,  $\beta$ -catenin signaling requires simultaneous alterations of one of these pathways to have an effect. However, our RNA sequencing analysis did not reveal a gene or pathway consistently altered in more than two cell lines. Thus, this scenario would imply that each cell line/HCC may have other genes/pathways that cooperate with  $\beta$ -catenin,

which seems unlikely. Along the same line of reasoning, it seems unlikely that one of these alternative pathways promotes tumorigenesis independent of  $\beta$ -catenin.

We have looked in more detail to Hippo YAP/TAZ signaling as it was recently suggested to be directly regulated by AXIN1<sup>19,34</sup>. In short-term knockdown and overexpression experiments, Liang et al. showed that low/absent AXIN1 expression levels correlated with increased YAP/TAZ stability and signaling<sup>19</sup>. They also confirmed a previous observation that both proteins can associate with each other<sup>19,34</sup>. They used these observations to support their mouse analysis in which simultaneous Axin1 knockout and MET overexpression, led to higher Yap/Taz signaling than observed in oncogenic  $\beta$ -catenin/MET induced HCCs. Both tumor groups showed a near-complete loss of Lats1/2 expression, critical kinases for YAP/TAZ turnover, which will have had a big impact on Yap/Taz signaling. The authors proposed that Axin1 mutation further increased Yap/Taz levels, specifically in this tumor group. However, in our analysis of five AXIN1-repaired cell lines we cannot find any correlation between AXIN1 expression and YAP/TAZ protein levels and signaling. In fact, several cell lines show the opposite correlation, that is increased expression of YAP/TAZ target genes when *AXIN1* is repaired. Our analyses were done on cell clones grown for prolonged times, which may have led to adaptations in YAP/TAZ signaling. Nevertheless, our analyses show that the association between AXIN1 and YAP/TAZ is not as clear-cut as suggested by Liang et al<sup>19</sup>.

A second scenario may be that AXIN1's main function is not to regulate nuclear signaling, but serves as a more structural component in cells. In a small number of publications, AXIN1 has been linked to centrosomal functions. Centrosomes have an important function in nucleation of the microtubular skeleton, and are especially important for proper regulation of chromosomal cell division. AXIN1 was suggested to associate with  $\gamma$ -tubulin, a major component of centrosomes, and its knockdown resulted in reduced microtubule nucleation<sup>35</sup>. Also in *Drosophila* embryos, AXIN appears to contribute to mitotic fidelity<sup>36</sup>. Thus, by restoring AXIN1 expression one could speculate that mitotic checkpoints are more robustly activated during mitosis, thereby delaying mitosis and effectively resulting in longer cell cycle times and overall reduced growth.

Taken together, we identify in **Chapter 2** which AXIN1 mutations affect  $\beta$ -catenin signaling and to which degree they are impaired in their regulation. This research line focused entirely on  $\beta$ -catenin signaling, which seems to be in partial contrast with the results described

in **Chapter 3**. Although we show in that chapter that AXIN1 repair leads to reduced  $\beta$ -catenin signaling, it may not be the sole explanation for the reduced growth characteristics that we simultaneously observe. At present, we do not know how to reconcile this apparent discrepancy. However, one aspect of liver tumorigenesis that is neither addressed in our analyses nor in most liver tumor inductions in mice, is that virtually all liver cancers emerge in patients with chronic liver injury, inflammation and cirrhosis. As we hypothesized previously, under such harsh circumstances, the modest increase in  $\beta$ -catenin signaling present in AXIN1-mutant cells may impose a selective advantage, for example by more readily inducing proliferation, survival or maintenance of stem cell characteristics<sup>20</sup>. Moreover, these AXIN1-mutant cells depend almost entirely on sufficient AXIN2 activity to counterbalance  $\beta$ -catenin signaling, as shown by the strong increase in signaling following *AXIN2* knockdown (**Chapter 3**)<sup>20</sup>. This makes AXIN1-mutant liver cells much more vulnerable to aberrantly increase signaling. Stochastically, AXIN2 will every now and then be too low to keep  $\beta$ -catenin signaling in check in an AXIN1-mutant cell, which may result in the emergence of a cluster of AXIN1-mutant cells that survive in the inflamed, cirrhotic liver. Once these cells acquire additional alterations in other signaling pathways such as Notch and YAP/TAZ, they may ultimately progress to full carcinomas.

### **Evaluating the quality of RNF43 antibodies**

RNF43 plays a role in inhibiting Wnt signaling by removing Wnt receptors from the cell membrane. However, recent studies have suggested that RNF43 might have additional functions in the nucleus<sup>37,38</sup>. These supposed nuclear functions are supported by commonly used RNF43 antibodies that reveal nuclear staining patterns. Our own investigation in **Chapter 4**, however, raises doubts about these findings. In this study, we used various techniques like western blotting, immunofluorescence, and immunohistochemistry on cell lines with modified RNF43 expression or entirely lacking the epitopes recognized by these antibodies. Surprisingly, none of the tested antibodies reliably detected the presence of endogenously expressed RNF43 in any of our experiments. Only non-specific bands or staining patterns were observed. This strongly suggests that the proposed nuclear location of RNF43 is an antibody artefact, and also raises doubts about the presumed nuclear functions of RNF43.

These same antibodies have also regularly been used to evaluate RNF43 expression levels using western blotting, or to evaluate the prognostic relevance of RNF43 protein expression for various tumor types using immunohistochemistry. As we show here that none of the applied antibodies is specific for RNF43, all these findings should be interpreted cautiously, at least for the RNF43 protein aspects described in these papers.

## **Role of tRNA biology in cancer development**

Cancer cells have a higher rate of global protein synthesis compared to noncancerous cells. The oncogenic activity observed across various types of cancer has been linked to translational reprogramming of the cancer peptidome, which leads to an increase in cell proliferation through increased protein translation<sup>39-41</sup>. tRNAs play a crucial role in this process, as they are small RNA molecules responsible for decoding genetic information from DNA, transcribed into RNA and ultimately translated into proteins. Emerging evidence suggests that dysregulation of tRNAs may contribute to the development of cancer<sup>42</sup>. Thus, it is of utmost importance to accurately quantify the expression levels of tRNAs in order to better understand their underlying mechanisms for cancer development.

The human tRNAome encompasses more than 600 gene loci that encode tRNA molecules. After transcription, tRNAs undergo post-transcriptional modification, and a common CCA ribonucleotide sequence is added to their 3' end, resulting in the mature form. This mature tRNA serves as the substrate for protein synthesis. It adopts a distinct cloverleaf structure and typically consists of 70-90 base pairs. The tRNA carries an anticodon that matches mRNA codons and an acceptor stem that binds to amino acids. Aminoacyl-tRNA synthetases (AARS) are enzymes responsible for accurately attaching the appropriate amino acids to tRNA, ensuring the accurate assembly of proteins. Insight into the nature of the tRNAome in general and the mature tRNAome in particular, is still primarily in its infancy, mainly because of the technical difficulties associated with their investigation.

Detection of tRNAs has traditionally been done through techniques such as thin layer chromatography<sup>43</sup>, liquid chromatography mass spectrometry<sup>44</sup>, microarrays<sup>45-47</sup>, and single tRNA-based qPCR<sup>48</sup>. Recently, the field has seen advancements in high-throughput sequencing<sup>49,50</sup>, which has made the quantification of the tRNAome at the transcriptional level more efficient. However, this method relies on complicated bioinformatics and requires the

use of specific reagents. In my **Chapter 5** of this thesis, I introduced a simplified qPCR method for rapid quantification of the mature tRNAome. This method involves a length-extension step, a universally compatible adaptor, and degenerate primers that can be used for the entire mature tRNAome. This method has been successfully used to study tRNA expression in macrophages and organoid models<sup>51,52</sup>. Given that disturbances in the tRNAome have broad implications in various diseases, including cancer development<sup>42,53,54</sup>, it is important to have more straightforward techniques available to detect and quantify these molecules. This convenient method introduced in my thesis has the potential to be broader applicable in more laboratories and advance many aspects of biomedical tRNA research.

Dysregulation of mature tRNAs expression can lead to aberrations in protein synthesis, which may contribute to the tumorigenic process. However, the specific role of tRNAs in liver cancer remains unknown. Using the qPCR method described above, we have studied the role of tRNA biology in liver cancer development by determining the mature tRNAome in HCC samples and their corresponding normal tissues (**Chapter 6**). Our results identified that high levels of *tRNA-Lys-CUU* expression in HCC tumors were associated with increased tumor recurrence and worse patient survival, indicating that sufficiently high Lysine levels may be relevant to sustain optimal HCC growth.

Therapies targeting the tRNA system have emerged as potential treatment approaches for cancer. For example, manipulating amino acid availability can disrupt proliferation<sup>55,56</sup>. Lysine is one of the nine essential amino acids that cannot be produced by the body. We show that removal from the culture medium of SNU398 liver cancer cells, resulted in the strongest growth inhibitory effect relative to other essential amino acids. Possibly, this explains why high *tRNA-Lys-CUU* levels are observed in patients with worse prognosis. One somewhat surprising observation from the amino acid deprivation experiments is that the tumor cells can still maintain a minimal growth capacity for some time, while nevertheless lacking an essential amino acid. Although amino acid deprivation can decrease overall levels of amino acids, the complete removal of a specific amino acid is often not achievable. First, cells are grown in the presence of serum, whose protein component maybe provides a minimal source of amino acids, such as the lysine investigated in **Chapter 6**. Second, cells activate feedback mechanisms that allow them to maintain some growth with reduced amounts of a specific amino acid. For example, cells can still survive for several days without methionine, although



it is required as the amino acid for initiating protein translation<sup>57-59</sup>. Methionine metabolism involves various pathways, including the methionine cycle and salvage pathway. In particular, methionine can be replenished through the methionine salvage pathway using methylthioadenosine (MTA), a by-product of polyamine biosynthesis<sup>60</sup>.

A second option to therapeutically affect the tRNA system, is to target the catalytic sites of aminoacyl-tRNA synthetases (ARSs)<sup>61</sup>. By inhibiting the enzymes responsible for charging the specific amino acids to tRNA, the process of protein translation can be disrupted. This strategy holds potential for interfering with essential cellular functions and inhibiting cancer cell growth<sup>61</sup>. Likewise, we observed that both knockdown and pharmacological inhibition of KARS1, the enzyme charging *tRNA-Lys-CUU* with lysine, results in reduced growth of HCC cell lines.

Building upon these findings, future cancer treatments may implement amino acid deprivation in their anti-cancer regimen by making dietary modifications to customize the specific amino acid restrictions, or by using the inhibitors that specially target aminoacyl-tRNA synthetases. Simultaneously, treatment strategies should be developed to selectively deprive target cells of essential amino acids while minimizing the impact on normal cells.

The research described above, focuses on studying the dysregulation of the mature tRNA<sup>ome</sup> in HCC and cancer in general. However, the field of tRNA biology has become much more complex through the discovery of various RNA fragments derived from pre-tRNAs or mature tRNAs, such as tRNA halves (tiRNAs) and shorter tRNA-derived fragments (tRFs). These fragments have the potential to be generated under different cellular conditions, including stress, and are believed to have crucial roles in the regulation of gene expression, RNA interference, and other cellular processes<sup>62-64</sup>. However, measuring these tRNA fragments can pose challenges due to their small size and potential low abundance. Current methods for detection and quantitation of tRNA fragments include northern blotting, RNA sequencing, microarray analysis, cross-linking, ligation and sequencing of hybrids (CLASH), photoactivatable-ribonucleoside-enhanced cross-linking and immunoprecipitation (PAR-CLIP), or custom Taqman-based PCR assays<sup>65-67</sup>. These tRFs can regulate gene expression and participate in processes like gene silencing, RNA processing, and protein translation, and impact on various physiological processes like cell stress, growth, and differentiation<sup>62-64,68-70</sup>. Their relevance in tumor biology is also emerging. For example, the tRF-315 (derived from

tRNA-Lys-CTT) was significantly upregulated in all prostate cancer groups and associated with aggressive tumor growth<sup>71</sup>. They also have potential as clinical biomarkers for cancer diagnosis and prognosis and as therapeutic targets.

In conclusion, tRNAs and their derivatives have a vital part in protein synthesis and gene expression regulation. Abnormal levels of tRNAs may contribute to cancer through the disruption of gene expression. Therefore, tRNA biology can be of potential interest for developing novel cancer diagnosis, prognosis, and therapeutics.

## Reference

- 1 Perugorria, M. J. *et al.* Wnt- $\beta$ -catenin signalling in liver development, health and disease. *Nat Rev Gastroenterol Hepatol* **16**, 121-136 (2019).
- 2 Hanahan, D. Hallmarks of Cancer: New Dimensions. *Cancer Discov* **12**, 31-46 (2022).
- 3 Bugter, J. M., Fenderico, N. & Maurice, M. M. Mutations and mechanisms of WNT pathway tumour suppressors in cancer. *Nature Reviews Cancer* **21**, 5-21, doi:10.1038/s41568-020-00307-z (2021).
- 4 Liu, P. *et al.* Oncogenic Mutations in Armadillo Repeats 5 and 6 of  $\beta$ -Catenin Reduce Binding to APC, Increasing Signaling and Transcription of Target Genes. *Gastroenterology* **158**, 1029-1043.e1010, doi:10.1053/j.gastro.2019.11.302 (2020).
- 5 Rebouissou, S. *et al.* Genotype-phenotype correlation of CTNNB1 mutations reveals different  $\beta$ -catenin activity associated with liver tumor progression. *Hepatology* **64**, 2047-2061 (2016).
- 6 Buchert, M. *et al.* Genetic dissection of differential signaling threshold requirements for the Wnt/beta-catenin pathway in vivo. *PLoS Genet* **6**, e1000816 (2010).
- 7 Mazzoni, S. M. & Fearon, E. R. AXIN1 and AXIN2 variants in gastrointestinal cancers. *Cancer Lett* **355**, 1-8, doi:10.1016/j.canlet.2014.09.018 (2014).
- 8 Schatoff, E. M. *et al.* Distinct Colorectal Cancer–Associated APC Mutations Dictate Response to Tankyrase Inhibition. *Cancer Discovery* **9**, 1358-1371, doi:10.1158/2159-8290.Cd-19-0289 (2019).
- 9 Eek-hoon, J. *et al.* Wnt/ $\beta$ -Catenin/Tcf Signaling Induces the Transcription of Axin2, a Negative Regulator of the Signaling Pathway. *Molecular and Cellular Biology* **22**, 1172-1183, doi:doi:10.1128/MCB.22.4.1172-1183.2002 (2002).
- 10 Martínez-Jiménez, F. *et al.* A compendium of mutational cancer driver genes. *Nature Reviews Cancer* **20**, 555-572, doi:10.1038/s41568-020-0290-x (2020).
- 11 Albuquerque, C., Bakker, E. R., van Veelen, W. & Smits, R. Colorectal cancers choosing sides. *Biochim Biophys Acta* **1816**, 219-231 (2011).
- 12 Li, S. *et al.* Commonly observed RNF43 mutations retain functionality in attenuating Wnt/ $\beta$ -catenin signaling and unlikely confer Wnt-dependency onto colorectal cancers. *Oncogene* **39**, 3458-3472 (2020).
- 13 Cruciat, C. M. Casein kinase 1 and Wnt/ $\beta$ -catenin signaling. *Curr Opin Cell Biol* **31**, 46-55 (2014).
- 14 Zucman-Rossi, J. *et al.* Differential effects of inactivated Axin1 and activated  $\beta$ -catenin mutations in human hepatocellular carcinomas. *Oncogene* **26**, 774-780, doi:10.1038/sj.onc.1209824 (2007).
- 15 Feng, G. J. *et al.* Conditional disruption of Axin1 leads to development of liver tumors in mice. *Gastroenterology* **143**, 1650-1659(2012).
- 16 Abitbol, S. *et al.* AXIN deficiency in human and mouse hepatocytes induces hepatocellular carcinoma in the absence of  $\beta$ -catenin activation. *J Hepatol* **68**, 1203-1213 (2018).
- 17 Qiao, Y. *et al.* Axis inhibition protein 1 (Axin1) Deletion-Induced Hepatocarcinogenesis Requires Intact  $\beta$ -Catenin but Not Notch Cascade in Mice. *Hepatology* **70**, 2003-2017 (2019).
- 18 Fodde, R. & Tomlinson, I. Nuclear beta-catenin expression and Wnt signalling: in defence of the dogma. *J Pathol* **221**, 239-241, doi:10.1002/path.2718 (2010).

- 19 Liang, B. *et al.* Differential requirement of Hippo cascade during CTNNB1 or AXIN1 mutation-driven hepatocarcinogenesis. *Hepatology* **n/a**, doi:10.1002/hep.32693 (2022).
- 20 Wang, W. *et al.* Evaluation of AXIN1 and AXIN2 as targets of tankyrase inhibition in hepatocellular carcinoma cell lines. *Scientific Reports* **11**, 7470, doi:10.1038/s41598-021-87091-4 (2021).
- 21 Gilgenkrantz, H. & Perret, C. Letter to the Editor: Comment on Qiao et al. *Hepatology* **70**, 763-764 (2019).
- 22 Chen, X., Monga, S. P. & Calvisi, D. F. Reply. *Hepatology* **70**, 764-765 (2019).
- 23 Broutier, L. *et al.* Human primary liver cancer-derived organoid cultures for disease modeling and drug screening. *Nature Medicine* **23**, 1424-1435, doi:10.1038/nm.4438 (2017).
- 24 Nuciforo, S. *et al.* Organoid Models of Human Liver Cancers Derived from Tumor Needle Biopsies. *Cell Rep* **24**, 1363-1376 (2018).
- 25 van Tienderen, G. S. *et al.* Hepatobiliary tumor organoids for personalized medicine: a multicenter view on establishment, limitations, and future directions. *Cancer Cell* **40**, 226-230 (2022).
- 26 Gao, D. *et al.* Organoid Cultures Derived from Patients with Advanced Prostate Cancer. *Cell* **159**, 176-187, doi:<https://doi.org/10.1016/j.cell.2014.08.016> (2014).
- 27 van de Wetering, M. *et al.* Prospective Derivation of a Living Organoid Biobank of Colorectal Cancer Patients. *Cell* **161**, 933-945, doi:<https://doi.org/10.1016/j.cell.2015.03.053> (2015).
- 28 Sachs, N. *et al.* A Living Biobank of Breast Cancer Organoids Captures Disease Heterogeneity. *Cell* **172**, 373-386.e310, doi:<https://doi.org/10.1016/j.cell.2017.11.010> (2018).
- 29 Caruso, S. *et al.* Analysis of Liver Cancer Cell Lines Identifies Agents With Likely Efficacy Against Hepatocellular Carcinoma and Markers of Response. *Gastroenterology* **157**, 760-776 (2019).
- 30 Arnold, H. K. *et al.* The Axin1 scaffold protein promotes formation of a degradation complex for c-Myc. *Embo J* **28**, 500-512 (2009).
- 31 Rui, Y. *et al.* Axin stimulates p53 functions by activation of HIPK2 kinase through multimeric complex formation. *EMBO J* **23**, 4583-4594(2004).
- 32 Guo, X. *et al.* Axin and GSK3- control Smad3 protein stability and modulate TGF- signaling. *Genes Dev* **22**, 106-120(2008).
- 33 Li, Q. *et al.* Axin determines cell fate by controlling the p53 activation threshold after DNA damage. *Nat Cell Biol* **11**, 1128-1134 (2009).
- 34 Azzolin, L. *et al.* YAP/TAZ incorporation in the beta-catenin destruction complex orchestrates the Wnt response. *Cell* **158**, 157-170(2014).
- 35 Fumoto, K., Kadono, M., Izumi, N. & Kikuchi, A. Axin localizes to the centrosome and is involved in microtubule nucleation. *EMBO Rep* **10**, 606-613 (2009).
- 36 Poulton, J. S., Mu, F. W., Roberts, D. M. & Peifer, M. APC2 and Axin promote mitotic fidelity by facilitating centrosome separation and cytoskeletal regulation. *Development* **140**, 4226-4236(2013).
- 37 Loregger, A. *et al.* The E3 ligase RNF43 inhibits Wnt signaling downstream of mutated beta-catenin by sequestering TCF4 to the nuclear membrane. *Sci Signal* **8** (2015).
- 38 Neumeyer, V. *et al.* Loss of RNF43 Function Contributes to Gastric Carcinogenesis by Impairing DNA Damage Response. *Cell Mol Gastroenterol Hepatol* **11**, 1071-1094 (2021).

- 39 Silvera, D., Formenti, S. C. & Schneider, R. J. Translational control in cancer. *Nat Rev Cancer* **10**, 254-266 (2010).
- 40 Ruggero, D. Translational control in cancer etiology. *Cold Spring Harb Perspect Biol* **5** (2013).
- 41 Truitt, M. L. & Ruggero, D. New frontiers in translational control of the cancer genome. *Nat Rev Cancer* **16**, 288-304 (2016).
- 42 Huang, S. Q. *et al.* The dysregulation of tRNAs and tRNA derivatives in cancer. *J Exp Clin Cancer Res* **37**, 101 (2018).
- 43 Spears, J. L., Gaston, K. W. & Alfonzo, J. D. Analysis of tRNA editing in native and synthetic substrates. *Methods Mol Biol* **718**, 209-226 (2011).
- 44 Gaston, K. W. & Limbach, P. A. The identification and characterization of non-coding and coding RNAs and their modified nucleosides by mass spectrometry. *RNA Biol* **11**, 1568-1585 (2014).
- 45 Grelet, S. *et al.* SPOt: A novel and streamlined microarray platform for observing cellular tRNA levels. *PLoS One* **12**, e0177939 (2017).
- 46 Dittmar, K. A., Sørensen, M. A., Elf, J., Ehrenberg, M. & Pan, T. Selective charging of tRNA isoacceptors induced by amino-acid starvation. *EMBO Rep* **6**, 151-157 (2005).
- 47 Mahlab, S., Tuller, T. & Linial, M. Conservation of the relative tRNA composition in healthy and cancerous tissues. *Rna* **18**, 640-652 (2012).
- 48 Honda, S., Shigematsu, M., Morichika, K., Telonis, A. G. & Kirino, Y. Four-leaf clover qRT-PCR: A convenient method for selective quantification of mature tRNA. *RNA Biol* **12**, 501-508 (2015).
- 49 Schwartz, M. H. *et al.* Microbiome characterization by high-throughput transfer RNA sequencing and modification analysis. *Nat Commun* **9**, 5353 (2018).
- 50 Zheng, G. *et al.* Efficient and quantitative high-throughput tRNA sequencing. *Nat Methods* **12**, 835-837 (2015).
- 51 Li, P. *et al.* Recapitulating hepatitis E virus-host interactions and facilitating antiviral drug discovery in human liver-derived organoids. *Sci Adv* **8**, eabj5908 (2022).
- 52 Li, Y. *et al.* Hepatitis E virus infection remodels the mature tRNAome in macrophages to orchestrate NLRP3 inflammasome response. *Proceedings of the National Academy of Sciences* **120**, e2304445120, doi:doi:10.1073/pnas.2304445120 (2023).
- 53 Goodarzi, H. *et al.* Modulated Expression of Specific tRNAs Drives Gene Expression and Cancer Progression. *Cell* **165**, 1416-1427 (2016).
- 54 Grewal, S. S. Why should cancer biologists care about tRNAs? tRNA synthesis, mRNA translation and the control of growth. *Biochim Biophys Acta* **1849**, 898-907 (2015).
- 55 Feun, L. *et al.* Arginine deprivation as a targeted therapy for cancer. *Curr Pharm Des* **14**, 1049-1057 (2008).
- 56 Tang, X. *et al.* Cystine Deprivation Triggers Programmed Necrosis in VHL-Deficient Renal Cell Carcinomas. *Cancer Res* **76**, 1892-1903 (2016).
- 57 Qian, F., Xu, H., Zhang, Y., Li, L. & Yu, R. Methionine deprivation inhibits glioma growth through downregulation of CTSL. *Am J Cancer Res* **12**, 5004-5018 (2022).
- 58 Strekalova, E., Malin, D., Good, D. M. & Cryns, V. L. Methionine Deprivation Induces a Targetable Vulnerability in Triple-Negative Breast Cancer Cells by Enhancing TRAIL Receptor-2 Expression. *Clin Cancer Res* **21**, 2780-2791 (2015).

- 59 Wang, K. *et al.* IL1RN mediates the suppressive effect of methionine deprivation on glioma proliferation. *Cancer Lett* **454**, 146-157 (2019).
- 60 Li, Z. *et al.* Methionine metabolism in chronic liver diseases: an update on molecular mechanism and therapeutic implication. *Signal Transduct Target Ther* **5**, 280 (2020).
- 61 Kim, S., You, S. & Hwang, D. Aminoacyl-tRNA synthetases and tumorigenesis: more than housekeeping. *Nat Rev Cancer* **11**, 708-718 (2011).
- 62 Guzzi, N. & Bellodi, C. Novel insights into the emerging roles of tRNA-derived fragments in mammalian development. *RNA Biol* **17**, 1214-1222 (2020).
- 63 Zhu, L., Liu, X., Pu, W. & Peng, Y. tRNA-derived small non-coding RNAs in human disease. *Cancer Lett* **419**, 1-7 (2018).
- 64 Kumar, P., Kuscu, C. & Dutta, A. Biogenesis and Function of Transfer RNA-Related Fragments (tRFs). *Trends Biochem Sci* **41**, 679-689 (2016).
- 65 McArdle, H. *et al.* Quantification of tRNA fragments by electrochemical direct detection in small volume biofluid samples. *Sci Rep* **10**, 7516 (2020).
- 66 Xie, Y. *et al.* Action mechanisms and research methods of tRNA-derived small RNAs. *Signal Transduct Target Ther* **5**, 109 (2020).
- 67 Honda, S. & Kirino, Y. Dumbbell-PCR: a method to quantify specific small RNA variants with a single nucleotide resolution at terminal sequences. *Nucleic Acids Res* **43**, e77 (2015).
- 68 Emara, M. M. *et al.* Angiogenin-induced tRNA-derived stress-induced RNAs promote stress-induced stress granule assembly. *J Biol Chem* **285**, 10959-10968 (2010).
- 69 Goncalves, K. A. *et al.* Angiogenin Promotes Hematopoietic Regeneration by Dichotomously Regulating Quiescence of Stem and Progenitor Cells. *Cell* **166**, 894-906 (2016).
- 70 Pandey, K. K. *et al.* Regulatory roles of tRNA-derived RNA fragments in human pathophysiology. *Mol Ther Nucleic Acids* **26**, 161-173 (2021).
- 71 Olvedy, M. *et al.* A comprehensive repertoire of tRNA-derived fragments in prostate cancer. *Oncotarget* **7**, 24766-24777 (2016).

# **Chapter 9**

**Nederlandse Samenvatting**

**Dutch Summary**





## Samenvatting

### De Wnt/ $\beta$ -catenine signaleringsroute in leverkanker

Hepatocellulair carcinoom (HCC) vertegenwoordigt de meest voorkomende vorm van leverkanker. HCC-tumorigenese hangt sterk samen met genmutaties die leiden tot abnormale activatie van de Wnt/ $\beta$ -catenine signaalroute<sup>1-3</sup>. Mutaties in AXIN1, een scaffold-eiwit in het afbraakcomplex dat Wnt/ $\beta$ -catenine afbreekt, worden vaak waargenomen in HCC (8-10%), maar komen ook frequent voor in verschillende andere soorten kanker, waaronder die van de huid, baarmoeder en het maagdarmkanaal<sup>4-7</sup>. In dit proefschrift is ons eerste doel om te bepalen welke functionele domeinen van AXIN1 waarschijnlijk de grootste impact hebben op  $\beta$ -catenine signalering wanneer ze worden verwijderd, en om te identificeren welke specifieke tumor-geassocieerde aminozuurveranderingen en truncaties waarschijnlijk drivermutaties zijn die  $\beta$ -catenine signalering verhogen. Vervolgens beschrijf ik de generatie van vijf AXIN1-herstelde HCC-cellijnen en hun functionele analyse met betrekking tot  $\beta$ -catenine signalering, groeikarakteristieken en andere genen/signaalroutes die mogelijk worden beïnvloed. In het volgende hoofdstuk presenteren we de kwaliteitsanalyse van vier veelgebruikte RNF43-antilichamen. Ten slotte beschrijf ik in de laatste twee hoofdstukken een nieuwe methode om niveaus van tRNA-expressie te detecteren, en gebruik ik deze nieuwe methode om te analyseren welke tRNA's mogelijk differentieel worden gereguleerd bij leverkanker.

In **Hoofdstuk 2** laten we zien dat de meerderheid van de AXIN1-mutaties in kanker, inclusief missense- en truncatiemutaties, gelijkmatig verdeeld zijn over de coderende regio van het eiwit. Allereerst hebben we vastgesteld welke functionele domeinen van het eiwit de grootste impact hebben op  $\beta$ -catenine signalering wanneer ze worden verwijderd uit een AXIN1-expressieconstruct. Verwijdering van de GSK3 $\beta$ - of  $\beta$ -catenine-interactiedomeinen had een sterke invloed op signalering, gevolgd door verwijdering van het RGS/APC-interactiegebied. De relevantie van deze domeinen werd bevestigd door genbewerking in cellijnen. Vervolgens hebben we tumor-geassocieerde missense-varianten die in deze domeinen werden waargenomen opgehaald uit de cBioPortal en COSMIC-databases. Van de 18 geteste varianten in het GSK3 $\beta$ -interactiedomein had alleen de R395P-variant een sterke invloed op signalering. Van de 15 geteste varianten in het  $\beta$ -catenine-domein beïnvloedden er 4 de  $\beta$ -catenine-regulatie, waarvan de V478G-variant de grootste impact op signalering

vertoonde. De meeste van deze variaties resulteerden ook in verminderde of verloren binding aan hun overeenkomstige interactiepartner.

Van de 37 geteste varianten binnen het RGS/APC-interactiedomein resulteerden er 13 in verhoogde  $\beta$ -catenine signalering. Over het algemeen observeerden we twee klassen van varianten. De eerste klasse beïnvloedde ofwel de interactie met APC rechtstreeks, of indirect doordat ze zich bevonden in aangrenzende structuren die de AXIN1-interface met APC ondersteunen. De tweede klasse van varianten trad op binnen de hydrofobe kern van de RGS/APC-structuur en wordt verondersteld het gehele RGS/APC-domein te destabiliseren. Een gemeenschappelijk kenmerk van beide klassen is het verlies van APC-binding, wat waarschijnlijk hun falen verklaart om efficiënt cytoplasmatische puncta te vormen in cellen. Deze puncta worden zogenaamde degradasomen genoemd, waarin eiwitten van het afbraakcomplex samenkomen om  $\beta$ -catenine efficiënt af te breken. Naast het verlies van APC-binding is gemeld dat sommige varianten in de hydrofobe kern de vorming van nano-aggregaten induceren die  $\beta$ -catenine signalering op een dominant-negatieve manier beïnvloeden door te binden aan een nieuw repertoire van eiwitten<sup>8</sup>. Dienovereenkomstig vertonen deze varianten (bijv. L106R, C121F) een sterker defect in  $\beta$ -catenine regulatie dan de varianten die alleen APC-binding verliezen. Echter, in een directe vergelijking behielden zelfs deze sterkere RGS/APC-mutanten meer functionaliteit dan de defecte GSK3 $\beta$ - of  $\beta$ -catenine-domeinvarianten.

In totaal hebben we 18 missense-varianten geïdentificeerd die  $\beta$ -catenine signalering beïnvloedden, uit een totaal van 80 geteste varianten. De waargenomen effecten op  $\beta$ -catenine signalering overlaptten grotendeels met de voorspelde gevolgen van een uitgebreide eiwitstructuuranalyse.

In dit hoofdstuk hebben we ook de functionele gevolgen van AXIN1-truncatiemutaties bepaald. In HCC zijn dit de meest voorkomende soort AXIN1-mutaties die worden waargenomen. In totaal hebben we vijf Crispr-cas9 gemedieerde HEK293T-klonen gegenereerd die AXIN1-truncaties dragen met sequentieel verlies van C-terminale domeinen. Alle onderzochte truncatie-varianten, inclusief een variant die slechts de laatste 22 C-terminale aminozuren verloor, vertoonden verlies van  $\beta$ -catenine regulerende functie. Belangrijk is dat het verlies van functie omgekeerd evenredig lijkt te zijn met de lengte van het ingekorte AXIN1-eiwit, waarbij langere eiwitten meer functionaliteit behouden. Onze analyses

suggereren dus dat alle truncerende mutaties ten minste gedeeltelijk invloed hebben op  $\beta$ -catenine-regulatie, terwijl dit alleen het geval is voor een subset van missense-mutaties. Ter ondersteuning van het laatste verwerven de meeste colorectale en leverkankers die missense-varianten dragen, mutaties in andere  $\beta$ -catenine-regulerende genen zoals APC en CTNNB1. Deze resultaten zullen bijdragen aan de functionele annotatie van AXIN1-mutaties die zijn geïdentificeerd in grootschalige sequentieonderzoeken of bij individuele patiënten. Bovendien dragen ze bij aan een beter begrip van hoe het AXIN1-eiwit betrokken is bij het reguleren van  $\beta$ -catenine signalering op een juiste manier.

De analyses die hierboven worden beschreven, richten zich allemaal op de rol van AXIN1 in de regulatie van  $\beta$ -catenine. Er zijn echter verschillende rapporten met betrekking tot HCC die suggereren dat AXIN1-mutatie niet leidt tot verhoogde  $\beta$ -catenine signalering en dat deze signaalroute niet relevant is voor door AXIN1 gestuurde tumorigenese. Deze veronderstelling is grotendeels gebaseerd op het ontbreken van nucleaire accumulatie van  $\beta$ -catenine in AXIN1-gemuteerde tumoren en een lage/geen activering van  $\beta$ -catenine doelgenen. Zoals uitgebreid uiteengezet in de discussie van mijn proefschrift, zijn deze argumenten op zichzelf onvoldoende om een belangrijke rol voor  $\beta$ -catenine uit te sluiten. Ter ondersteuning hiervan toonden Qiao et al. aan dat de ontwikkeling van AXIN1-gestuurde HCC bij muizen vrijwel geheel afhankelijk is van functioneel  $\beta$ -catenine<sup>9</sup>. Om deze controverse te onderzoeken, hebben we de CRISPR/Cas9 genoombewerkingstechniek gebruikt om de AXIN1-truncatiemutatie te herstellen die aanwezig is in vijf HCC-cellijnen, zoals beschreven in **Hoofdstuk 3**. In totaal hebben we 14 succesvol herstelde klonen verkregen (2-4 per cellijn) die allemaal verminderde  $\beta$ -catenine signalering vertoonden. In combinatie met andere gepubliceerde gegevens toont dit duidelijk aan dat AXIN1-truncatie in HCC leidt tot verhoogde signalering, zij het bescheiden in vergelijking met bijvoorbeeld  $\beta$ -catenine-gemuteerde tumoren. Een tweede observatie was dat alle herstelde AXIN1-klonen verminderde groeikarakteristieken vertoonden, aangetoond met behulp van een kolonievormings- en MTT-test. Op het eerste gezicht lijkt dit te leiden tot de voor de hand liggende conclusie dat de verminderde groei kan worden verklaard door het lagere niveau van  $\beta$ -catenine signalering. Echter, het herstellen van  $\beta$ -catenine signalering tot het oorspronkelijke gemuteerde niveau door de cellen aan te vullen met exogeen WNT3a-ligand, slaagde er niet in de groei van deze klonen te herstellen.

Aangezien verminderde  $\beta$ -catenine signalering de gewijzigde groeikarakteristieken van herstelde AXIN1-cellen niet volledig kon verklaren, hebben we andere genen en signaalroutes onderzocht die mogelijk worden beïnvloed door AXIN1. Hiervoor hebben we RNA-sequencing gebruikt in combinatie met een gedetailleerd onderzoek naar specifieke genen/signaalroutes. We hebben tussen de 37 en 283 significant verhoogde of verlaagde genen geïdentificeerd per cellijn. Echter, bij het vergelijken van differentieel tot expressie gebrachte genen tussen cellijnen bleek er weinig consistentie te zijn in de geïdentificeerde genen of signaalroutes die mogelijk worden beïnvloed. Met betrekking tot  $\beta$ -catenine signalering waren slechts een klein aantal van de meer responsieve doelgenen (*AXIN2*, *NKD1*, *NOTUM*) gewijzigd in expressie in de meeste klonen, terwijl andere veronderstelde doelgenen meer variabiliteit vertoonden.

Recentelijk is gesuggereerd dat AXIN1 ook direct de niveaus en signalering van YAP/TAZ-proteïnen reguleert in HCC-cellen<sup>10</sup>. De Hippo-YAP/TAZ-signaleringsroute is een belangrijke signaalroute om orgaanomvang en weefselgroei te controleren, en de activiteit ervan is verhoogd in de meeste HCC's, vooral in AXIN1-gemuteerde tumoren. Echter, onze YAP/TAZ-immunoblot- en doelgenanalyse kon geen correlatie vinden tussen de mutatiestatus van AXIN1 en YAP/TAZ-signalering, wat de gepubliceerde link tussen AXIN1 en YAP/TAZ in twijfel trekt. Op dezelfde manier vonden we geen correlatie met Notch-signalering, wat ook is gemeld als verhoogd in veel AXIN1-gemuteerde HCC's. Samengevat laten we in dit hoofdstuk zien dat AXIN1-mutatie zowel de fitheid van HCC-cellen als de  $\beta$ -catenine signalering verhoogt, maar we vinden geen solide functionele correlatie tussen beide eigenschappen, noch met andere genen/signaalroutes die mogelijk worden beïnvloed door de mutatiestatus van AXIN1.

In **Hoofdstuk 4** beschrijven we de kwaliteitsanalyse van vier veelgebruikte RNF43-antilichamen. RNF43, net als zijn homoloog ZNRF3, is een belangrijke regulator van de Wnt-signaleringsroute door de hoeveelheid Wnt-receptor op het celmembraan te verminderen. Mutaties in RNF43 worden waargenomen in veel soorten kanker, vooral die van het maagdarmkanaal, en leiden tot abnormaal hoge niveaus van  $\beta$ -catenine-signalering wanneer cellen worden blootgesteld aan Wnt-liganden. Op basis van deze functie wordt aangenomen dat RNF43 zich bevindt op het celmembraan. Echter, verschillende rapporten hebben aanvullende nucleaire functies voor RNF43 geopperd. Deze waarnemingen worden ondersteund door duidelijke nucleaire kleuringspatronen te tonen met behulp van RNF43-

antilichamen. We hebben een cellijn gegeneerd die twee exonen mist die de epitopen coderen die door deze antilichamen worden herkend. Daarnaast gebruiken we meerdere cellijnen die naar verwachting geen RNF43 of ingekorte varianten ervan tot expressie brengen. Bij het gebruik van deze vier veelgebruikte RNF43-antilichamen op dit panel van cellijnen, kunnen we alleen niet-specifieke signalen waarnemen via Western blotting, immunofluorescentie of immunohistochemie. Met andere woorden, ze kunnen endogeen RNF43 niet betrouwbaar detecteren. Onze resultaten suggereren dat de nucleaire kleuringpatronen het gevolg zijn van een antilichaamartefact en dat RNF43 waarschijnlijk niet in de kern is gelokaliseerd. Meer in het algemeen moeten rapporten die gebruikmaken van RNF43-antilichamen voorzichtig worden geïnterpreteerd, althans wat betreft de aspecten van het RNF43-eiwit die in deze papers worden beschreven.

### **Rol van het tRNA-decoderingsstelsel in de ontwikkeling van leverkanker**

tRNA's spelen een cruciale rol bij de synthese van eiwitten uit aminozuren tijdens de translatie, gebaseerd op de genetische code. Afwijkingen in de tRNA-pool zijn in verband gebracht met de ontwikkeling van kanker, omdat ze kunnen bijdragen aan de transformatie van normale cellen in kankercellen. Veranderingen in de hoeveelheid tRNA of modificatiepatronen daarvan, kunnen leiden tot een verhoogde productie van door oncogenen gecodeerde eiwitten of een verminderde generatie van tumorsuppressoreiwitten, die beide kunnen bijdragen aan de ontwikkeling van kanker<sup>11-13</sup>. Daarnaast is ontregeling van tRNA-verwerkings- en modificatie-enzymen in verband gebracht met de ontwikkeling en progressie van bepaalde soorten kanker<sup>14,15</sup>.

Op dit moment is het uitdagend om tRNA op transcriptieniveau te detecteren en te kwantificeren vanwege redundantie in genkopieën, extreem korte sequenties, een rigide secundaire structuur en post-transcriptionele modificaties. Dit maakt het moeilijk om de niveaus van volledig gemodificeerde functionele tRNA's nauwkeurig te bepalen. In **Hoofdstuk 5** hebben we een eenvoudigere methode ontwikkeld voor het detecteren van tRNA met behulp van qPCR. Deze methode omvat een lengte-extensiestap, een universeel compatibele adapter en degeneratieve primers die kunnen worden gebruikt voor het volledige volwassen tRNA-oom. Door deze methode toe te passen, heb ik ontdekt dat HEV-infectie aanzienlijke veranderingen veroorzaakt in het hepatische tRNA-oom, waarbij mogelijk de vertaling van

genen die coderen voor de virale capsid-eiwitten wordt bevorderd ten koste van gastheer-antivirale genen zoals interferon-stimulerende genen. Deze herprogrammering van het tRNA-oom draagt waarschijnlijk bij aan de replicatie van het virus.

In **Hoofdstuk 6** was het doel van onze studie om de rol van tRNA bij de ontwikkeling van leverkanker (HCC) te onderzoeken en potentiële tRNA-gerelateerde doelwitten voor therapie te identificeren. Onze analyse van het tRNA-oom in HCC-tumoren en aangrenzend normaal leverweefsel onthulde dat een hoge expressie van tRNA-Lys-CUU was geassocieerd met een verhoogd risico op tumorrecidief en een slechtere overleving van de patiënt. We hebben ook significante verhoging waargenomen van Lysyl-tRNA Synthetase (KARS), het enzym verantwoordelijk voor het koppelen van lysine aan tRNA-Lys-CUU, in HCC-tumoren in vergelijking met normaal leverweefsel. Om de functies van tRNA-Lys-CUU en KARS verder te onderzoeken in HCC, hebben we experimenten uitgevoerd met HCC-cellijnen en organoïden afkomstig van patiënten. Onze resultaten toonden aan dat lysine-depletie, KARS-afname of behandeling met de KARS-remmer cladosporine effectief de celgroei, kolonievorming en migratie remde, via mechanismen die celcyclus-arrest en apoptose omvatten. Onze studie benadrukt het potentieel van tRNA-moleculen en KARS als therapeutische doelwitten voor de behandeling van HCC.

## Referenties

- 1 Parsons, M. J., Tammela, T. & Dow, L. E. WNT as a Driver and Dependency in Cancer. *Cancer Discov* **11**, 2413-2429 (2021).
- 2 Perugorria, M. J. *et al.* Wnt- $\beta$ -catenin signalling in liver development, health and disease. *Nat Rev Gastroenterol Hepatol* **16**, 121-136 (2019).
- 3 Xu, C. *et al.*  $\beta$ -Catenin signaling in hepatocellular carcinoma. *J Clin Invest* **132** (2022).
- 4 Timbergen, M. J. M. *et al.* Activated Signaling Pathways and Targeted Therapies in Desmoid-Type Fibromatosis: A Literature Review. *Front Oncol* **9**, 397 (2019).
- 5 Zucman-Rossi, J., Villanueva, A., Nault, J. C. & Llovet, J. M. Genetic Landscape and Biomarkers of Hepatocellular Carcinoma. *Gastroenterology* **149**, 1226-1239 e1224 (2015).
- 6 Ledinek, Ž., Sobočan, M. & Knez, J. The Role of CTNNB1 in Endometrial Cancer. *Dis Markers* **2022**, 1442441 (2022).
- 7 Bugter, J. M., Fenderico, N. & Maurice, M. M. Mutations and mechanisms of WNT pathway tumour suppressors in cancer. *Nature Reviews Cancer* **21**, 5-21, doi:10.1038/s41568-020-00307-z (2021).
- 8 Anvarian, Z. *et al.* Axin cancer mutants form nanoaggregates to rewire the Wnt signaling network. *Nature Structural & Molecular Biology* **23**, 324-332, doi:10.1038/nsmb.3191 (2016).
- 9 Qiao, Y. *et al.* Axis inhibition protein 1 (Axin1) Deletion-Induced Hepatocarcinogenesis Requires Intact  $\beta$ -Catenin but Not Notch Cascade in Mice. *Hepatology* **70**, 2003-2017 (2019).
- 10 Liang, B. *et al.* Differential requirement of Hippo cascade during CTNNB1 or AXIN1 mutation-driven hepatocarcinogenesis. *Hepatology* **n/a**, doi:10.1002/hep.32693 (2022).
- 11 Dai, Z. *et al.* N(7)-Methylguanosine tRNA modification enhances oncogenic mRNA translation and promotes intrahepatic cholangiocarcinoma progression. *Mol Cell* **81**, 3339-3355 e3338 (2021).
- 12 Passarelli, M. C. *et al.* Leucyl-tRNA synthetase is a tumour suppressor in breast cancer and regulates codon-dependent translation dynamics. *Nat Cell Biol* **24**, 307-315 (2022).
- 13 Orellana, E. A. *et al.* METTL1-mediated m(7)G modification of Arg-TCT tRNA drives oncogenic transformation. *Mol Cell* **81**, 3323-3338 e3314 (2021).
- 14 Goodarzi, H. *et al.* Modulated Expression of Specific tRNAs Drives Gene Expression and Cancer Progression. *Cell* **165**, 1416-1427 (2016).
- 15 Huang, S. Q. *et al.* The dysregulation of tRNAs and tRNA derivatives in cancer. *J Exp Clin Cancer Res* **37**, 101 (2018).





# **Appendix**

**Acknowledgements**

**Publications**

**PhD Portfolio**

**Curriculum Vitae**



## Acknowledgements

I arrived in the Netherlands five years ago to begin my Ph.D., and it has been an entirely enjoyable and memorable experience. I'd like to thank everyone, including my supervisors, friends, colleagues, and families.

To **Ron**, my respected co-promoter, who has assisted me in entering the field of molecular biology, I want to express my deepest gratitude. Despite our collaboration spanning less than three years, the wealth of invaluable experiences I have gained from you is immeasurable. Your patience in guiding me through each experiment and your unwavering enthusiasm for science have been truly inspiring. Furthermore, your perceptiveness allows you to understand my thoughts and provide timely assistance. The most impressive thing you did was sending me an email about the renewal project. Your action alleviated my embarrassment, as I was contemplating reaching out to you, and I was genuinely pleased with the way you used the words "under my wing". It is a great honor for me to be your student.

I am deeply grateful to my promotor, **Maikel P. Peppelenbosch**, for whom I have great respect and admiration. Your valuable advice and questions have been instrumental in the success of my project. Your expertise in multiple disciplines, including biochemistry, molecular medicine, virology, and cancer biology, has been an invaluable resource for me. Your creative thoughts and insights have truly inspired me, and I am grateful for the opportunity to work with such a brilliant and knowledgeable individual. Thank you for your guidance and support.

To **Abdullah**, my ex-co-promoter, I would like to express my sincere gratitude for giving me the opportunity to pursue my Ph.D. Your hard work and brilliance as a scientist are an inspiration to me, and I am grateful for the opportunity to work with you. Your guidance and support have been invaluable, and I am grateful for the knowledge and skills I have gained from you.

To **Gwenny**, your kind smile always brings happiness to my day when I see you in the MDL. Thank you for your valuable project suggestions during the MDL seminar. To **Luc van der Laan**, you are a funny professor and I appreciate the organoids you provided for our experiments. To **Monique**, thank you for your suggestions on the tRNA papers and for your assistance with the AXIN1 project. To **Jaap**, I am very grateful for the HCC samples you

provided, which form the basis of my first project. To **Lisanne Noordam**, I am glad to have you as my second author on my first project. You have been a great help in analyzing data and creating beautiful graphs. Thank you for your kindness and assistance.

To **Jan**, you are my friend and are always sensitive to my mood, kindly asking me what has happened. Every greeting from you makes me feel more cordial. Thank you for assisting us with ordering and organizing incoming goods and for your efforts in keeping the lab running smoothly.

To **Buyun**, as my most respected former colleague, you have a solid theoretical foundation in biology, you work extremely hard and are solely focused on experiments. Thank you for providing step-by-step instructions on culturing organoids. To **Xumin**, I appreciate your intelligence and consciousness of your objectives. Even though we only worked together for a short while, I valued the advice you gave me during my experiments. I am looking forward to collaborating with you in the future. To **Jiaye**, I am extremely grateful for your help when I first arrived at the lab and for your valuable suggestions on my experiments. Your support was instrumental in getting me settled and comfortable in my new environment. To **Sunrui**, you are always nice and taking care of Yunlong and me.

To **Wanlu**, you are incredibly smart and provided me with detailed guidance for my experiments and suggestions for my first presentation. To **Meng**, you are a kind and considerate person, and I really appreciate your help in evaluating the feasibility of my project. I am also very thankful for the opportunity you gave me to be your paranymp, it was a truly valuable memory that I will cherish forever.

To my ex-roommates in EE830, **Changbo**, **Peifa**, and **Zhijiang**, I am very grateful for having the opportunity to share an office with all of you. You are all hardworking individuals and I have learned a lot of valuable experience from each of you.

To **Zhouhong**, I appreciate your valuable advice when I felt lost in my scientific pursuits. To **Shaojun**, you are an excellent researcher, and I am grateful for your guidance on how to use the coffee machine. I am fortunate to have had the chance to work with all of you, and I wish you all the best in your future endeavors.

To **Ling**, you are an extremely warm-hearted person. You are always available whenever and wherever I need assistance. My husband always feels at ease when he knows

you are in the lab, because he knows that you will wait for me until the evening and then accompany me home. Your kindness and support have been invaluable to me. To **Yang**, I first met you while talking with my husband; you were a great help to us during that time. You are always courteous and have a great sense of humor, and we shared a memorable experience together. I consider myself fortunate to have met you guys in the Netherlands and to have you as a friend.

To my roommates in EE-830b, I would like to express my heartfelt gratitude to all of you. To **Bingting**, thank you for providing me with food from my hometown when I was feeling homesick, and for taking care of my feelings when I was sad. I also appreciate your girlfriend, **Shirong**, for joining us and creating happy memories while watching women's volleyball together. Furthermore, I am grateful to Bingting for sharing three unforgettable paraphernalia memories with me. Special thanks to **Luochengling** and **Wunan**, you guys have been with me through some of the toughest times and I will always remember the good moment when I opened my door and saw you guys standing outside. I hope you both achieve your goals within the next two years. To **Hangrui**, you are an interesting and funny person, and I admire your determination to maintain a healthy diet and physical fitness, even though it can be challenging at times. I want to express my heartfelt gratitude for your provision of delectable food and weekly supply of milk throughout the past challenging year, as they have been instrumental in keeping me nourished and alive.

To my colleagues in Ron's group, I would like to express my appreciation. To **Shanshan**, you are a hardworking and smart individual and have shown great efficiency in the experiments. Thank you for your help in our group, for providing me with necessary materials, and for your contributions to my projects. I sincerely wish you all the best for your upcoming PhD defense. To **Kelly**, I am grateful for your help in generating plasmids and performing some experiments. Although we worked together for a short time, you were always trying to finish as much work as possible. To **Boaz**, I initially had concerns that you were careless and thought it would be difficult to work together. However, you quickly proved me wrong. You are incredibly smart and able to learn quickly when you focus. Thank you for your contributions to my projects. To **Marla**, for your kind help to analyze images on the confocal. To **Jiahui**, it was a pleasure meeting you in the MDL. I hope everything goes well for you in the coming years in Ron's group.

Thanks to **Xiaofang**. We have known each other for eight years and even though you have become a mother to a cute and intelligent daughter, **Fatimah**, you will always be the cute girl in my heart. To **Junhong**, you are a hardworking individual, and I am confident that you will be given more opportunities to realize your vision. I sincerely wish you all the best in your future endeavors and hope that all your goals will be achieved.

To **Zhou** and **Lushun**, we arrived in the Netherlands almost at the same time and lived in the Holland2stay apartment during that period. When you moved to Leiden, I was initially sad but then happy to hear about your accomplishments there. Thank you for sharing your Polaroid cameras with me and for taking so many interesting photos together during our trip to Iceland. I will always cherish those memories. To **Pengfei**, heartfelt congratulations on your impressive achievements during your PhD journey. Best wishes for your ongoing success and personal growth.

I would like to extend my sincere gratitude to my colleagues in MDL, **Suk, Xiaopei, Yining, Siyu, Jiajing, Jiahua, Kuan, Guige, Anny, Amy**,.... Your companionship throughout my PhD journey have been invaluable. While I cannot possibly list everything, I will always cherish the wonderful memories we made together. Thank you for being a part of one of the best times in my life. I wish you all the best for your future endeavors.

To **Peipei, Jie, Heng, hongzhen, Wenchao, Ying**, regretting not having met you guys earlier. I truly treasure the time we spent together. Our shared experiences brought us even more happiness. I wish you all the best for a bright and successful future.

To **Chunjing**, I would like to express my gratitude for your accomplishments and for the warm and heartfelt moments we have shared. I have never hesitated to share everything, both my happiness and my sadness, with you, and I appreciate your willingness to listen and offer your support. Thank you for always being there for me when I needed help. You are a true friend, and I am lucky to have you in my life.

To **Elisa (Yang)**, my dear little sister. I regret not spending more time with you during the first three years. Whenever we were together, you always took care of everything, and I felt freer and more relaxed. Even though we were just sitting at home doing nothing, I was happy just being with you. I hope that in the future, we will be able to create even more priceless memories together.

To my families:

I would like to express my deepest gratitude to all of you for your understanding and support, which allowed me to pursue my work in the Netherlands. Special thanks to my parents and my brother and his wife, for your unwavering support and understanding. You have always been my backbone, giving me the strength and freedom to pursue my goals. To my parents-in-law and sister-in-law and her husband, thank you for your understanding and support for me and my husband. Your encouragement and support have been invaluable to us. To my uncle and his wife, thank you for always caring about our lives and for supporting us in every way possible. And to all my families, one sentence is not enough to express my immense gratitude and appreciation for everything you have done for me. I am truly blessed to have such a loving and supportive family.

Lastly, I must express my full appreciation to my beloved husband, **Yunlong**. You possess an extraordinary ability to maintain a calm and patient demeanor, and you are a loving and attentive husband. I am deeply grateful to have you as my husband. You take care of my daily needs and allow me to focus on my experiments without any distractions. Furthermore, you never cease to amaze me with your loving moments and delicious meals. I am truly fortunate to have you in my life.





## Publications list

1. **Zhang, R**, Noordam, L, Ou, X, et al. The biological process of lysine-tRNA charging is therapeutically targetable in liver cancer. *Liver Int.* 2021; 41: 206–219.
2. Li, Y.#, **Zhang R.#**, Wang Y., Li P., Li Y., Janssen H L. A., de Man R. A., Peppelenbosch M. P., Ou X., & Pan Q. (2023). Hepatitis E virus infection remodels the mature tRNA<sup>ome</sup> in macrophages to orchestrate NLRP3 inflammasome response. **Proceedings of the National Academy of Sciences of the United States of America**, 120(25), e2304445120. <https://doi.org/10.1073/pnas.2304445120> (# equal contribution)
3. Ou X#, Ma B#, **Zhang R#**, Miao Z, Cheng A, Peppelenbosch MP, Pan Q. A simplified qPCR method revealing tRNA<sup>ome</sup> remodeling upon infection by genotype 3 hepatitis E virus. *FEBS Lett.* 2020 Jun; 594(12): 2005-2015. (# equal contribution)
4. **Ruyi, Zhang**, et al. Identification of tumor-associated AXIN1 missense variants that affect  $\beta$ -catenin signaling. **Manuscript in submission.**
5. **Ruyi, Zhang**, et.al. Unraveling the Impact of AXIN1 Mutations on HCC Development: Insights from CRISPR/Cas9 repaired AXIN1-mutant liver cancer cell lines. **Manuscript in submission.**
6. Li, S., **Zhang, R.**, Lavrijsen, M., van den Bosch, T. P. P., Peppelenbosch, M. P., & Smits, R. (2023). Issues with RNF43 antibodies to reliably detect intracellular location. **PLoS one**, 18(4), e0283894. <https://doi.org/10.1371/journal.pone.0283894>.
7. Miao Z, **Zhang R**, Yu P, Li Y, Pan Q, Li Y. The macrolide antibiotic azithromycin potently inhibits hepatitis E virus in cell culture models. *Int J Antimicrob Agents.* 2021 Sep;58(3):106383.
8. Li Y, Miao Z, Li P, **Zhang R**, Kainov DE, Ma Z, de Man RA, Peppelenbosch MP, Pan Q. Ivermectin effectively inhibits hepatitis E virus replication, requiring the host nuclear transport protein importin  $\alpha$ 1. *Arch Virol.* 2021 Jul;166(7):2005-2010.
9. Wang W, Liu P, Lavrijsen M, Li S, **Zhang R**, Li S, van de Geer WS, van de Werken HJG, Peppelenbosch MP, Smits R. Evaluation of AXIN1 and AXIN2 as targets of tankyrase inhibition in hepatocellular carcinoma cell lines. *Sci Rep.* 2021 Apr 2;11(1):7470.
10. Liu J, Li P, Wang L, Li M, Ge Z, Noordam L, Lieshout R, Verstegen MMA, Ma B, Su J, Yang Q, **Zhang R**, Zhou G, Carrascosa LC, Sprengers D, IJzermans JNM, Smits R, Kwekkeboom J, van der Laan LJW, Peppelenbosch MP, Pan Q, Cao W. Cancer-Associated Fibroblasts Provide a Stromal Niche for Liver Cancer Organoids That Confers Trophic Effects and Therapy Resistance. *Cell Mol Gastroenterol Hepatol.* 2021;11(2):407-431.

11. Li Y, Qu C, Spee B, **Zhang R**, Penning LC, de Man RA, Peppelenbosch MP, Fieten H, Pan Q. Hepatitis E virus seroprevalence in pets in the Netherlands and the permissiveness of canine liver cells to the infection. *Ir Vet J*. 2020 Apr 2;73:6.
12. Li Y, Li P, Li Y, **Zhang R**, Yu P, Ma Z, Kainov DE, de Man RA, Peppelenbosch MP, Pan Q. Drug screening identified gemcitabine inhibiting hepatitis E virus by inducing interferon-like response via activation of STAT1 phosphorylation. *Antiviral Res*. 2020 Dec;184:104967.
13. Jiaye Liu, Pengfei Li, Ling Wang, Meng Li, Zhouhong Ge, Lisanne Noordam, Ruby Lieshout, Monique M.A. Verstegen, Buyun Ma, Junhong Su, Dave Sprengers, **Ruyi Zhang**, Guoying Zhou, Ron Smits, Jaap Kwekkeboom, Luc J.W. van der Laan, Maikel Peppelenbosch, Qiuwei Pan, Wanlu Cao. FRI488 - Modelling liver tumor organoids and cancer-associated fibroblasts interaction reveals the robust effects of stromal niche in cancer nurturing and treatment resistance. *Journal of Hepatology*. 2020; 73(1):S638-S63
14. Wang L, Li M, Yu B, Shi S, Liu J, **Zhang R**, Ayada I, Verstegen MMA, van der Laan LJW, Peppelenbosch MP, Cao W, Pan Q. Recapitulating lipid accumulation and related metabolic dysregulation in human liver-derived organoids. *J Mol Med (Berl)*. 2022 Mar;100(3):471-484.
15. Li P, Li Y, Wang Y, Liu J, Lavrijsen M, Li Y, **Zhang R**, Verstegen MMA, Wang Y, Li TC, Ma Z, Kainov DE, Bruno MJ, de Man RA, van der Laan LJW, Peppelenbosch MP, Pan Q. Recapitulating hepatitis E virus-host interactions and facilitating antiviral drug discovery in human liver-derived organoids. *Sci Adv*. 2022 Jan 21;8(3):eabj5908.
16. Li Y, Li P, He Q, **Zhang R**, Li Y, Kamar N, Peppelenbosch MP, de Man RA, Wang L, Pan Q. Niclosamide inhibits hepatitis E virus through suppression of NF-kappaB signalling. *Antiviral Res*. 2022 Jan;197:105228.
17. Gao K, Zong H, Hou K, Zhang Y, **Zhang R**, Zhao D, Guo X, Luo Y, Jia S. p53N236S Activates Autophagy in Response to Hypoxic Stress Induced by DFO. *Genes (Basel)*. 2022 Apr 26;13(5):763.

---

## PhD Portfolio

<b>Name PhD Student</b>	Ruyi Zhang
<b>Erasmus MC Department</b>	Gastroenterology and Hepatology
<b>Ph.D Period</b>	October 2018 – October 2023
<b>Promoter</b>	Prof. Dr. Maikel P. Peppelenbosch
<b>Co-promoter</b>	Dr. M.J.M. Smits

### PhD training

---

#### Seminars

- 2018-2022, Weekly MDL seminar program in experimental Gastroenterology and Hepatology (attending); (42 weeks/year; @1.5h) (ECTS, 9.0)
- 2018-2022, Weekly MDL seminar program in experimental Gastroenterology and Hepatology (presenting); (preparation time 16h; 2 times/year) (ECTS, 4.6)
- 2018-2022, Biweekly research group education(attending); (20 times/year; @1.5h) (ECTS, 4.3)
- 2018-2022, Biweekly research group education(presenting); (preparation time 8h; 8 times/year) (ECTS, 8.6)

#### General Courses

- 2019, The Microscopic Image Analysis: From Theory to Practice (ECTS, 0.8)
- 2019, The Basic course on R (ECTS, 1.80)
- 2019, The Introduction in Confocal Course
- 2021, Scientific Integrity (ECTS, 0.30)
- 2021, The Basic and Translational Oncology (ECTS, 1.80)

### **National and International Conferences**

---

- 2019, Annual Day of the Molecular Medicine Postgraduate School, Rotterdam, the Netherlands.

### **Academic Awards**

---

- 2018, China Scholarship Council (CSC) Scholarship (File No. 201808530490)

## Curriculum Vitae

Ruyi Zhang was born on April 20, 1990 in Gongzhuling, Jilin province, China. She was raised and completed her primary, secondary, and high school education in her hometown.

In 2010, she began her college studies at the Jilin Institute of Chemical Technology in China, and received her bachelor's degree in 2014. In 2014, she began her master's studies at the Kunming University of Science and Technology in China, and started her master's research training at the Medical Faculty under the supervision of Dr. Shuting Jia. In the laboratory of molecular genetics of aging and tumor, her master's thesis was on "The mechanism of the RAS-MAPK pathway cooperating with p53N236S in anti-apoptosis."

In 2018, with the support of the China Scholarship Council (CSC), she had the opportunity to start her PhD research at the Department of Gastroenterology and Hepatology at the Erasmus University Medical Center in Rotterdam, Netherlands. Under the supervision of Prof. Maikel P. Peppelenbosch and Dr. Abdullah Pan, she focused on tRNA decoding biology, followed by a research project on the Wnt/ $\beta$ -catenin pathway in liver cancer supervised by Dr. Ron Smits.